Electromagnetic Forming of Friction Stir Welded Aluminium Sheets

A thesis submitted in partial fulfillment
of the requirements for the Degree of

DOCTOR OF PHILOSOPHY

by

Mr. Jyoti Kumar Doley
(Roll No. 11610321)

Department of Mechanical Engineering
Indian Institute of Technology Guwahati
Guwahati: 781039, India.

2018

Declaration

I hereby certify that the information presented in this dissertation '**Electromagnetic Forming of Friction Stir Welded Aluminium Sheets**' is entirely my own account of research performed under the supervision of Prof. Sachin Dnyandeo Kore. Any part of this work has not earlier been submitted for the award of any degree, diploma, associate-ship, fellowship or its equivalent to any Institute or University.

Jyoti KumarDoley
Roll no. (11610321)
Department of Mechanical Engineering
Indian Institute of Technology Guwahati
Assam – 781039, India

Certificate

To whomsoever it may concern it is to certify, that the work contained in the thesis report titled **Electromagnetic Forming of Friction Stir Welded Aluminium Sheets** by Jyoti Kumar Doley (Roll no. 11610321) has been carried out under my supervision, that the work is original, and that the work has not been submitted elsewhere for a degree.

Dr. Sachin D. Kore
Associate Professor
Department of Mechanical Engineering
Indian Institute of Technology Guwahati
Assam – 781039, India

Dedicated to Babu

The hero of my life.

Acknowledgments

First and foremost, I would like to render my utmost gratitude to Dr. Sachin D. Kore who has accepted me as a research scholar under his guidance and introduced to me this wonderful research subject. Under his kind supervision and with his intellectual inputs, this work has been completed in the best of the environment. He always encourages my research work and guided me in all scientific as well as personal aspects, for which I shall always be indebted to him.

I am extremely thankful to my doctoral committee chairman Prof. P. S. Robi and committee members Prof. S. Senthivelan and Prof. R. Bhattacharjee for their valuable suggestions and encouragements through out of my research work. I would like to address my gratitude to past and present head of the mechanical engineering department Prof. A. K. Dass and Prof. S. K. Diwedy for the generosity they have shown in providing experimental facilities and needs. I would also like to extend a special note of thanks to Prof. U. S. dixit for extending emotional and moral support to me during my difficult days.

My thanks are due to the technical staff of mechanical engineering department, who have helped me at all stages in my research work. I am thankful to Mr. N. K. Das, Mr. Sanjib Sarma, Mr. Jiten Basumatary, Mr. Amal Kalita, Mr. P. Paul, Mr. Nip Borah and Mr. S. Ahmed for helping me in solving problems related to experimental issues. I am also extremely thankful to workshop staff, Mr. B. Chandan, Mr. Dilip Chetri, Mr. M. Sarma, Mr. U. Gohain, Mr. D. Khaklary, Mr. D. Deka and Mr. M. C. Medhi, who have helped me during setup design and fabrication.

I wish to acknowledge my heartfelt and deep sense of appreciation towards my research group members cum friends Dr. Chandrahas Patel, Dr. Ashish Rajak, Mr. Ramesh Kumar, Mr. Piyush Singh, Mr. Sagar Pawar and Mr. Getu T. Areda. I sincerely thanks them for making my stay in the institute most memorable. I would also like to express my gratitude to my friend Mr. Randeep Singh Chaudhary who always encourages me to go to the extreme and many thanks to all who directly or indirectly contributed to the completion of this thesis.

It wouldn't be possible to express my gratitude to my mother because no words are enough to define my feelings for her. Further I would thank from the depth of my heart to my siblings Dr. Mrs. Jyotimai bora and Mr. Hichendra Doley for their support and understanding.

Finally, I would like to thank Pronita for being there and believed in me. Her continuous source of unconditional love, support and encouragement always provided me the required patient and energy to go ahead.

Abstract

Friction stir welding (FSW) process is a solid state joining technique considered to be a significant development in the area of welding particularly for light metals considering their poor weldability like aluminium, magnesium, titanium alloys. Further issues related to forming difficulties of the above materials can be effectively solved by High velocity forming (*HVF*) process. Electromagnetic forming (*EMF*) is one of such *HVF* processes, which is gaining popularity due to its clean and simplicity of operation. Again, in modern vehicle constructions alloys are used as Tailor welded blanks (*TWB*), primarily for rigidity and weight saving, in which blanks are welded first and then formed into desired shapes.

In this thesis aluminium alloys *AA* 6061 and *AA* 5052 were chosen for studies because of their wide applicability in automotive sector. First a number of experimental studies were carried out with Friction stir welding (*FSW*) process to study weld-ability of these alloys as a different material combination and different thickness *TWBs* respectively. Successful welding with optimum welding parameters was found out supported by good mechanical and microstructure results. Like, defect free *TWBs* with different grade combination were obtained by friction stir welding *AA*5052-*H32* to *AA* 6061-*T6* in thicknesses of 1 *mm* and 1.5 *mm* respectively. The optimum process parameters were found to be tool rotational speed of 1500 *rpm* and welding speed of 63 *mm/min* and 98 *mm/min*. During tensile test welded blanks failed at weld zone near *AA* 5052 alloy. During welding intermetallic compounds were formed in weld zone which contribute negatively in the fracture strength of the joint.

In another case, successful welding of different thickness blanks with thickness combination of 1 *mm* with 1.5 *mm* were obtained for *AA* 5052 -*H32* and *AA* 6061-*T6* respectively. Tool rotational speed of 1500 *rpm* and tool traverse speed of 36, 63 and 98 *mm/min* were the parameters for successful weld joint. All the weld samples fractured at weld zone near thinner 1 *mm* side during tensile testing.

In second phase formability study of these *TWBs* with *EMF* were carried out. Comparative study was done to access formability of base material and *TWBs* by high velocity (*EMF*) process and by conventional quasi-static forming process. Formability was analysed in terms of Limit dome height (*LDH*) test and Forming limit diagram (*FLD*).

Effect of orientation of weld line on *EM* forming of different grade *TWB* was found to bring significant change in their formability. Test results showed more deformation obtained when weld line is offset by 25 *mm* towards *AA* 6062 side. Among quasi-static and *EMF* processes, more deformation was achieved in case of *EMF* process by the *TWBs*. There is a significant increase in *FLC* of *TWB* formed by *EMF* process against conventional process. Similarly, *EMF* process gave more deformation than the conventional quasi-static process for different thickness *TWB* of *AA* 5052. Base materials also showed the same trend of increase in formability with *EMF* process. Also, there is a significant increase in the *FLCs* of the *TWBs* which were formed by *EMF* process as compared to quasi-static process.
Hence, experimental investigation revealed successful welding of thin sheet of *AA* 5052 and *AA* 6061 in form of *TWBs* can be obtained by *FSW* process. Further, *EMF* process tends to increase the formability of the *TWBs* as well as that of the base materials.

In addition, with the help of commercially available *FEM* software *LS Dyna* simulation work was done to predict the failure region in sheet metal during *EM* forming. The simulation result helped in die design and was successfully validated with experiment result.

Table of Contents

List of Figures

List of Tables

Chapter 1

Introduction

1 Introduction

1.1 Forming

Forming – is defined as manufacturing process through the three-dimensional or plastic modification of a shape while retaining its mass and material cohesion. In contrast to deformation, forming is the modification of a shape with controlled geometry. Forming processes are categorized as chip-less or non-material removal processes.

The processes mentioned above are termed as fixed tools or conventional forming processes where there are certain mechanical defects and limitations arising from various metal forming processes.

1.1.1 Defects Caused by Conventional Forming

The processes mentioned above are termed as fixed tools or conventional forming processes where there are certain mechanical defects and limitations arising from various metal forming processes. The various defects reported are due to necking, the instability and fracture of metals, wrinkling and buckling, spring-back, void or cavity formation and surface and structural damage. While fixed tools are highly productive they do not offer the local control that was provided by hammer forming. Even today, difficult components in prototype production and aerospace manufacture are commonly produced with the aid of manually operated hammers. High velocity metal forming techniques are more akin to hammers than fixed tools as the impulse is controlled rather than forces or displacements. Also like hammer work, when properly implemented, one can control the spatial distribution of the impulse.

1.1.2 High Velocity Forming

As the name itself hints, high velocity forming (*HVF*) refers to a set of techniques which are used for metal forming. The velocities achieved during these techniques are in the range from 100- 300 *m/s* with a strain rate of the order of 10^3/ *sec*. These techniques include methods such as Explosive forming, Electromagnetic forming, Electro-hydraulic forming and so forth. All these techniques involve imparting a high kinetic energy to the work piece by accelerating it to a very high velocity, before it is made to hit the work die. *HVF* process increases the formability of many metals and alloys even to those difficult to form material like alloys of aluminium and magnesium. Due to very low strain rate sensitivity, aluminium

alloys have poor forming characteristics and difficult to formed by conventional forming method [1, 2, and 3]. High velocity forming technique is one of the processes to increase the formability of aluminium alloy. High kinetic energy associated with the high velocity forming process brings inertial effect to the deforming work-piece resulted in a plastic deformation.

1.1.3 Advantages of *HVF*

HVF techniques have several advantages over conventional forming techniques, apart from reducing the number of processes required in manufacturing. These are as follows:

a) One of the main advantages of using *HVF* techniques is that very complex shaped parts can be formed in a single operation, rather than carrying out a series of operations to achieve the same results via conventional forming techniques.

b) Plane strain elongation increases for aluminium alloy subjected to a single room temperature high velocity forming process. A full understanding of high velocity formability is still not available, but it appears one primary reason is a resistance to sheet metal necking that is developed by inertia.

c) When sheet metal strikes a tool at high velocity large compressive impact stresses are developed. These coin the sheet into the die surface. This can reduce spring-back, improve surface finish and enhance formability.

d) When a sheet is deformed with a particular velocity profile each part of the sheet would like to travel along its launch path creating a wrinkling. At high velocity wrinkling is repressed due to the material momentum.

e) The strain distribution is much more uniform in a single operation of *HVF* as compared to conventional forming techniques. This results in making it easy to produce complex shapes without inducing unnecessary strains in the material.

f) Since the basic principle of a high velocity formation technique is quite opposite to that of a conventional forming technique, the tools and other equipment used in the process has quite lightweight compact relatively speaking.

g) High velocity techniques can be used to improvise upon various joining methods such as say for example fusion welding. Impact welding using highly velocity techniques can produce much better results than the conventional fusion welding techniques.

1.2 Motivation

In 1970s the sudden rise in crude oil prices and dwindling sales of bulky inefficient vehicles have made automobile manufacturer to realise the importance of lighter and fuel efficient vehicles. So after that there is segment of smaller, lighter and efficient cars which became prominent in the car market. Many new innovations like front wheel drive, monoque body construction have taken place during that era to save weight and space. Recently the interest is shifting to material selection like lighter but stiff material e.g. aluminium and magnesium alloys. The use of aluminium alloy can provide reduction in vehicle weight with an advantage of excellent corrosion resistant. But aluminium has lower formability behaviour than traditionally used material like steel. Popular method to overcome this difficulty is either forming at elevated temperature or with forming at high speed. Forming at elevated temperature increases time and cost since extra stage of warming the material to desired temperature is added in the manufacturing process. High speed forming provides a solution to the formability issue of the aluminium alloys within manufacturing chain. Electromagnetic forming in particular which is a high speed forming process is gaining acceptance among industries for its simplicity and ease of operation.

The strength of aluminium is one third of that steel. To maintain crash worthiness of the vehicle we need a structure giving enough strength. Further to conserve weight of the vehicle the use of light weight material like aluminium alloys is necessary. Tailor welded blanks are used where extra strength and stiffness is required in vehicle body. Again aluminium alloys are difficult to weld by fusion welding due to formation of oxide layer on its surface. It can be weld by solid state welding process like friction stir welding. To be deformed by *EMF* process the thinner material dimension is desirable for better result. Though successful welding of aluminium alloy thinner than 2 *mm* by *FSW* process is still a challenge though few researchers have studied *FSW* of less than 2 *mm* thin sheets [45, 46, 47 &, 48]. So, the main motivation of the current work is to study the weld-ability of aluminum alloys of less than 2 *mm* thickness in form of *TWBs* by *FSW* process and then investigate the high speed formability of the *TWBs* by *EMF* process. The *TWBs* will be in the form of different grade and of different thickness combination.

1.3 Objective of the Research Work

AA 5052-*H32* and *AA* 6061-*T6* materials which have a major application in automobile industry for car body constructions were considered in this study. A sheet thickness of both 1 *mm* and 1.5 *mm* for each *AA* 5052 and *AA* 6061 were taken for welding by *FSW*.

The first part of the objectives are:

1. To characterize the mechanical and microstructural behaviour of friction stir welded blanks of dissimilar grade material combination, i.e., *AA* 6061 with *AA* 5052.
2. To characterize the mechanical and microstructural behaviour of friction stir welded blanks of different material thickness, i.e., 1 *mm* to 1.5 *mm*.

Forming behaviour of friction stir-welded blank is essential to study for its application in automotive and aero- space structures. Hence, formability behaviour of *FSWed* blanks will be studied with the help of high velocity forming process. Formability analysis will be done at both high velocity and at quasi-static speed. There is no previous literature found on electromagnetic forming of aluminium *TWB*. In our study electromagnetic forming and hydraulic press forming process will be utilized for high velocity and quasi-static forming test respectively. Formability was analysed in terms of Forming Limit Diagram (*FLD*) through Limit Dome Height (*LDH*) test.

The second part of the objectives are:

1. To characterize the forming behaviour of *FSWed* blanks of dissimilar grade material combination, i.e., *AA* 6061 with *AA* 5052.
2. To characterize the forming behaviour of *FSWed* blanks of different material thickness, i.e., 1 *mm* to 1.5 *mm*.

In order to successfully conduct the *LDH* test the die should be able to provide desirable failure region and deformation in the deforming work-piece. Simulating the process could provide the required die entry radius to avoid unwanted fracture at undesirable zone.So, in the last part, work will be done to predict the failure region in *EM* sheet metal forming through simulation.

1.4 Contribution of the Research Work

High speed forming of welded blanks has not been reported in any research paper till the writing of this thesis. Therefore, by addressing the specified research gap and challenges in the respective field of solid state welding and high speed welding of tailor welded blanks of

aluminium alloys a major contribution for future researcher can be made. The major findings or contribution of the research work can be summarized as:

1. Determining the optimum process parameters for difficult to weld thin sheet aluminium alloys of different grade combination (i.e. *AA* 5052 with *AA* 6061) by friction stir welding.
2. Determining the optimum process parameters for successful welding of thin sheet aluminium alloys of different thickness combination (i.e. 1 *mm* with 1.5 *mm*) by friction stir welding.
3. Formability analysis of aluminium alloy tailor welded blanks (of different thickness as well as of different grade combination).
4. Quantifying the high speed formability of aluminium alloy tailor welded blanks (of different thickness as well as of different grade combination) in terms of forming limit diagram.

1.5 Outline of the Thesis

The thesis is organised into seven chapters. First chapter is dedicated to introduction to high speed forming and friction stir welding. The second and third chapters are about review of background literature and experimental procedure respectively. Fourth chapter deals with friction stir welding of thin sheets of aluminium alloys, while chapter fifth concerned about high speed forming of the friction stirred welded blanks by electromagnetic forming process. Chapter sixth is about numerical simulation for predicting failure zone in *EMF* process. Last chapter seven present the conclusions and future scope. The following are the brief introduction of each chapter:

Chapter 1: Introduction to various high speed forming techniques such as explosive, electrohydraulic and, electromagnetic forming process followed by tailor welded blanks and friction stir welding process. Objective and contribution of the present research work.

Chapter 2: Literature review of work done by various researchers in the field of electromagnetic forming of aluminium alloys and friction stir welding of thin sheet aluminium alloys particularly *AA* 5052 and *AA* 6061.

Chapter 3: Description about electromagnetic forming and friction stir welding experimental set ups. Briefing about experiment methodology.

Chapter 4: First section of this chapter provides description about experimental work done to join different grade aluminium alloy *AA* 5052 with *AA* 6061 by friction stir welding process, supported by report on post weld mechanical behaviour and microstructural transformation of the joint.

In the second section joining of same material different thickness *AA* 5052 and *AA* 6061 aluminium alloys were reported. Discussion on optimum process parameters for successful welding along with mechanical behaviour and microstructural analysis of the joint was reported.

Chapter 5: In the first section, description of experimental work done to analysis the effect of weld line movement during high speed forming of friction stir welded blanks (different grade combination). While in second section, description of high speed formability study of different thickness friction stir tailor welded blanks of aluminium alloy *AA* 5052 by electromagnetic forming process has been reported. In both the sections comparative study of high speed forming process with quasi-static forming process of welded blank were reported. The formability was studied in terms of limit dome height test and forming limit diagram.

Chapter 6: Finite element simulation of *EMF* process to predict the failure zone of the work piece.Validation of the simulation result with experimental result.

Chapter 7: Conclusions of the presented research work with defined scope of future work.

Chapter 2

Literature Review

2 Literature Review

In this chapter, detail descriptions on various types of High velocity forming (*HVF*), Tailor welded blanks and Friction stir welding are presented. Followed by description on experimental work done in electromagnetic forming process of sheet metal and on the later part, review of friction stir welding process of aluminium alloys has been reported. There are number of literatures available dealing with flat sheet deformation by EMF process as well as in the area of friction stir welding of aluminum alloys, the review will concern on history and advancement of the respective field.

2.1.1 Explosive Forming

Explosive forming is distinguished from conventional forming in which the punch or diaphragm is replaced by an explosive charge. The explosives used are generally high explosive chemicals, gaseous mixtures, or propellants. There are two techniques of high explosive forming, stand – off technique and the contact technique [4]. The use of water as the energy transfer medium ensures a uniform transmission of energy and muffles the sound of the explosive blast. The process is versatile a large variety of shapes can be formed, there is virtually no limit to the size of the work piece, and it is suitable for low quantity production as well [5].

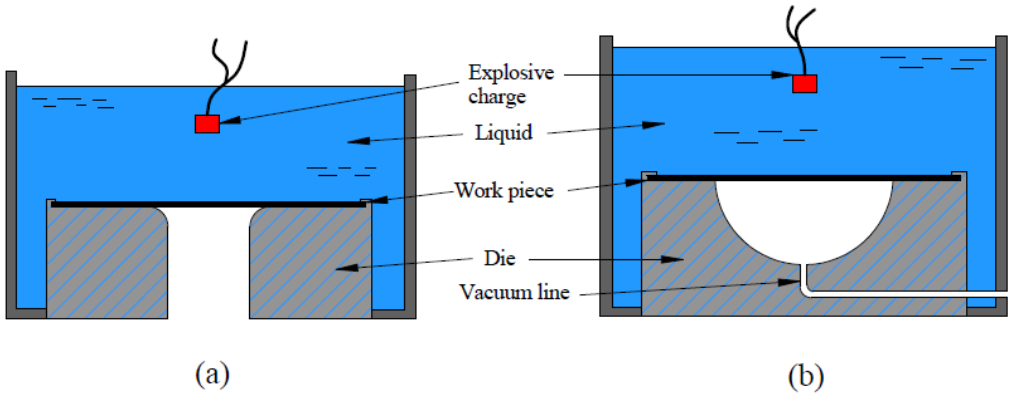

Fig. 2.1 Example of (a) free forming and (b) die forming as accomplished with explosive forming.

2.1.2 Electrohydraulic Forming

Electro hydraulic forming (*EHF*), also known as electro-spark forming, is a process in which electrical energy is converted into mechanical energy for the forming of metallic parts. A bank of capacitors is first charged to a high voltage and then discharged across a gap between two electrodes, causing explosions inside the hollow work piece, which is filled with some suitable medium, generally water. These explosions produce shock waves that

travel radially in all directions at high velocity until they meet some obstruction. If the discharge energy is sufficiently high, the work piece is deformed at high strain rate into the die [6, 7, 8, 9, and 10]. The deformation can be controlled by applying external restraints in the form of die or by varying the amount of energy released.

2.1.3 Electromagnetic Forming

Electromagnetic forming (*EMF*) is a non-contact technique where large forces can be imparted to any electrically conductive work-piece by a pure electromagnetic interaction. The force application is contact free and no working medium is required. The principle is based on physical effects described by Maxwell [11]. Maxwell reported that a temporarily time varying magnetic field induces electrical currents in nearby conductors with consequent exerts forces (Lorentz forces) to these conductors. Depending on the magnetic flux density, *B* and the current density, *J* in the tool coil as well as in the work-piece, the volumetric magnetic force, *F* also acts on both and can be determined by

$$\vec{F}_{Lorent}=\vec{J}\times\vec{B} \tag{2.1}$$

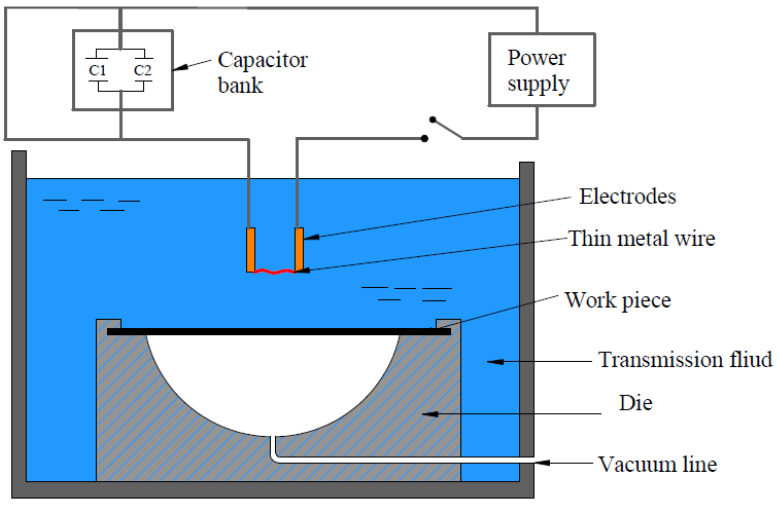

Fig. 2.2 Schematic of electrohydraulic forming.

A schematic diagram with key elements for the process is provided in *Fig. 2.3*. A significant amount of energy (usually between 5 and 200 *kJ*,) is stored in a large capacitor, or bank of capacitors, by charging to a high voltage (usually between 3,000 and 30,000 *volts*). The charge is switched over low inductance conductive bus work through a coil or actuator. Large currents run through the coil. The currents take the form of a damped sine wave and

can be understood as a ringing Inductance-Resistance-Capacitance (*LRC*) circuit [12]. The peak current is typically between about 10 to 1000 *kA* and the time to peak current is on the orders of tens of microseconds. This creates an extremely strong transient magnetic field in the vicinity of the coil. The magnetic field induces eddy currents in any conductive materials nearby; in much the way the primary circuit of a transformer induces voltage and current in the secondary [13]. Hence any metallic work-piece nearby will have currents induced and these will generally be opposite in direction to the primary current. The opposed fields in the coil and work piece set up an electromagnetic repulsion between the coil and work-piece [14]. That electromagnetic force can produce stresses in the work-piece that are several times larger than the material flow stress. Ultimately, this can cause the work-piece to deform plastically and to be accelerated at velocities exceeding 100 *m/s*. Work-piece material of electrical resistivity up to 15 $\mu\Omega.cm$ can be formed by the process [13].

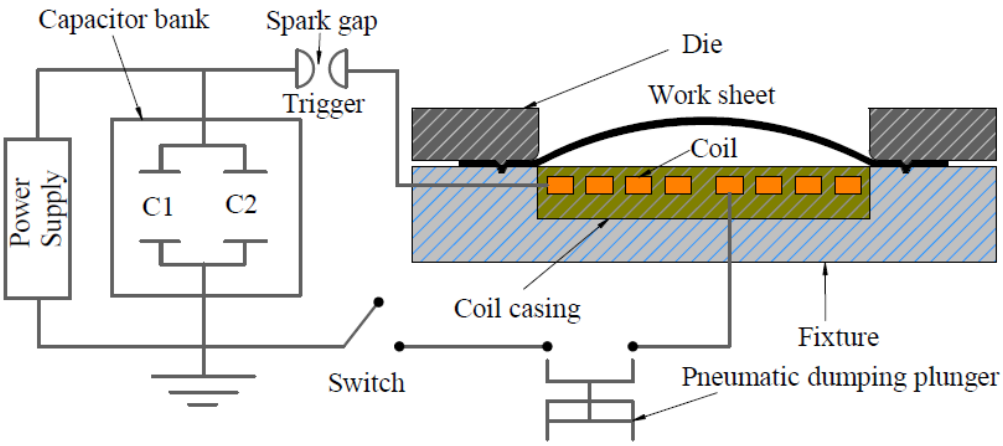

Fig. 2.3 Schematic of the general electromagnetic forming process.

Developing a relatively high system ringing frequency is often quite important. If the electrical oscillation frequency is too low, intense eddy currents are not induced in the work-piece, and the force developed is low. The ringing frequency is directly related to the *LRC* circuit characteristics and, low capacitance and low inductance favour a high ringing frequency. Materials of lower conductivity demand higher ringing frequency for effective forming. For these reasons metals with high conductivity such as aluminium and copper are very well suited to electromagnetic forming. Carbon steel can be formed, but special attention should be given to the system ringing frequency. Metals with relatively low electrical conductivity such as titanium and austenitic stainless steels are almost impossible to directly form by electromagnetic forming, but they can be formed with the aid of a more conductive driver plate.

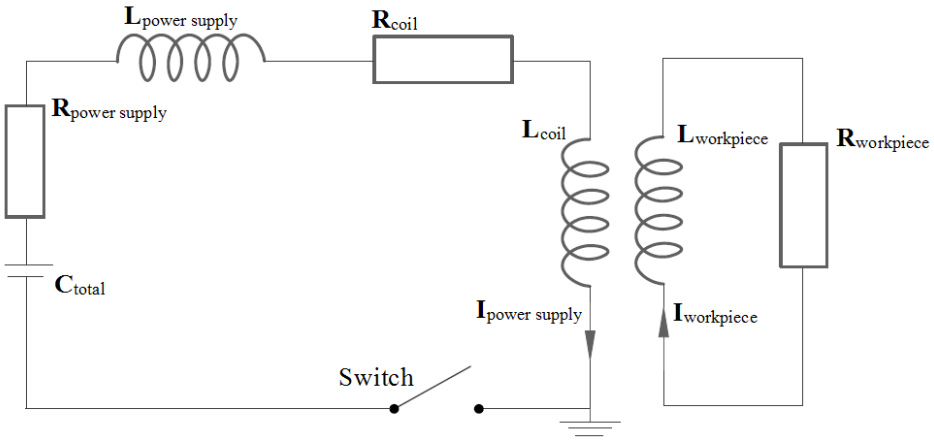

Fig. 2.4 Schematic of simplified EMF circuit.

The peak current generated by a capacitor bank discharge $I(t)$, can be estimated from standard *LRC* equations for the primary circuit (*Fig. 2.4*). So, long as the circuit resistance is low this can be estimated as:

$$I(t) = V_0 \sqrt{\frac{C_{total}}{L_{total}}} \tag{2.2}$$

Here, V_0 is the voltage of the capacitor bank initially charged up-to, C_{total} and L_{total} is the total system capacitance and inductance ($L_{total} = L_{power\ supply} + L_{coil}$) respectively.

Thus, the current density in the coil can be obtained from the pulse current *I(t)*, which is a sinusoidal damped current generated from a *RLC* circuit of the *EMF* devices and can expressed as:

$$\frac{d^2I(t)}{dt^2} + 2\xi\omega\frac{dI(t)}{dt} + \omega^2 I(t) = 0 \tag{2.3}$$

Where,
$$\xi = \frac{1}{2} R_{total} \sqrt{\frac{C_{total}}{L_{total}}} \tag{2.4}$$

Solving the above differential equation by setting initial $I(t) = 0$, thus, in the *EMF* process the discharging pulse current is approximately expressed as below:

$$I(t) = -I_0\, exp(-\gamma t) sin(\omega t) \tag{2.5}$$

Where, I_o is the current of coil and could be represented as

$$I_0 = \frac{V_0}{L_{total}\,\omega} \tag{2.6}$$

The damping constant γ is defined as

$$\gamma = \frac{R_{total}}{2L_{total}} \tag{2.7}$$

The angular frequency ω, is expressed as

$$\omega = \sqrt{\frac{1}{L_{total}C_{total}}} \tag{2.8}$$

At a fixed primary circuit current, the magnetic pressure (electromagnetic field intensity) is increased by increasing the number of windings in the forming coil or solenoid, but this will increase the inductance of the system. This in turn reduces the peak current. The result is that for any situation, there are an optimum number of coil windings. As a general rule for efficient forming most of the total system inductance should reside in the forming coil. There is an engineering trade-off; however, as the number of turns increases, the inductance of the system rises, reducing ringing frequency. This reduces the peak current and will allow more flux to leak through the work-piece. The correspondence between electromagnetic field intensity and magnetic pressure can be exploited in the design of electromagnetic forming coils. In regions where the current paths are closely packed there will be a much higher pressure than in regions where the coil has thick sparse conductors. This ultimately determines the launch velocity distribution for the sheet and the free-form shape the sheet metal shape would take.

The depth of penetration of the current through work-piece called skin depth δ, which mainly depends on the resistivity ρ [15], of the work-piece and the frequency ω, of the closed electrical circuit:

$$\delta = \sqrt{\frac{2\rho}{\mu_0\,\omega}} \tag{2.9}$$

Where,μ_0, is the absolute permeability of the material.

Joule heating is also known as Ohmic heating and resistive heating, in which a current pass through a conductor releasing heat because of its internal resistance. Generally, in an *EMF*

process, Joule heat generated by a large current could be observed at the coil and work-piece. This heat can be calculated by the following formula:

$$Q = I^2 \times R \times t \tag{2.10}$$

Where, Q is the heat generated by a current, I, flowing through a conductor with electrical resistance, R, during a time period, t. The resistance of a material that is dependent on temperature, $R\ (T)$, can be calculated by the temperature coefficient of resistance α in the following formula:

$$R(T) = R(T_0)\alpha(\Delta T) \tag{2.11}$$

Where, $R\ (T_0)$ is the resistance at reference temperature (T_0 = 20^0C) and ΔT is the temperature difference between T_0 and T.

2.1.4 EMF Process Characteristics

The main apparatuses which constitute an electromagnetic forming system are discussed below.

2.1.4.1 Equipment

An electromagnetic forming system has two essential electrical components; a capacitor bank and a forming coil that do work on a work-piece to be formed. Also, some tool or die system that produces the final part shape may also be important. There are two opposed philosophies one may follow in developing an electromagnetic forming system. One could develop a general-purpose setup that is useful, but not optimal, for a range of metal forming activities. Or, a system may be designed that is optimal for a particular operation. In this latter case one can be much more efficient (developing equivalent metal forming with less stored electrical energy). These approaches become clear when system details are discussed.

a) Capacitor Banks

The heart of an electromagnetic (or electrohydraulic) forming system is a capacitor bank. The essential components are a number of capacitors that store energy E, (typically in the range of 5 to 200 kJ) by storing electrical charge at voltages V, between 3kV and 30kV. The associated bank capacitance, C can be determined from:

$$E = \frac{CV^2}{2} \tag{2.12}$$

The energy is provided to the capacitors by a charging system. A transformer steps the voltage up from line voltage to that required by the capacitor bank. The capacity of the transformer will largely control the time required to charge the bank between discharge events. In repeated use, active cooling of the elements that dissipate energy will limit the ultimate cycle period for such a bank. The capacitors are tied to the current output with bus work. Two considerations are key in the design of the bus work, it must have low inductance (in general the majority of the system inductance should be at the forming coil), and long-lasting spark-free electrical contacts are required [16].

In use, the capacitors are relatively slowly charged to the forming voltage and once this is reached a fast-action switch is used to provide the current pulse to the coil. Several types of switches have been used, including rattrap type switches, semi-conductor switches [17] and fairly simple spark gaps [18].

Commercial capacitor banks typically have either mercury-filled ignitron-type switches or solid-state Silicon Controlled Rectifier (*SCR*) switches. The former performs well, but can be temperamental and have a somewhat limited life; while the latter can be inefficient if not designed well and it can be expensive to equip the bank with the required number of switches required to handle the large currents seen in electromagnetic forming. In a simple *LRC* type circuit, the current will ring with a damped sinusoidal current-time profile.

(b) Coils

Like the punch tool in a conventional forming process, the coil of the electromagnetic process similarly plays an important role in the electromagnetic forming process. The main purpose of the actuator is to transmit current and completing the electrical circuit as a whole. It provides required force for deformation in terms of magnetic field and pressure. The instantaneous nature of current and magnetic force requires important consideration while designing the tool coil. So, the shape of the coil along with mechanical properties of the material, like, the strength, and the electrical properties, like, inductance and resistance, also need to be considered while designing the coil [19].The simplest way to make an electromagnetic compression coil is to simply cut a slot and hole in a conductive plate. High material conductivity will improve system efficiency and high material yield strength provides a strong, robust, long life coil. So, the desired material choices are high strength aluminium alloys, copper-beryllium alloys, and brasses. Generally, electromagnetic forming coils are fabricated by placing spiral coil of conductive wire over strong insulated mandrel laminated with phenolic composite [20]. Reinforced epoxy or urethane is often

used as a structural and insulating over layer. Compression, expansion or flat coils can all be made following this same general approach.

Various operation of compression or expansion of tubes and deformation of flat sheets can be achieved by electromagnetic forming with the help of different arrangement of coil and work piece and tool geometry itself (*Fig. 2.5*). So, mainly three types of coils are identified according to above operations. The spiral helical coils are generally used for compression and bulging of tubes while flat spiral coil are used for expansion of sheets.

For tube compression operation the coil encloses the work-piece, while for the expansion of tube it is in the other way around. Generally, tubes with a diameter from 3 *mm* up to 2 *m* and with thicknesses of up to 5 *mm* can be processed by electromagnetic tube forming process [16]. For electromagnetic sheet metal forming the area of the formed work-piece can be from $10^{-4}\ m^2$ to 0.02 m^2 while the sheet thickness can be up to 5 *mm*.

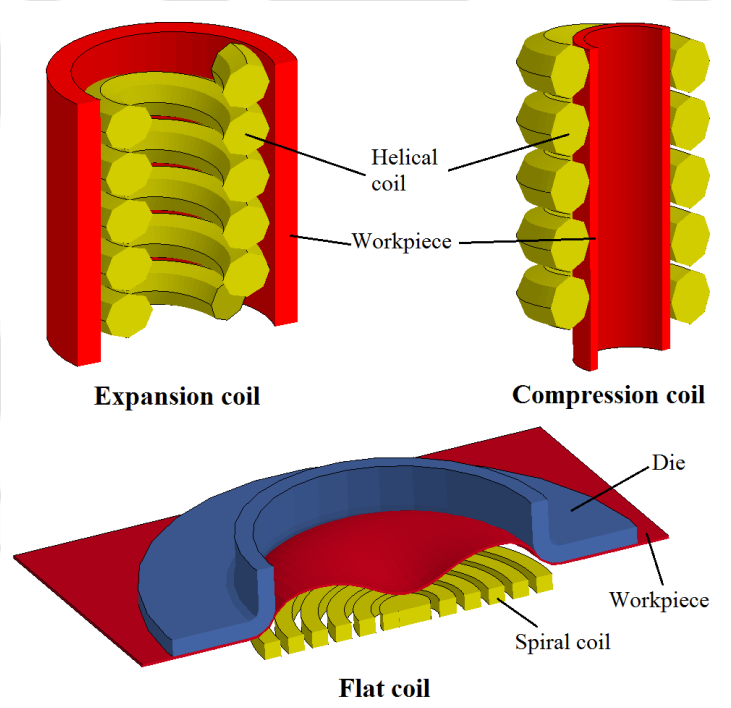

Fig. 2.5 Different coil types for the electromagnetic forming processes.

There are two important limitations of this type of tool coil. First, the forces on the work-piece and coil are equal and opposite (in addition to other magnetic interactions within the coil). Therefore, the coil construction materials determine the pressure the coil can withstand. Second, it is usually difficult to use a very fine winding pitch to increase local field intensity. This also limits the local pressures that can be generated from this kind of

coil. Both these issues can be partly treated in short-run production by using inexpensive coils that are essentially disposable.

(c) Fieldshaper

To generate the highest electromagnetic pressures work-piece and tool coil surface, the coil should be made from a monolithic block of a high strength and high conductivity metal [21]. However, monolithic block or single turn coils usually have quite low inductance, which makes them quite inefficient.

So, with the help of fieldshaper regular coils can be used to develop high electromagnetic pressure while being maintaining suitable inductance of the coil. Compared to the outer surface of the field shaper the concentration area is typically much smaller as shown in *Fig. 2.6*, resulting in a higher current density and higher field strength at the smaller zone. Due to this magnetic field another current is induced in the work-piece in the region of the concentration area, which in turn shields the magnetic field. However, the tool coil, the field shaper and the work-piece are electrical conductors in a magnetic field, so that Lorentz forces are acting on all components as soon as the currents are flowing. These so-called Lorentz forces initiate a plastic deformation of the work-piece as soon as the resulting stresses in the work-piece reach the flow stress.

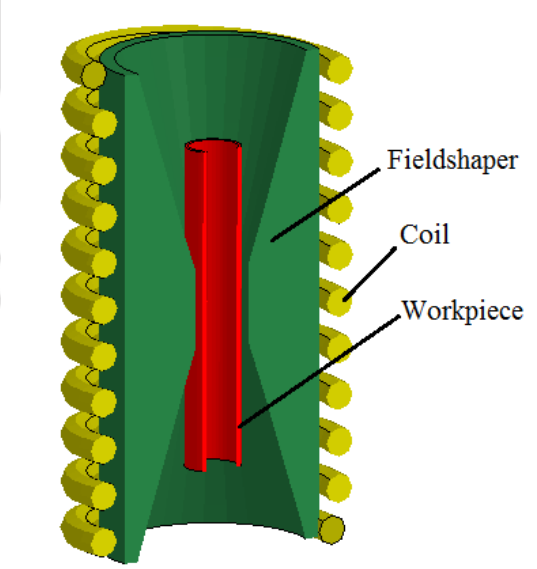

Fig. 2.6 Helical coil with an internal work piece tube for compression operation by featuring a fieldshaper.

2.1.5 Applications of EMF

The *EMF* technology can be applied in various different manufacturing processes especially in the field of sheet metal processing and it is also possible to perform joining or cutting operations or even a combination of the mentioned applications. While electromagnetic force can be used in very general and creative ways to form conductive sheet metal, to date it has been almost exclusively used to form crimped assemblies. Such assemblies can be designed to optimize axial or torsional strength, and in either case, the joint strength can often exceed the strength of the parent tube. Despite this, most of the assemblies that have been produced do not require high mechanical performance. Instead, the high reproducibility and dimensional tolerance afforded by the process are more typically the reasons for choosing electromagnetic crimping. The technology has also found application in the aircraft maintenance industry. Magnetic hammers are used, and a somewhat more complex application of this has been developed as to create electromagnetic dent-pullers.

2.1.6 Advantages and Disadvantages of Electromagnetic Forming

Electromagnetic forming offers several advantages:

At high strain rates or velocities sheet metal experiences improvement in mechanical properties in terms of reduce spring back and wrinkling. Stretching exceeds conventional process limits thus improving the ductility of the material. So, electromagnetic forming has the potential to improve material formability. The reduction in spring back and wrinkling gives the final product a close dimensional tolerance and good surface appearance.

Deformation happens in EMF due to large pressure generated by the tool coil against the metal sheet, which happens for a fraction of a section. Therefore, fixture design should be focus on only to accelerate or decelerate the low mass thin sheet of metal rather than to accommodate additional punch forces. This simplifies tooling and fixture design associated with electromagnetic forming process and reduces the overall size and mass.

In electromagnetic sheet metal forming process usually single-sided tooling is used for deformation of sheet. Thus reducing tooling cost significantly, moreover, single tool can be used for many operations involving different die profile [22]. Additional advantages include elimination of alignment of precisely machined matched punch and die set, every time while forming in conventional forming operation.

High productivity. Since the operation time is in microsecond, electromagnetic forming could be highly productive if automated [23].

a) The elimination of lubricants while forming the process is environmentally friendly. That also makes the operation zone out of messy and smelly discomfort [24].

b) However, there are some disadvantages of the electromagnetic forming process:

c) The main disadvantage of the process is that it is limited to high electrical conducting material only. However, non-conducting or low conducting material can be formed with the help of a driver. But this increases the complexity of the operation.

d) Short tool life due to large pressure involved.

e) Low efficiency of *EMF* system as only up-to 20% of the charging energy is actually utilized for plastic deformation operation [25].

f) There is a constraint of thickness of the sheet involving deformation and operation involving deep drawing.

g) Because of high currents and high voltages involved in *EMF* operation, safety concerns are there.

2.2 Tailor Welded Blanks

As discussed earlier for lightweight construction of automobile, aluminium and magnesium alloys have the advantages of lightweight, corrosion resistance, and very good thermal and electrical conductivity. To take advantages of its above-mentioned properties in vehicle constructions, aluminium alloys are being use as tailor made blanks. In Tailor Welded Blanks (*TWB*), the sheets are welded together prior to the desired forming operation using advanced welding techniques. The tailoring of the sheets provides optimal distribution of thickness, strength, etc. with several advantages to the product like reduced production costs, reduced weight, and improved structural performance.

Today a conventional car structural body parts composed of different thickness material or of more than one material, or even have different types of coatings and geometries, so, *TWB* are therefore sheet metal assemblies that include areas with different thicknesses, materials,

coatings, etc. [26]. Applications of *TWB* include car door inner panel, deck lids, bumper, side frame rails etc. in automotive sector [27]. Designer can optimize the structural performance of the car parts as *TWB* of different thicknesses, strengths, and/or other material properties can be made. Optimal performance of the part means lighter structures, higher strengths, and joining before forming results in lower production costs.

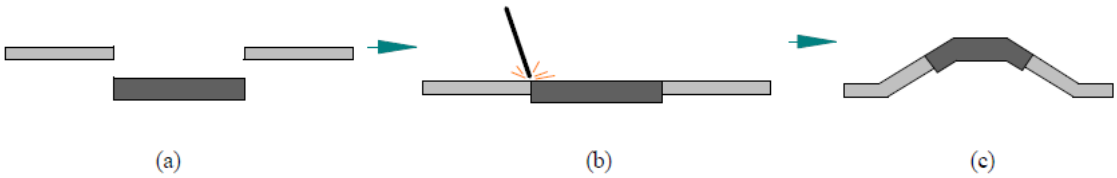

Fig. 2.7 Principle of tailor welded blanks (a) Blanks, (b) Joined by a welding process and, (c) Forming.

The principles of tailor welded blank processing are shown in *Fig. 2.7*. So, the tailor welded blanks are defined as two or more separate pieces of flat material, dissimilar thickness, and/or mechanical properties, jointed together before forming to provide customized and superior qualities in the finished stamping [28].

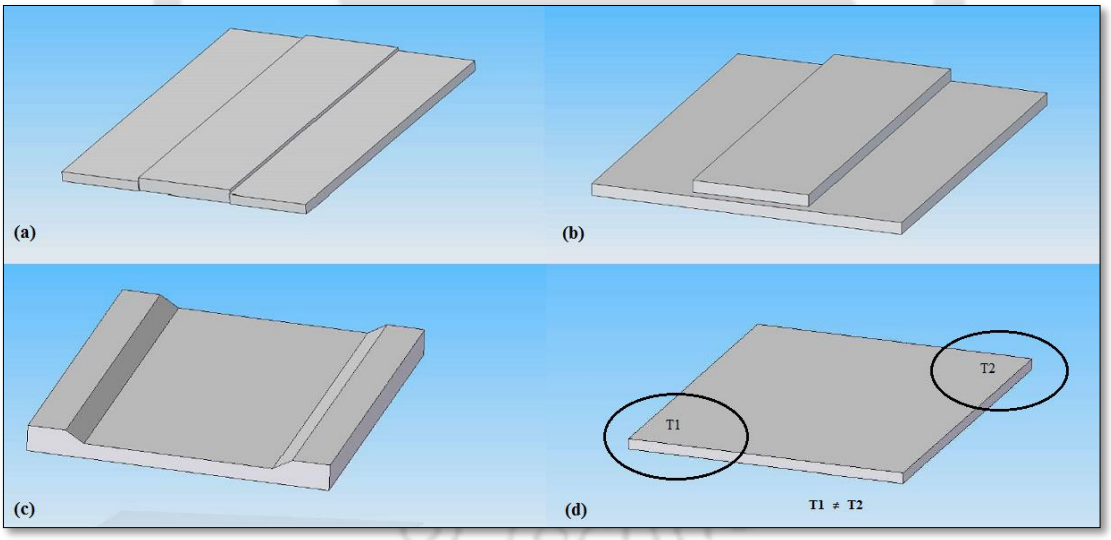

Fig. 2.8 Types of tailor blanks (a) Tailor Welded Blanks, (b) Patchwork Blanks, (c) Tailor Rolled Blanks and, (d) Tailor Heat Treated Blanks.

There are generally four sub-groups of tailor blanks- tailor welded blanks, patch-work blanks, tailor rolled blanks and tailor heat-treated blanks (*Fig. 2.8*). Every types of blanks have its own purpose and advantages, for e.g. tailor welded blanks and tailor rolled blanks are used in car parts were no reinforcing is required or avoids excess joining elements, thus contributing to light weight design. Whereas, patch work blanks add to a process integration since blank and reinforcing patch are formed simultaneously in one tool. In tailor heat

treated blanks a local heat treatment is used to improve the forming behaviour of the materials for the construction of the body in white. Conventionally car parts with different thickness and of different material grades are first formed into smaller pieces, and then these formed parts are welded together to obtained one piece of complete automobile part. But, with the application of tailor welded blank technique, the different thickness and materials grades are first joined by means of *LASER* beam welding, Friction stir welding or by using adhesive etc. and then the *TWBs* are formed into one piece of the complete automobile part.

2.2.1 Advantages of Tailor Welded Blanks

Due to the possibility of obtaining a *TWB* of different thickness, coating, geometry, and /or strength constituent material, Tailor welded blanks can have several benefits:

a) Car body weight reduction, thus greater fuel efficiency.
b) Improvement in raw material utilization and reduction of scrap material.
c) Automobile parts reduction due structural rigidity of *TWB*s [29].
d) Improvement in anti-crash property of the car.
e) Larger width parts can easily be made.
f) Costs benefits as the joining materials prior to the forming reduces the number of the required forming tools, so the higher accuracy increases and the use of material is enhanced in the forming process leading to less production costs.
g) In addition, part integration eliminates production steps in press shop and assembly and, thus, arguably reduces capital investments as well as personnel and variable costs. Also, tailor blanking may involve additional cost savings in material handling and in other, less directly related operations of production. Possible technological improvements include increased dimensional accuracy of components, and improved structural and corrosion properties due to continuous welds in tailored blanks compared to ordinary stampings assembled by spot welding.
h) The high investment costs for welding processes involve in the manufacture of tailor welded blanks are being its disadvantages.

The sheets which constitute the tailor-made blank are welded or adhesively bonded. They can be joined by various welding process, i.e., laser welding, friction stir welding, micro-plasma arc welding or gas tungsten arc welding. The joining, welding, or machining process is followed by a forming process which brings the tailor-made blank to its functional shape as a structural part.

However, aluminium has poor weld-ability characteristics due to its high reflectivity, low molten viscosity and the existence of oxide layers. This leads to change in microstructure, porosity, hot cracking in the fusion zone, loss of alloying elements and reduction of strength. So, aluminium and its alloys are hard to weld by conventional fusion welding processes. Unconventional welding method like Friction stir welding is most suitable for poor weld-ability material like aluminium, since during the welding process the constituent materials do not undergo melting and solidification [30].

2.3 Friction Stir Welding

Friction Stir Welding (*FSW*) creates high quality, high-strength joints with low distortion and is capable of fabricating either butt or lap joints, in a wide range of materials thickness and lengths. The process uses no outside (filler) material, no shielding gases, and requires low energy input when compared to other welding processes (*Fig. 2.9*). The solid phase bond between the two pieces is made solely of parent material. The grain structure in the weld zone is finer than that of the parent material and has similar strength, bending, and fatigue characteristics.

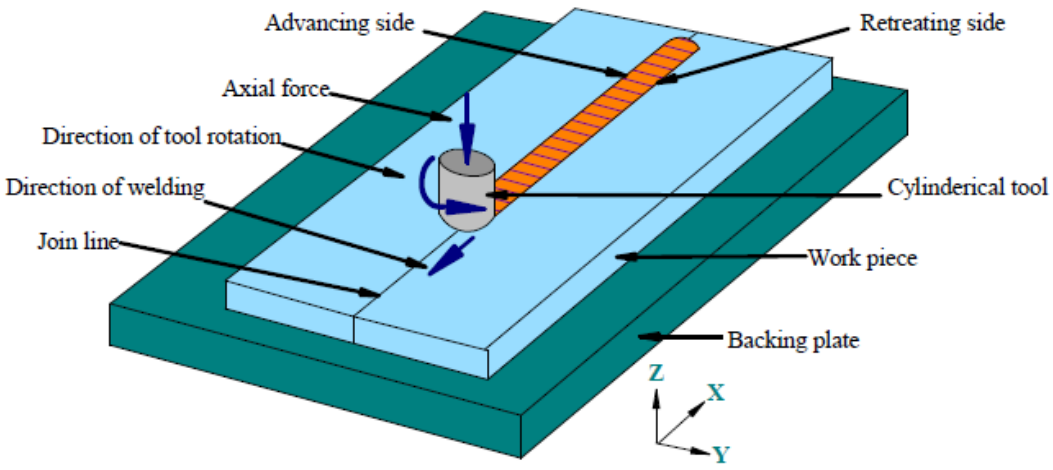

Fig. 2.9 Schematic diagram of Friction stir welding process.

2.3.1 FSW Process Overview

In *FSW* a non-consumable spinning cylindrical tool bit is plunged between two clamped plates. The rotation of the tool creates friction that heats the material to a plastic state. The rotating tool moves along the joint, it extrudes material in a distinctive flow pattern and forges the material in its wake. The resulting solid phase bond joins the two pieces into one. The terminology associated with *FSW* tool is depicted in *Fig. 2.10*.

The tool contributes to two main functions for welding: (*a*) heating of work piece, and (*b*) moving the material to produce the joint. As the heat is generated by friction between the tool and the work piece, plastic deformation of work piece takes place. The localized heating softens the material around the pin and the combination of tool rotation and translation leads to movement of material from the front of the pin to the back of the pin [31, 32, 33, 34, and 35]. As a result of this process, a joint is produced in solid state.

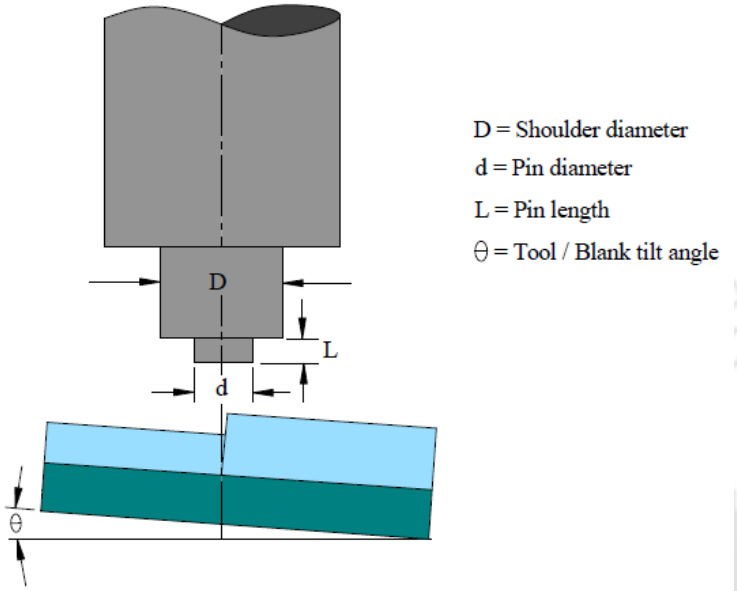

Fig. 2.10 FSW tool nomenclature.

Input variables include the tool rotation speed, welding speed, plunge depth, tilt angle, sideways tilt angle, shoulder geometry, shoulder features, probe geometry, and probe features such as Threads, Straights, Tapered, Squares and Triangles as shown in *Fig. 2.11*. Tool tilt angle is the angle between the tool axis and the normal to the surface of the sheets being welded.

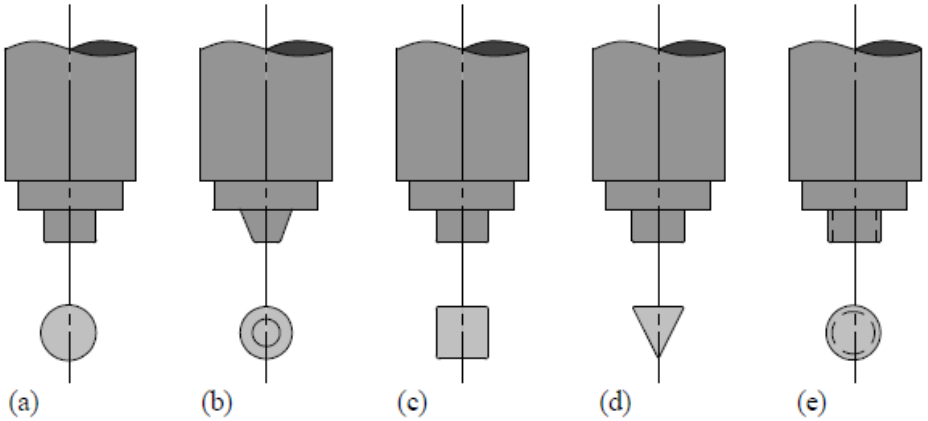

Fig. 2.11 Schematic diagram of different types of pin profile (a) Straight cylindrical, (b) Tapered cylindrical, (c) Square, (d) Triangle and (e) Threaded cylindrical.

For welding aluminium, magnesium, and copper which have low melting point the material of the tool is chosen harden steel such as *H13* and joining of higher melting point, higher hardness metals, such as steel, titanium, and nickel based super alloys, or to metal matrix composites (*MMC*s) are used [36].

The advancing-retreating sides of the weld line is a dominant characteristic of the process and greatly influences how heated, plasticized material is extruded around the tool probe before it is forged together behind the probe under significant shoulder pressure [37, 38]. The advancing side (*AS*) is the side where the velocity vectors of tool rotation and traverse direction are similar and the side where the velocity vectors are opposite being referred as retreating side (*RS*).

Normally, the microstructural investigation reveals that the friction stir weld blank has four different regions based on the microstructural features which are the region that is affected by heat only is known as the Heat affected zone (*HAZ*), which is shown in *Fig 2.12*. The region outside of this, which is unaffected by heat or deformation is the parent material or base metal.

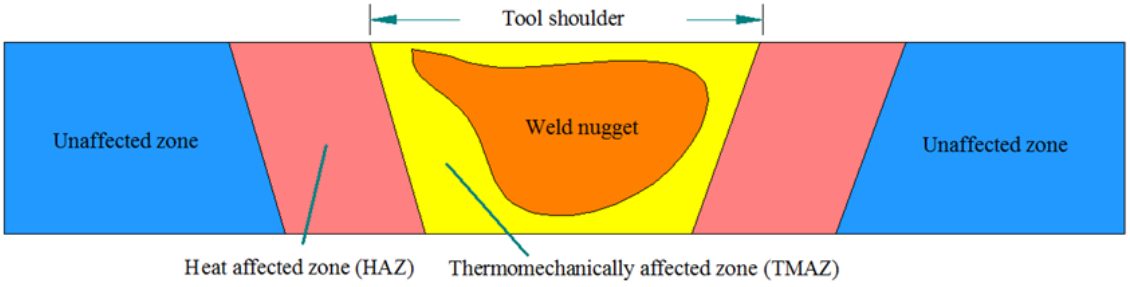

Fig. 2.12 Illustration of different microstructural regions in the transverse cross section of an FSWed material.

The region that is affected by both heat and plastic deformation is known as the Thermo-mechanically affected zone (*TMAZ*), which is defined by a trapezoid bounded by the diameter of the shoulder and the diameter of the probe at the weld root. In welds of certain materials, the *TMAZ* region may not be completely recrystallized. In this case, a special region within the *TMAZ* called the weld nugget, in which all material is recrystallized, is designated as nugget [39, 40, 41, 42, 43, & 44]. Another term for the 'nugget' that is often referred in the literature is the 'dynamically recrystallized zone'.

Apart from *FSW* joint types involve in pipe welds, corner welds, hemispherical welds, double *T*-joint welds and fillet welds, the most common types of joint configuration are the square butt joint, lap joint and the *T*-joint. The joints are shown in *Fig. 2.13*.

Compare to other weld technique *FSW* has the advantage of typically little joint preparation necessity.

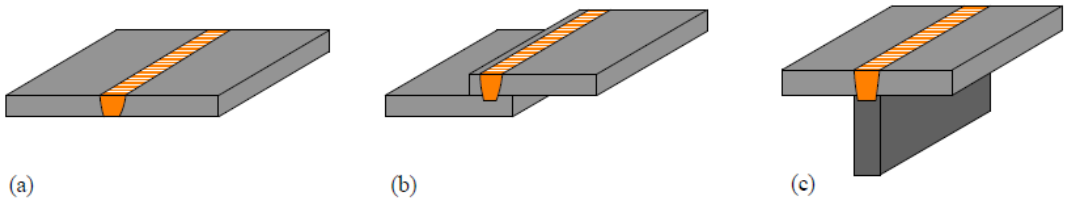

Fig. 2.13 Common friction stir welding joint configuration (a) square butt, (b) lap, and (c) tee joint.

2.3.2 FSW Applications

There are many commercial uses of *FSW* in Ship building, aerospace and land transport industries. *FSW* process is being used as an alternative to riveting and machining because of advantages like weight savings and reduced manufacturing costs. The process is generally used for welding:

a) Tailored blanks, e.g. welding of different sheet thicknesses or of different material combinations.
b) Space frames, e.g. welding of extruded tubes to nodes.
c) Window frames, pipeline fabrications, facade panels.
d) Structural component made from aluminium, copper, magnesium or titanium and,
e) Various ancillary components like fuel tanks, heat exchanger, wheel rims, engine and chassis cradles etc.

2.3.3 Advantages and Disadvantages of FSW

Generally, *FSW* is well-known for little or defect free welding process and is able to sustain large variations in process parameters. Many problems which are related with fusion welding such as porosity, solidification cracking, liquation cracking and solute redistribution are absent in *FSW*. The advantage of being a solid state welding process saves *FSW* from complications associated with cooling from liquid phase which occurs in fusion welding. There many potential advantages of *FSW* typical to non-conventional welding processes, the major of which are listed below:

a) Environment friendly due to absence of toxic fumes or the spatter of molten material.
b) No gas shielding or filler wire required for welding.
c) Energy efficient and can be automated on simple milling machines.
d) One tool made of tool steel can typically be used for over 1000 *m* of weld length in welding aluminium alloys.
e) Lower setup costs and running cost, with a versatility to operate in all positions (horizontal, vertical, etc.) due to the absent of weld pool.
f) Good mechanical properties in fatigue, tensile and bend tests with good weld appearance.
g) Can weld aluminium and copper with a thickness greater than 75 *mm* in one pass.

However, there are some disadvantages of the process which are listed below:

a) Leaves an exit hole when the tool is withdrawn after welding.
b) Initial cost of the machine is very high compared by fusion welding which is further escalated by the necessity to heavy duty clamping of the materials to counter the large tool force.
c) Welding is difficulty if the weld gap is greater than 10 % of material thickness.
d) Welding speeds are often slower than those of some fusion welding processes.
e) Flexibility limitation associated with welding of non-linear weld line profile and thickness variations through weld line.

2.4 Electromagnetic Sheet Forming

In late 1950's Wagner *et al.* [49] proposes the use of electromagnetic forming process for high velocity metal working in defence application, before that Harvey and Brower [50] had patented a system for metal forming based on electromagnetic forming principle in 1958. However, there is no significant commercial utilization of the process was achieved. At the same time Wood *et al.* [51] and Wilson *et al.* [13] submitted a report confirming that the increase in formability of metal with respect to high rate forming process. The phenomenon of increase in ductility of many metals at high velocity is also observed by Tobe*et al*. [52], Kobayashi *et al*. [53], Winter *et al*. [54] and, Daehn [21]. During the recent years there is an increase in interest in high speed forming of aluminium alloys (for light weight construction), which was accelerated by availability of high capacity and efficient equipment. There are numbers of formability studies done on commercial aluminum alloys by electromagnetic forming process which has been reported by Balanethiram*et al*. [7, 8], Takatsu *et al.* [55], Wiemar [25], Daehn *et al.* [56], Jablonski *et al.* [57] and Seth *et al.* [58]. Daehn *et al.* [56] examined the generation of large through thickness compressive stresses in the sheet termed as inertial ironing when the sheet impact with the die wall at high velocity. Hu *et al*. [59] studied the role of inertial effect during high speed forming which enhances the metal formability. To predict the magnetic pressure distribution Hassani *et al.* [60] designed different types of coil geometry for electromagnetic forming and also analytically compared it. Yudaev *et al*. [61] studied *EM* forming of flanges and stiffeners with 1.5 *mm* aluminum sheet and reported that forming limits were higher compared to quasi-static forming. Vohnout [62] combined quasi-static process and *EM* forming and concluded that the combined process yielded increased formability compared to a quasi-static process. Oliveira *et al*. [63] reported experiments and numerical analysis to compare free forming and cavity die forming by constructing forming limit diagrams.

With the help of conical die Imbert *et al.* [64] found that formability improved over free forming due to tool sheet interaction and combined effect of high hydrostatic stresses, high strain rates and non-linear strain paths. Padmanabhan *et al.* [65] studied the relation between wrinkling of the sheet and magnitude of magnetic pressure during EM forming and found out an inverse relation. Ning Li *et al.* [66] confirmed that conventional forming is governed by planar slip mechanism while for electromagnetic forming it is cellular wavy slip mechanism. Kamal *et al.* [67] performed a micro-embossing in a case with the help a two stage EM forming process. Golowin *et al.* [68] conceived a uniform actuator for *EM* forming

process for coining operations. Noh *et al.* [69] successfully achieved a desired shape by using two step *EMF* process involving the use of two coils and a middle-block die. Li *et al*. [70] analysed the formability of a low conductive metal sheet by electromagnetic forming process by employing a new method to generate data for the forming limit diagram. Recently Cui *et al*. [71] found that for a given discharge both the sheet thickness and current damping exponent plays an important role in achieving the optimum current frequency.

A comprehensive review of electromagnetic forming process was reported by Mamalis *et al.* [72] and Psyk *et al*. [73]. They discussed the process principle, research works and latest development with applications.

2.5 History of Tailor Welded Blank

The use of Tailor welded blanks (*TWB*) technology date goes back to 1980s; because of the several advantages, it provides the automobile and aircraft industries had a particular interest in the technology. The first experimental use of *LASER* welded blanks for a car part was done by Rover Swindon processing facility in 1982 according to Rooks [74]. The practical use of the technology in actual production car was used in 1985 for the production of under-body for the *Audi 100* car model. Kusuda *et al.* [75] mentioned the use of *TWB* by Toyota Motor Corporation in Japan since 1985 implying the emergences of the technology in Europe, Japan and United states almost at the same time. The use of aluminium *TWB* is more recent as generally steel alloys were used a common material in automotive industry. Merklein *et al.* [76] did an in-depth review on *TWB* production, applications and evaluation. The welding methods used were Laser Beam Welding (*LBW*) and mash seam welding in which CO_2 and *Nd:YAG* laser welding accounts for almost *99%* of all *TWB* application according to Montgomery *et al.* [77]. The other welding techniques are friction stir welding, electron-beam welding, and induction welding which are commonly for *TWBs* [78].In *TWB* technology laser beam welding is prevailing joining method for steel alloys while friction stir welding technique is often used for aluminium alloys. Due to weight advantages of aluminium alloy over steel alloys there is increase use and study of aluminium *TWB* in recent year [79]. Among the aluminium alloys, 5xxx and 6xxx series have large applicability in the automotive industry so preferred choice of material in studies. Zhao *et al.* [80] listed various problems and difficulties in laser welding of 5xxx, 6xxx and some 2xxx series automotive aluminium alloys such as alloying element vaporization, changed structural properties in welded blanks and various defects associated in laser welding of theses alloys.

Cao *et al.* [81, 82] presented a complete overview of laser welding of wrought aluminium alloys related to processes, parameters and metallurgical issues. Daeyong *et al.* [83] stated that there are several difficulties in producing aluminium alloy *TWB* because of their lower formability and less familiar weld-ability requirements.

Since the emergence of *TWB* technology in 1980s, it has attracted a much attention from the research community that results in rapid progress and vast publication in this field. The attention is shifting to friction stir welding technique for joining difficult to weld aluminium *TWB* over fusion based welding processes. Staud *et al.* [84] accordingly reported the advantages of friction stir welding technique in joining aluminium alloys over laser welding process. Taban and Kaluc [85] found superior mechanical strength by *FSW* process when compared between conventional welding processes like *MIG* and *TIG* for aluminium alloy 5086-*H32*. Similarly, Malarvizhi and Balasubramanium [86] reported a superior tensile property for *AA* 2219 alloy joint by *FSW* process among *GTAW, EBW,* and *FSW*. The following part of literature review will be more related to friction stir welding of aluminium alloys specially 5*xxx* and 6*xxx* series.

2.6 Friction Stir Welding of thin Sheets

Friction Stir Welding (*FSW*) was invented by Thomas et al. at *TWI Ltd* in 1991 [87] which overcomes many of the problems associated with fusion welding techniques such a shrinkage, solidification cracking and porosity. More importantly, it can weld alloys that are difficult or impossible to weld using fusion welding techniques. *FSW* is a solid-state process which produces welds of high quality in difficult to weld materials such as aluminium and is fast becoming the process of choice for manufacturing lightweight transport structures such as boats, trains and aeroplanes. The elevated temperature during operation generally stay below 500^0 *C*, which is below the melting temperature of aluminium alloys ($\approx 660.3^0$ *C*), as reported by Tang *et al.* [88], Mahoney *et al.* [89] and, Reynolds *et al.* [90]. A more comprehensive overview of research and progress of friction stir welding and processing is reported by Mishra *et al.* [33].

2.6.1 Process Principle

A distinguish feature about *FSW* process is that in the weld region heat generated is aided by the movement of material in plastic state with the help of a plunge tool [91]. *FSW* process involves interaction of various complex thermo-mechanical phenomena occurring at the same time. This thermo-mechanical phenomenon is further affected by the process

parameters like tool geometry and welding parameters. The interactions affect the material flow and plastic deformation, heating and cooling rates, quality of joint and dynamic recrystallization [33, 34, 83, and 92]. The tool design effects heat generation, material low and, thrust required. The function of tool shoulder is to generate enough heat and to maintain the plasticized material to stay within the work piece [93, 94]. According to Mishra *et al.* [33] a FSW tool should have following desirable properties: (i) maintain optimum welding force, (ii) facilitate easier plastic flow of material, (iii) maximum interface between the tool pin and, (iv) plasticized material for more pressure and heat generation and enable downward auguring effect. The welding parameters include (i) tool rotational speed and (ii) weld speed along the join line, which have a major influence on the weld quality [95]. The rotation of the tool helps in stirring and mixing of the plasticized material below the tool shoulder while the traverse motion of the tool moves the stirred material from the front to the back of the pin. The rate of stirred material increases the dislocation density at the weld region and the amount of grain surface and grain edge per unit volume [96].

In addition to the tool rotational speed and traverse speed, important process parameter is tool tilt angle. An optimum tool tilt angle is required to ensures that the tool shoulder hold the stirred material and moves it efficiently front to the back of the tool pin [37]. The influence of tool design, welding parameters and, microstructure and properties of weld joints have been extensively reviewed by McClure *et al.* [97] and Mishra *et al.* [33].

Weld joint in *FSW* is obtained by instance extrusion and forging of the material at high strain rates. Jata*et al.* [98] found out deformation strain rate by using a correlation between grain-size and *Zener- Holloman* parameter, they estimated the value in the order of 10 s^{-1}. And Masaki *et al.* [99] approximate the effective strain rates in the range of 2-3 $s^{-1}$by using plane- strain compression test. During instance extrusion of the material, a mixture of recrystallization phenomena and recovery of grain structure takes place in the weld zone [100]. The heat generated during extrusion is the resultant of shear stress and the velocity of the work-piece material that had struck to the tool as it moves [101]. Aluminium alloys are classified into two groups, heat-treatable (precipitation- hardenable) alloys and non- heat treatable (solid-solution-hardened) alloys. Aluminium alloys 2 *xxx*, 6 *xxx*, and 7 *xxx* series are heat treatable while 1 *xxx*, 3 *xxx*, 4 *xxx*, and 5 *xxx* series are not-heat treatable. The two groups show different hardness characteristics at the weld region. A heat treatable or age hardenable *AA* 6082 alloy shows minimum hardness in the heat affected zone of the weld region while non-heat treatable *AA* 5083 alloy shows uniform hardness across the weld [102]. Many studies on the mechanical properties of *FSW* joints of heat-treatable aluminium

alloys were done in the past. Luckwood *et al.* [103] studied mechanical and microstructure properties along with simulation model of the *FSWed AA* 2024 blanks. Sutton *et al.* [104] reported the residual stress and microstructure properties associated with *FSW* butt joint of *AA* 2024 *T3* alloy. While Genevois *et al.* [105] examined the precipitation phenomena of *FSWed AA* 2024 aluminium alloy. The influence of local heat input on the hardness of stir zone of *FSWed AA* 2024-T3 aluminium alloy was studied by Fu *et al.* [108]. Zhang *et al.* [109] investigated the effect of water-cooling on microstructure properties of *FSWed AA* 2014 alloy. *AA* 2195 aluminium alloy was butt welded by Fonda *et al.* [110] to study the grain refinement and precipitation during *FSW* process. Similarly Elangovan *et al.* [111] studied the influences of tool pin profile and welding speed during *FSWed* butt weld of *AA* 2219 alloy. Further, Jie *et al.* [112] investigated the mechanical properties of underwater *FSWed* joint of *AA* 2219 alloy. *FSWed AA* 2519 aluminium alloy was studied by Sree Sabari *et al.* [114] to investigate the influence of post weld heat treatment on tensile properties. Rodrigues *et al.* [115] studied the influence of welding parameters on the microstructural as well as on mechanical properties of *FSWed AA* 6016-*T4* alloy. Cavaliere *et al.* [116] and Cabibbo *et al.* [117] investigated the effect of welding parameters on mechanical and microstructure properties of *AA* 6056 weld joints. Many of researchers have focused on *AA* 6061 alloys for *FSW* studies, since this alloy is commonly used in automobile industries. Earliest report includes Shigematsu *et al.* [118] in which they used recycled *AA* 6061 aluminium plates manufactured by hot-extrusion of machined chips. A thermo-mechanical model was studied for *FSW* of *AA* 6061 alloys with adaptive boundary conditions by Soundararajan *et al.* [119]. Dinaharan *et al.* [120] and Heidarzadeh *et al.* [121] studied the influence of process parameters on the tensile strength of *FSWed AA* 6061 joints. Further, Trueba Jr. *et al.* [122] reported the effect of tool shoulder parameters on the tensile properties of *FSWed AA* 6061-*T6* blanks. Sato *et al.* [123] studied *FSWed* joint of *AA* 6063 alloys they investigated the distribution of tensile property at the weld joint. While Imam *et al.* [124] studied the effect of post weld natural-aging on the tensile and hardness properties of the *FSWed* joint of *AA* 6063.Cavaliere*et al.*[125] and scialpi *et al.* [126] reported the influence of welding parameters on microstructure and mechanical properties of *FSWed AA* 6082 weld joints. A study on formability of *FSWed* blanks were done by Kim *et al.* [127] with respect to joining direction for *AA* 6111-T4 aluminium alloy. Gaafer *et al.* [128] friction stir welded *AA* 7020-O aluminium plates to study the microstructural and mechanical properties of the weld joints. Through *FSW* of *AA* 7050 aluminium alloy plates London *et al.* [129] studied the material flow characteristics and temperature distribution

pattern in the weld joint. Working on the material Rebecca *et al.* [130] investigated the effects of multi pass *FSW* on weld joint properties. Further, Fu *et al.* [131] reported an improvement in weld quality and temperature distribution during butt joining of *AA* 7050 aluminium blanks by submerged *FSW* process. Rhodes *et al.* [132] and Fratini *et al.* [133] studied the microstructure behaviour of *AA* 7075 alloy during *FSW*. While Rajakumar *et al.* [134] worked on optimizing the *FSW* process parameters to obtain a maximum tensile strength for *FSWed AA* 7075 joints.

In the case non-heat-treatable alloys such as *AA* 1050 works has been reported by Liu *et al.* [135] on the mechanical properties of the joint made by *FSW*. While Murr *et al.* [136] reported on *FSW* of *AA* 1100 alloy analyzing dynamic recrystallization at the joint. The common 5 series alloys used in industries like *AA* 5052 were also given much interest by many researchers. Kwon *et al.* [137] reported a work on *FSW* of *AA* 5052 alloy plates. While Sato *et al.* [138] analyzed the post weld formability of *FSWed AA* 5052 blanks. Further Moshwan *et al.* [139] discussed the effect of tool rotational speed on the microstructure and mechanical properties of *FSWed* joint of *AA* 5052-O alloy. Peel *et al.* [140] and Hirata *et al.* [141] studied the influence of *FSW* process parameters on the residual stresses in *AA* 5083 alloy. While James *et al.* [142] analyzed the relationship between process mechanisms and crack paths in *FSWed* blanks of *AA* 5083-*H321* and *AA*5383-*H321* aluminium alloys. *FSW* of *AA* 5086 aluminium alloy was studied by Etter *et al.* [143] they analyzed the mechanical properties of the joint obtained. The welding defects associated with *FSW* of *AA* 5456 alloy were investigated by Chen *et al.* [144]. The post weld corrosion along with microstructural and mechanical properties was investigated by Fonda *et al.* [145].

The common defects associated with FSW process is porosity and surface defects. Crawford *et al.* [146] observed initiation and enlarging of wormholes near the bottom of the weld if the traverse speed of the tool is increases while keeping the rotational speed constant. The reason is inadequate material flow towards the bottom of the weld. The intensity of defects increases with the increase in traverse speed to rotational speed ratio reported by Liu *et al.* [147], Long *et al.* [148], and Leal *et al.* [149], for the same material and tool geometry.

2.6.2 Work Done on FSW of Dissimilar Aluminium Alloys

FSW of dissimilar alloys is quite difficult to weld compared to welding similar aluminium alloys. Much care and precaution should be taken to weld dissimilar aluminium alloys since

different aluminium alloys have distinct deformation behavior at high temperature and high pressure. The location of the materials with respect to retreating or advancing position during *FSW* can have a significant effect on the joint quality as analyzed by Lee *et al.* [150].

Ahmed *et al.* [151] identified and reported the optimum levels of process parameters required for welding thin sheets of *AA* 5052-*H32* and *AA* 5754-*H22* by using Taguchi grey based method. They found out effect of welding speed almost was insignificant on ultimate tensile strength and fracture strain. Sivachidambaram *et al.* [152] reported the influence of *FSW* tool speed variables for joining *AA* 7075 to *AA* 5383 and found tool rotation speed of 700 *rpm* and traverse speed of 40 *mm/min* for optimum weld quality. The study on dissimilar *FSW* of *AA* 2219-*T87* to *AA* 5083-*H321* is done by Dilip *et al.* [153] and reported the microstructures, hardness and tensile properties of the joint, claiming joint efficiency of 90 %. Guo *et al.* [154] analyzed the magnesium concentration and *B4C* particle distribution in an *FSWed* dissimilar *AA* 1100-*B4CMMC* and *AA* 6063 aluminium alloy. They reported a uniform material mixing and seamless bonding around the interface between the *Al-B4C MMC* and the *AA* 6063 alloy during *FSW*. Sundaram *et al.* [155] reported the *FSW* of *AA* 2024-*T6* to *AA* 5083-*H321* using various pin profiles and observed that the increase in the tool axial force increases the tensile strength of the welded joints with an optimum tool rotational speed value. Cavaliere *et al.* [156] successfully studied the mechanical and microstructural properties and fatigue endurance curves of dissimilar aluminum sheets of *AA* 2024 and *AA* 7075 that were joined by *FSW*. Similarly Muruganandam *et al.* [157] *FSWed* the dissimilar *AA* 2024 and *AA* 7075 aluminum alloys, and reported that the welding the process led to recrystallized grain structure and precipitates distribution in weld nugget zone.

FSW of aluminium alloy *AA* 6082 to *AA* 2024 has been carried out by Cavaliere *et al.* [158] to study the mechanical and microstructural behaviour. They found out that by keeping the *AA* 6082 on the advancing side optimum tensile and fatigue properties for the joints are achieved, with a tool traverse speed of 115 *mm/min*. To investigate the peening effect on the residual stresses of dissimilar *AA* 2195 and *AA* 7075 welded joint. Hatamleh and DeWald [159] produced the welds. They found higher values of tensile stresses in the mid-thickness on the laser peened samples compared to *FSWed* samples. Rodriguez *et al.* [160] successfully welded *AA* 6061 to *AA* 7050 by *FSW* process and observed that the micro-hardness at the weld nugget is in-depended of tool rotational speed while level of materials intermixing at the stir zone depends on the tool rotational speed.

Ghosh *et al* [161] examined the effect of *FSW* parameters on the mechanical properties of dissimilar *FSWed A*356 and *AA* 6061 aluminum alloys. They concluded that welds produced at the lowest tool rotational and traversing speed exhibited superior mechanical properties. Further they observed that the interface microstructure within the weld nugget is dominated by the retreating side alloy. Kasman *et al*. [162] joined *AA* 5754 to *AA* 7075 aluminum alloys under different tool rotation and traversing speeds. They reported that the strength of the joints decreases with increasing welding speed or tool rotational rate. Further, the hardness values of the weld zones were found to be varying according to the welding speed and the tool rotational speed. Da Silva *et al.* [163] studied the microstructure and mechanical properties as well as the material flow behavior in *FSWed* dissimilar 2024-*T3* and 7075-*T6* joints. They observed that the lowest hardness value was at *HAZ* of 2024-*T3* which was about 88 % of the base material of the same and subsequently occurrence of failure at these region during tensile testing. Amancio-Filho *et al.* [164] reported an optimized value of the traverse speed and the tool rotation speed for *FSW* of dissimilar *AA* 2024-*T351* and *AA* 6056-*T4* aluminium alloys while keeping the axial force and the tool geometry constant. Koilraj *et al.* [165] conducted *FSW* of dissimilar *AA* 2219 and *AA* 5083 aluminium alloys and obtained optimized FSW process parameters. The optimum values of the rotational speed, transverse speed, and D/d ratio are 700 *rpm*, 15 *mm/min* and 3 respectively.

An artificial neural network (*ANN*) model was developed by Shojaeefard *et al.* [166] to simulate the correlation between the applied *FSW* parameters with resultant mechanical properties of the *FSW* of *AA* 7075-*O* to *AA* 5083-*O* aluminium alloys. They found that a good correlation exists between the predicted data obtained from an *ANN* model and the obtained results. Steuwer *et al.* [167] have studied *FSW* between *AA* 5083 and *AA* 6082, they reported that the tool rotation speed has a substantially larger influence than the transverse speed on the mechanical properties and the residual stresses in the weld joints. Gan *et al*. [168] investigated hardness and tensile properties of dissimilar Friction Stir Welded (*FSWed) AA* 5083-*H18* and *AA* 6111-*T4* alloys and found that the hardness of the weld zones in *AA* 6111 alloy is more than that of the *AA*5083-*H18* alloy. Gungor *et al.* [169] investigated the microstructure and mechanical properties of *FSWed* dissimilar *AA* 5083-*H111* to *AA* 6082-*T651* aluminium alloys. They found that defect-free structure along with long fatigue life and good weld strength could be obtained at low tool speed.

Leitao *et al.* [170] studied the influence of high temperature plastic behaviour of *AA* 5083-*H111* and *AA* 6082-*T6* during *FSW*. They concluded that *AA* 5083 has very poor weldability while *AA* 6082 displayed a good weldability, under same welding conditions. Aluminium

alloys of same series but different grade namely *AA* 6082-*T6* and *AA* 6061-*T6* were *FSWed* together by Moreira *et al.* [171]. They observed that failure occurs at weld zone edge which has minimum value of hardness reading. Aval *et al.* [172] studied the microstructures and mechanical properties of similar and dissimilar *FSW* of *AA* 5086-*O* and *AA* 6061-*T6*. They observed that finer grain structure was achieved in weld nugget of *AA* 6061 compared to *AA* 5086 but grain refinement was obtained in both the cases. Palanivel *et al.*[173] investigated the influence of tool rotational speed and pin profile on the microstructure and strength of the dissimilar *FSWed* AA5083-*H111* to *AA* 6351-*T6* aluminium alloys. According to their observation, the rotational speed and pin profile directly affect the strength of the joints and grain structure. Hong *et al.* [174] investigated the effect of the location of base materials during *FSW* of dissimilar *AA* 5052-*H32* and *AA* 6061-*T6* aluminium alloys. They concluded that the elongation at fracture, yield strength and tensile strength are more when *AA* 6061 were kept in advancing side. Similarly, Park *et al.* [175] studied the effect of base material location on microstructure character during joining of *AA* 5052 and *AA* 6062-*T6* by *FSW* process. They reported that the materials were more uniformly mixed when *AA* 5052 were kept in advancing side and the lowest value of microhardness were observed at *HAZ* of *AA* 5052 aluminium side.

2.6.3 Forming of FSWed Aluminium Blanks

Aluminum alloys are difficult to form by conventional forming method because of their lower formability characteristics [176]. However, several investigations have been performed on the formability of aluminium alloy *TWBs* by conventional forming process, giving us some useful insight into the formability characteristics of *FSWed* sheets. Sato *et al.*[177] and Hirata *et al.*[178 and 179] investigated the relationship between formability and microstructure of *FSWed* blanks of *AA* 5052 and *AA* 5083 respectively. They reported that microstructure at the stir zone having large grain size and low density of dislocations plays an important role on the joint's fracture limit strain. Similarly, Kang *et al.* [180] studied the formability behavior of *FSWed AA* 5052-*H32* sheets and found relation between obtained microstructure at weld zone with formability. They stated finer grain structure gives more strength to the joints. While Leitao *et al.* [181] investigated the influence of mechanical properties of the join with the formability; they reported that the formability of *FSWed* aluminium alloy *TWBs* are affected the type of mismatch in mechanical properties between the weld and the base materials.

Miles *et al.* [182] studied the formability of *FSWed* similar and dissimilar *TWBs* of *AA* 5754-*O*, *AA* 5182-*O*, and *AA* 6022-*T4* aluminium alloys. They found that weld combination of *AA* 5754- *AA* 5182 gives better formability compared to base materials. While, the combination of *AA* 5754- *AA* 6022 alloys have lower formability compared to base materials. In another study [183], they have reported that the *FSWed* sheets joints had more formability than those by gas tungsten arc welding. Kim *et al.* [184] investigated the effect of material direction combination on the formability of *FSWed* aluminium alloy *AA* 6111-T4 alloy of 1.5 *mm* thickness, by simple tension tests, hemisphere dome stretching, and cylindrical cup drawing tests. Leitao *et al.* [185] found that the crack initiation at the weld blanks could happen due to the presence of small defects at the bottom of the weld zone during dissimilar friction stir welding. Lee *et al.* [186] investigated the formability behavior of *FSWed* blanks of *AA* 6111-*T4*, *AA* 5083-*H18*, *AA* 5083-*O*, and *DP* 590 dual phase steel sheets by hemispherical dome stretching (*HDS*) tests.

Rodrigues *et al.* [187] performed formability test of *FSWed* thin sheets of *AA* 6016-*T4* with axisymmetric cups through deep drawing process. Saunders and Wagoner [188] through their experiment showed the dependence of *TWB* formability on weld line orientation. Buste *et al.* [189] investigated numerically and experimentally the influence of weld line movement on strain distribution in aluminium *TWBs*. Kusuda *et al.*[75] investigated the influence of weld orientation on failure pattern when aluminium alloys *TWBs* are deformed by spherical punch stretch test. They found that fracture occur at weld line for parallel orientation while for perpendicular weld orientation failure occur at the base material. Similarly, Shakeri *et al.* [190] observed failure of base material occurs when the loading direction is perpendicular to the weld line. Kim *et al.* [191] have also studied the effect of weld line movement on the formability of welded blanks. They concluded that the optimum formability is obtained when weld direction is parallel to the rolling direction. Parente *et al.* [192] investigated the formability performance of *FSWed* blanks of *AA* 5182 to *AA* 6061 by obtaining forming limit curves through *Nakajima* test. The results showed influence of weld line orientation on the formability along with decrease in formability compared to base materials. The thickness variation of *TWBs* also affects significantly on the formability evaluation. According to Cayssials *et al.* [193] the formability of welded blanks decreases as the thickness ratio between the base blanks increases. Similarly Chan *et al.* [194] also viewed the same outcome and stated that formability of dissimilar thickness *TWBs* is mainly depend on the thickness of the thinner blank. Ramulu *et al.* [195] studied the influence of shoulder diameter and plunge depth on the formability of *FSWed AA* 6061-T6 sheets

through limit dome height test and found that with increase in shoulder diameter and plunge depth the formability increases.

2.7 Conclusions

The presented literature review shows electromagnetic forming generated interest in the initial years after being invented in the late 1950s. Several publications originate during that period.

Important fundamental research work considering the process analysis and the analytical calculation of significant parameters, which is still relevant today, was already published at that time. However, numerous papers are limited to describing the process principle and listing potential process advantages showing high expectations, which were made on the new technology. Different applications ranging from the forming of very special and highly demanding parts in a small number of items to series production with large lot sizes and high production rates are reported.

Since the late 1990s a resurgence of electromagnetic forming in the scientific and industrial interest can be observed. This effect is related to the increasing importance of implementing lightweight construction concepts. Lightweight construction concepts are contributed by material choice and special design strategies as well. To reduce product weight e.g. in a vehicle, the most suitable material for each separate component has to be identified and applied. This results in an optimal mix of different materials, which need to be joined/connected to each other. However, modern lightweight materials typically offer a reduced formability compared to conventional steels.

Since electrically highly conductive materials as aluminum alloys are frequently involved in lightweight construction concepts, electromagnetic forming is a promising technology and consequently can be recognized as a right choice for normally difficult to form aluminium alloy.

When producing such components standard production concepts cannot be applied due to their limitation. With that innovative forming processes along with new joining processing strategies are required. Solid state welding technique is most suited for volatile metal like aluminium alloys. Friction stir welding process which was invented in early 1990s became popular within a short span of times. From the reviews it is learned that the welding parameters, including tool rotation rate, traverse speed, spindle tilt angle, and targetdepth,

are crucial to produce sound and defect-free weld. FSW results in significant temperature rise within and around the weld. A temperature rise of 400–500 ^{0}C has been recorded within the weld for aluminum alloys. Intense plastic deformation and temperature rise result in significant microstructural evolution within the weld, i.e., fine recrystallized grains of 0.1–18 mm, texture, precipitate dissolution and coarsening, and residual stress with a magnitude much lower than that in traditional fusion welding.

Three different microstructural zones have been identified in friction stir weld, i.e., nugget region experiencing intense plastic deformation and high-temperature exposure and characterized by fine and equiaxed recrystallized grains, thermo-mechanically affected region experiencing medium temperature and deformation and characterized by deformed and un-recrystallized grains, and heat-affected region experiencing only temperature and characterized by precipitate coarsening.

Compared to the traditional fusion welding, friction stir welding exhibits a considerable improvement in strength, ductility, fatigue and fracture toughness. Moreover, 80% of yield stress of the base material has been achieved in friction stir welded aluminum alloys with failure usually occurring within the heat-affected region, whereas overmatch has been observed for friction stir welded steel with failure location in the base material. Fatigue life of friction stir welds are lower than that of the base material, but substantially higher than that of laser welds and MIG welds. In addition to aluminum alloys, friction stir welding has been successfully used to join different grade materials and different thickness blanks.

From the detailed literature review it has been interpreted that there is an opportunity in the field of high speed forming of aluminium tailor welded blanks. Since no researcher till date has reported works done on this particular area where two non-conventional welding and forming process are combined together, therefore, this will be a challenging opportunity to achieve a new efficient production method.

Chapter 3

Experimental Procedure

3 Experimental Procedure

In this chapter the experimental setup and processes used to perform the experiment are described. Some of the experimental procedures and equipment details that are general to all are simply mentioned briefly.

In order to produce *TWB*s of aluminium alloys, thin sheet of *AA* 6061-*T6* and *AA* 5052-*H32* aluminium alloys were considered. The thickness requirements of the sheets were 1 *mm* and 1.5 *mm* which were cut in to 200 *mm* × 100 *mm* dimension each before welding it together. The welding of aluminium alloys were done with *FSW* process initially with trial and error method for obtaining optimum process parameters for successful welding. The welded blanks were considered in combinations of different thickness and of different grade. The combinations were chosen between *AA* 6061 and *AA* 5052 alloys for different grade and for different thickness the selection were between 1.5 *mm* and 1 *mm*. The defect free *TWB*s were then analyzed for mechanical and microstructure properties. The formability experiments of the TWBs were done by both electromagnetic forming (high speed forming) and by conventional hydraulic press punch forming (quasi static forming). The formability experiments were quantified in terms of both limit dome height test and forming limit diagram.

3.1 Friction Stir Welding Machine

Welding of the blanks were performed with the help a modified column and knee type vertical milling machine of *KNUTCH* make (model no. X5036) as shown in *Fig. 3.1*. The maximum rotational spindle speed is 1500 *rpm* and the tool traverse speed ranges in *mm/min* are 22, 36, 63, 98, 132 and 200.

Fig. 3.1Modified FSW machine.

3.1.1 Fixture Work-piece

Aluminium alloy *AA* 5052-*H*32 and *AA* 6061-*T*6 were used to create tailor welded blanks of different thickness and of different grade. Each sheet with a dimension of 200 *mm* × 100 *mm* was butt welded in the rolling directions. A mild steel plate of 25 *mm* thickness was used as a bottom backing plate. The chemical compositions of each alloy are listed in *Table 3.1*.

Table 3.1Nominal chemical composition of the base materials (wt. %).

Alloy	Al	Cr	Cu	Fe	Mg	Mn	Si	Zn	other
AA 5052 *H*32	95.7-97.7	0.15 - 0.35	Max 0.1	Max 0.4	2.2 - 2.8	Max 0.1	Max 0.25	Max 0.1	Max 0.15
AA 6061 *T*6	95.8-98.6	0.04 - 0.35	0.15-0.04	Max 0.7	0.8 - 1.2	Max 0.15	0.4 - 0.8	Max 0.25	Max 0.15

The dimensions of the plunge tools used in the process are given in *Table 3.2*, two no. of cylindrical tools of material stainless steel (*SS*)-*H13* were used for the present *FSW* process (*Fig.3.2*). The diameter of the circular tool pins was made equal to the one third of the shoulder diameter size as per the suggestion of *Arora et al.* [196]. The diameters for tool pins were kept 3.25 *mm* and 4 *mm* for different tool shoulder 10 *mm* and 12 *mm* respectively (*Table 3.2*).

Table 3.2 Tool parameters.

Tool no.	Shoulder dia.(D) (mm)	Pin dia. (d) (mm)	Pin length (L) (mm)
1	10	3.5	0.7
2	12	4	1.2

A mild steel plate of 250 *mm* × 200 *mm* × 15 *mm* dimensions with a slotting of 230 *mm* × 30 *mm* at the centre was machined (*Fig. 3.2.*). The plate was used has an upper plate above the work sheets as a clamping arrangement in order to arrest all the degrees of freedom of the thin blank sheets for the present *FSW* fixture. With the absence of the said upper plate it was difficult to weld with present sheet thickness and the occurrence of defects like tearing along weld direction and crack due to bending was found to happen.

3.2 Formability Test Setup

To analysis the limits of formability for tailor welded blanks, limiting dome height or bulge height test technique have been widely used. The *Nakazima* and the *Marciniak* tests are two most common experimental tests which provide information on formability of sheet material. The main difference between these tests is the shape of the punch that is being used, like for *Nakazima* test shape is hemispherical while for *Marciniak* it is a flat shape.

Forming Limit Diagram (*FLD*) constituting Forming Limit Curve (*FLC*) provide information regarding process limitations in sheet metal forming and are used to assess the formability characteristics, particularly stamping behaviour of the concern blank. The *FLD* were constructed after the plastic deformation of the blank, its different regions were categorized into safe, critical,and failed zones, according to the state of strains obtained from deformed circles. The circles were printed on the surface of the sheet before deformation. The strains from deformed circles were calculated in terms of major and corresponding minor strains, which are then plotted along two mutually perpendicular principal strain axes.

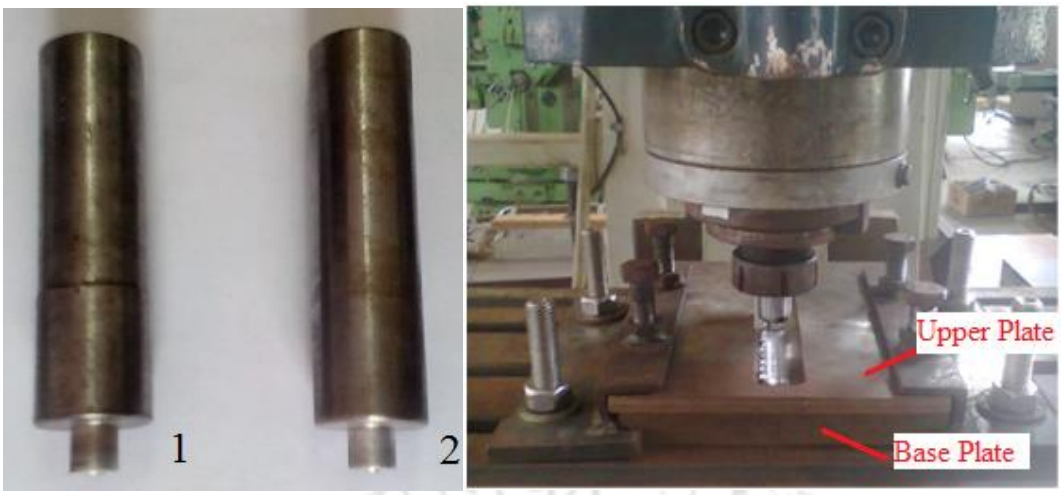

Fig. 3.2 Samples of the tools used & assembly of clamping fixture for FSW process.

The major strain (e_1) and minor strain (e_2) were determined by measuring changes of the principal directions l_f and w_f (*Fig. 3.3*) of the deformed circle with reference to the initial dimension, l_0 and w_o respectively by using the *Eqs.* (*3.1*) and (*3.2*).

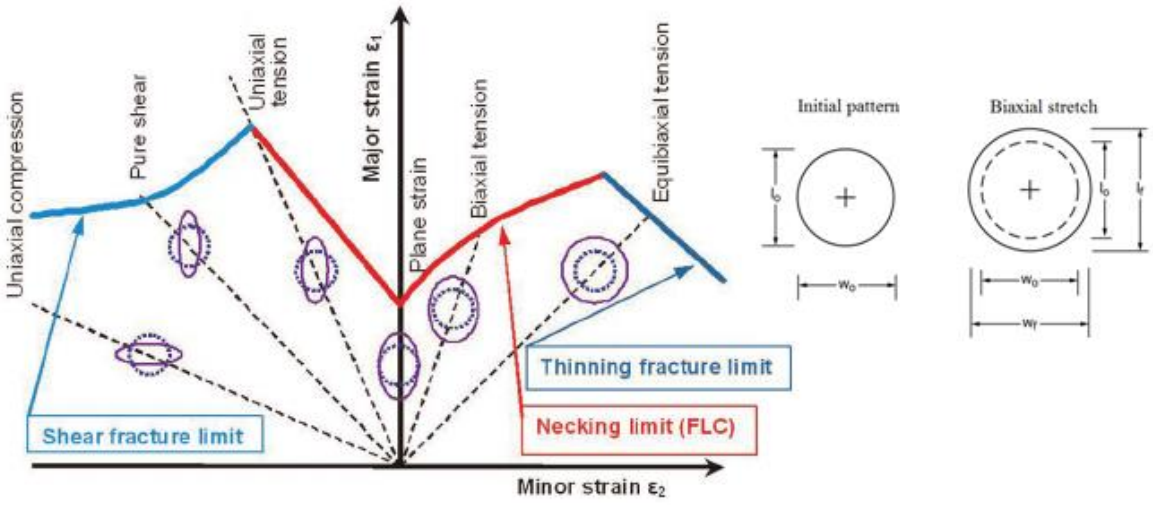

Fig. 3.3 Various deformation zone of FLD along with schematic of grid circles at initial and final stage of deformation.

$$\text{Major strain, } e_1\ (\%) = \frac{l_f - l_0}{l_0} \times 100 \qquad (3.1)$$

$$\text{Minor strain, } e_2\ (\%) = \frac{w_f - w_0}{w_0} \times 100 \qquad (3.2)$$

Where, *l* = length, *w* = width, *0* = original, and *f*= final.

The various zones of *FLD* from linear compression to equibiaxial tension are schematically represented in *Fig. 3.3*. The *FLD* of sheet in linear strain path is determined using tension

tests and stretch forming tests with a hemispherical punch. The *FLD* for negative minor strains are determined with notched tensile specimens of various widths.

FLDs are used during designing and manufacturing of a component as they provide information regarding formability behaviour of the blanks at different strain conditions. Another important application of *FLDs* is in numerical simulations of transformation processes, where the *FLC* of particular blanks represents characteristics material behaviour data for the forming simulations. Keeler *et al.* [197] first presented *FLD* concept for biaxial stretch test of metal. Goodwin [198] further developed the concept by adding different stress conditions in stretching of the blanks to generate negative minor strains. Hecker [199] later proposed a standardised process that requires different blank widths to develop different strains with the help of a limiting dome height test.

In our study, the *Nakazima* test [200] is selected for formability study due to its simplicity. High velocity uniaxial tension test for the specimen will be difficult to obtain by *EMF* process. The common apparatus for uniaxial high strain rate test is *Split-Hopkinson* pressure bar setup. Hence to construct the *FLC* of aluminium alloy formed at high velocity, we will focus on biaxial stretch zone of the *FLD*. The *Nakazima* test set-up is made of a hemispherical punch, a die, a blank-holder and a draw-bead that restrict the slippage of the blanks. In our case, the biaxial stretch forming tests were done using a hemispherical shaped punch with a diameter of 100 *mm*. The die, punch, and the blank holder used for the experiments are shown schematically in *Fig. 3.4*. The hollow die has an inner diameter of 108 *mm* and entry radius of 10 *mm*. A circular blank holder with a 145 *mm* draw bead diameter with 3.5 *mm* height was used to constraint metal movement near the flange area of the die. The blank holder ensures that the sheet metal exposed under the hollow die opening would only be deformed by the punch. The material for the punch tool was *AISI P20* tool steel and for die and blank holder, it was cast iron.

ASTM E2218 Standard test method [201] were followed for determining *FLC*s and for this purpose patterns of grid circles of diameter 2.5 *mm* were marked on the surface of the blanks by permanent ink printing process. Formability test for quasi-static process was done by a 50-ton hydraulic press and it was operated at a punch speed of 0.45 *mm/sec*. The punch load was stopped immediately after the initiation of the fracture. The measured strains points (major and minor strain) averaged from different specimen are connected to draw *FLD*. Similar approach and setup was used to draw *FLDs* of the TWBs for high velocity forming. Electromagnetic forming system was used for high velocity deformation of the *TWBs*.

3.3 Electromagnetic Forming System

The *EMF* system consists of two units, an *EMF* machine with current measurement system and a work-bench (*Fig. 3.5*). The *EMF* machine consists of capacitor banks, control unit and current measurement components. The work-bench is the unit where coil and die fixture is placed for experimentation. The fixture is consists of a coil tool, work-piece, die with clamping and blank holder plate. The fixture is connected to the current output channel of the *EMF* machine.

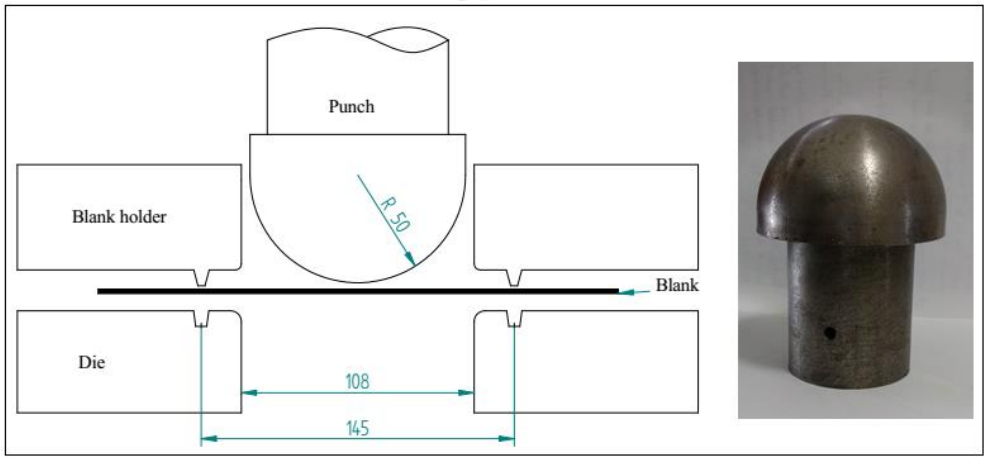

Fig. 3.4 Die and tool parameters for conventional LDH test with the image of actual punch used.

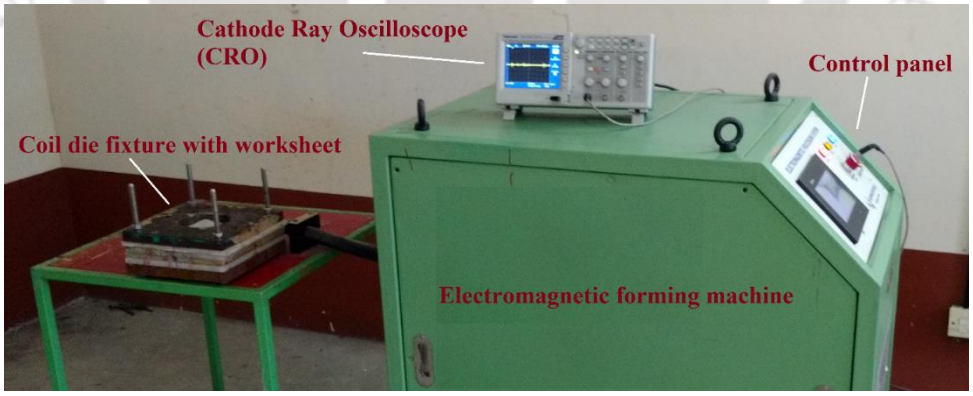

Fig. 3.5 The electromagnetic forming system.

3.3.1 Capacitor Bank

The *EMF* machine has a maximum energy storage capacity of 10 *kJ* at a voltage of 15 *kV* and it consists of two capacitor unit each with a capacitance of 45μF with a system inductance of 400 *nH*. The capacitors are charged by high voltage power supply. The control

system is integrated in the *EMF* machine, which is shown *Fig. 3.5*. The control panel consists of Graphical user interface (*GUI*) display, which enable to charge the capacitor up to a pre-determine voltage. Through the touch-sensitive switch of the *GUI* high voltage current is made to discharge from capacitor bank to the coil.

3.3.2 Measuring Unit

The measuring unit consist of an assembly of a Rogowski coil, an Intregrator and an Oscilloscope. The Rogowski coil and Intregrator are situated inside the machine while the Oscilloscope operates as external auxiliary equipment. The function of the Rogowski coil is to measure the voltage that is proportional to the rate of change of current passing through the conductor or coil. Further to convert the voltage proportional to the current, the integrator is used. The measured current is displayed in waveform by the oscilloscope, which is connected to the integrator output.

3.3.3 Actuator and Fixture

A six-turn spiral copper coil (*Fig. 3.6*) of 110 *mm* diameter was used as an actuator tool in *EM* forming process. The dimension of the coil along with complete fixture set up is shown in *Fig. 3.6*. The copper coil was engraved in a nylon cavity for strength and insulation. The cavity of the free-form die was open to the atmosphere eliminating the requirement to evacuate the die chamber (*Fig. 3.7*) and was of the same dimension as that of conventional forming test setup.

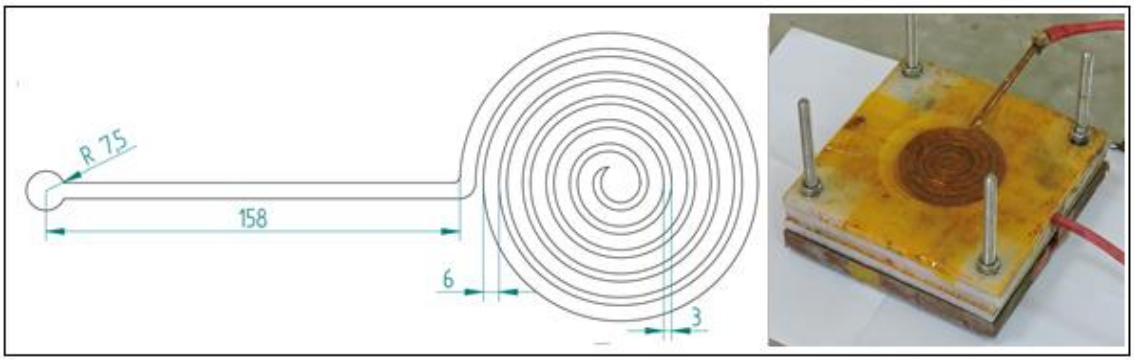

Fig. 3.6 Schematic diagram of the coil tool & the actual copper coil engraved in the nylon casing.

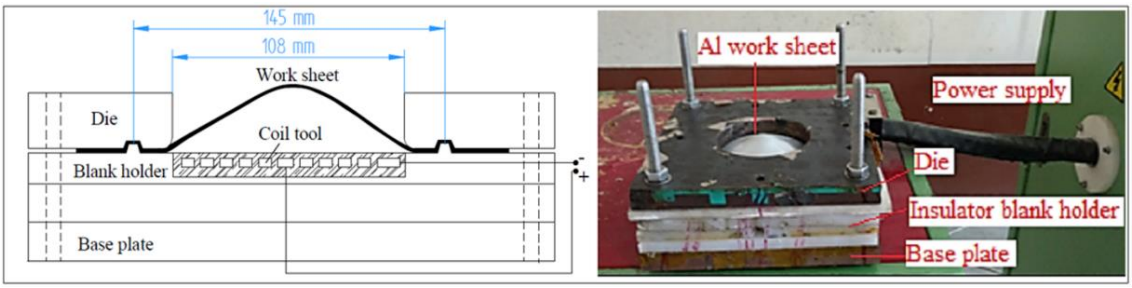

Fig. 3.7 Schematic of EMF fixture with actual EM forming setup.

For tensile test the friction stir welded samples were cut into sizes according to *ASTM E8M* standard specifications [202] and the weld line were kept in transverse direction.

Chapter 4

Friction Stir Welding of Aluminium Alloys

4 Friction Stir Welding of Aluminium Alloys

4.1 Friction Stir Welding of Dissimilar Grade of Aluminium Alloys AA 5052 with AA 6061

In this section, Friction stir welding (*FSW*) of *AA* 5052-*H32* to *AA* 6061-*T6* blanks were obtained for each thicknesses of 1 *mm* and 1.5 *mm* respectively. Generally, successful welding of aluminium thin sheets (below 2 *mm*) by *FSW* is quite difficult to obtain even though few researchers have studied *FSW* of less than 2 *mm* thin sheets [46, 47, 203, and 204]. The objective of the present work is to characterize the mechanical behaviour and microstructure properties. The comparison between dissimilar grade welded blanks of each thickness 1 *mm* to 1.5 *mm* has also been made.

4.1.1 Results and Discussions

AA 5052 to *AA* 6061 was welded for each blank thickness of 1 *mm* and 1.5 *mm* using tool no.1 and 2 respectively. The aluminium alloy *AA* 6061 was kept on advancing side of the tool path while *AA* 5052 was on retreating side. The tool spindle rotational speed was kept at 1500 *rpm* (maximum) for all the blanks and the traverse weld speed were varied to get successful welding. After a few trial successful welding were obtain at certain range of tool traverse speed. Nomenclature of final welded samples associated with the blank thickness and tool traverse speed combinations are given in *Table 4.1*. Mechanical and microstructure of the successful welded blanks are further analysis.

Table 4.1 Process parameters for each sample nos.

Sample nos.	Material Combination	Blank Thickness (mm)	FSW Tool Pin used (no.)	Tool Rotational Speed (rpm)	Tool Traverse Speed (mm/min)
1	*AA* 5052 &*AA*6061	1	1	1500	63
2	*AA* 5052 &*AA*6061	1	1	1500	98
3	*AA* 5052 &*AA*6061	1.5	2	1500	63
4	*AA* 5052 &*AA*6061	1.5	2	1500	98

4.1.1.1 Weld Bead Appearance

On visual inspection of the successful welded blanks it was found that the weld paths have visibly smooth surface without any macro defects (*Fig. 4.1*). However, there is a wavy distortion on the outer surface of the welded blanks due to the surface strain. This is due to the thermal stress generated from frictional heat between the tool and the blanks during *FSW* process. In addition, there is no notable change in the surface appearance of welded blanks at traverse speed of 63 *mm/min* and 98 *mm/min*. The average heights of flash formations along the edge of weld path were of around 1.5 *mm*, which were removed easily.

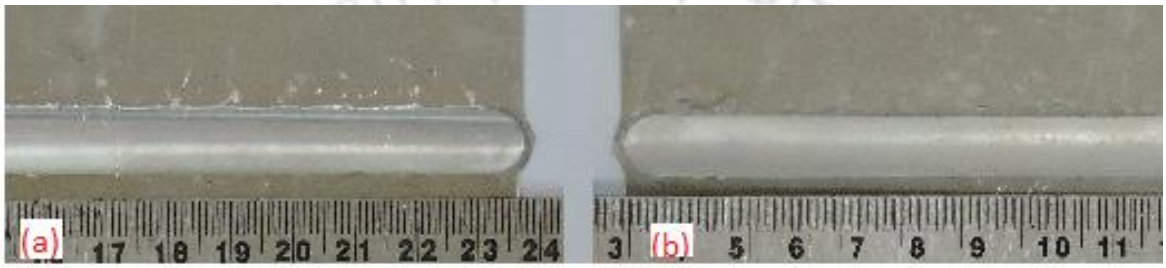

Fig. 4.1 Surface appearance of FSWed sample at tool traverse rate (a) 63 mm/min and (b) 98 mm/min.

4.1.1.2 Tensile Properties

To analyse weld strengths at varying tool traverse speeds with respect to similar blank thickness, comparison of tensile test results between *sample 1* and *sample 2*, and between *sample 3* and *sample 4* are done. All the tensile test samples fractured at weld zone near *AA* 5052 alloy (*Fig. 4.2*).

In *Fig. 4.3* we can see the Ultimate Tensile Strength (*UTS*) of *sample 1* (172.4 *MPa*) is almost equal to that of *sample 2* (170.5 *MPa*). Though the tensile stress at facture for both the samples is approximately similar (~150 *MPa*) the ductility of *sample 1* was found to be slightly more than that of *sample 2*. The elongation at break for *sample 1* is 1.26 *mm* which is 5.9 % more than that of *sample 2* (1.19 *mm*). Similarly, from *Fig. 4.4* which shows plotting of average tensile stress vs. strain of *sample 3* and *sample 4*, we can see that *UTS* of *sample 3* (210.4 *MPa*) is approximately equal to that of *sample 4* (208.7 *MPa*). The elongation at fracture for *sample 3* was 1.9 *mm* and for *sample 4* it was about 1.7 *mm*; this shows that *sample 3* has more ductility (11.8%) than that of *sample 4*. So, we can inference that specimens welded at lower welding speed shows better ductility.

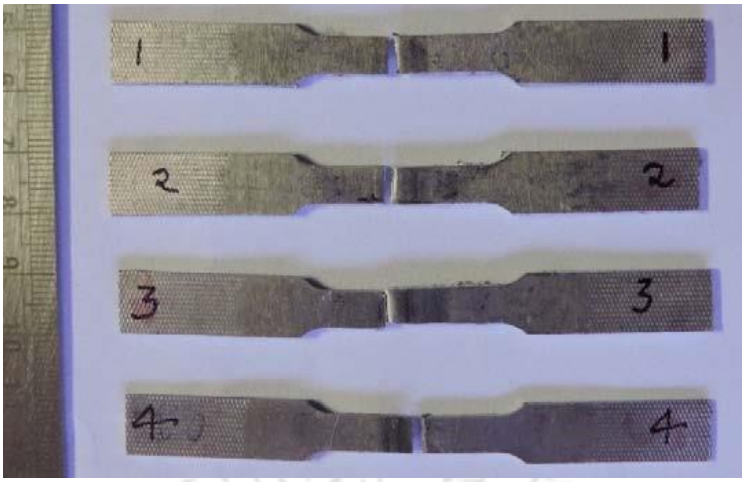

Fig. 4.2Tensile test specimens showing fracture at weld zone.

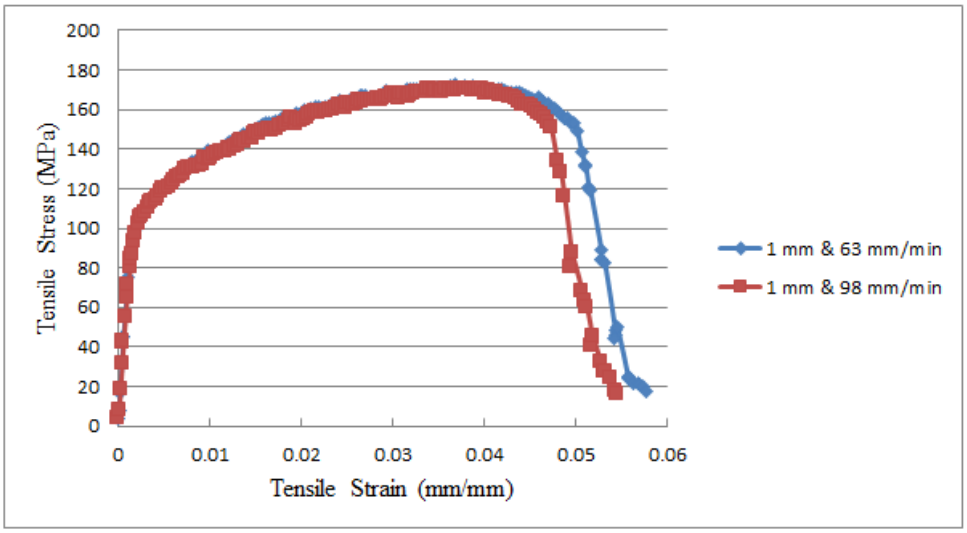

Fig. 4.3 Tensile test result of dissimilar grade welded blanks of 1 mm thickness.

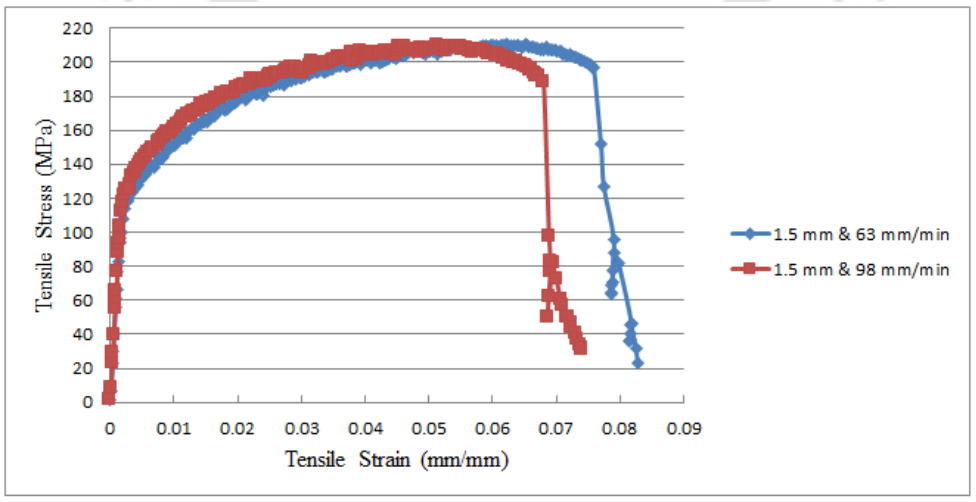

Fig. 4.4 Tensile test result of dissimilar grade welded blanks of 1.5 mm thickness.

Load vs. elongation (*Fig. 4.5*) data analysis of all the welded blanks depict that the thicker blanks, *sample 3*(1.5 *mm*) and *sample 4* (1.5 *mm*), have average higher load at fracture which is 58.55 % more than that of 1 *mm* thickness blanks (*sample 1* and *sample 2*). Similarly the average elongation is found to be 47 % more respectively.

The strength of base material is found to be higher than that of the welded samples as shown in *Fig. 4.6*, which explain the fracture at welded joint during tensile testing of the samples (*Fig. 4.2*). From *Table 4*, we can interpret that more the thickness of the blanks more will be the elongation even for welded blanks.

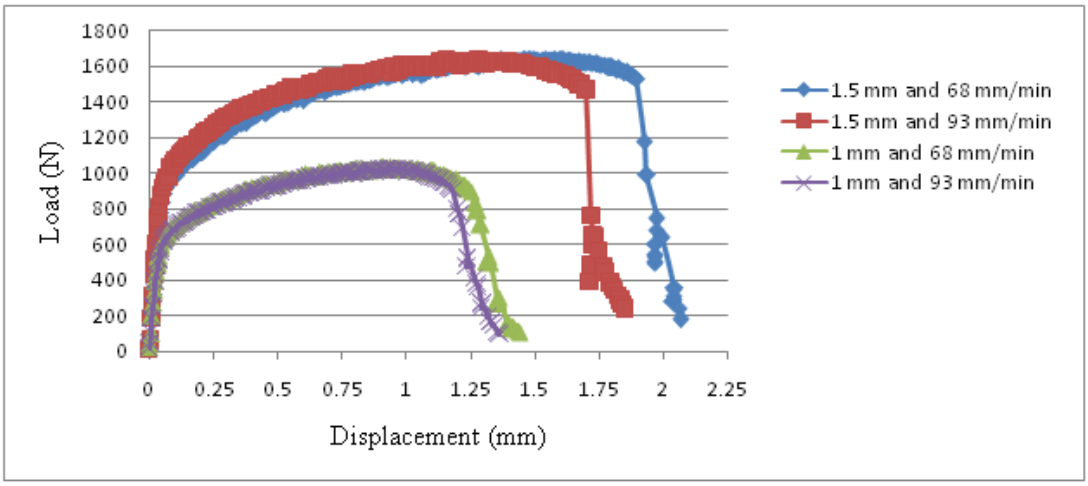

Fig. 4.5 Load vs. elongation plotting of samples 1, 2, 3 and 4.

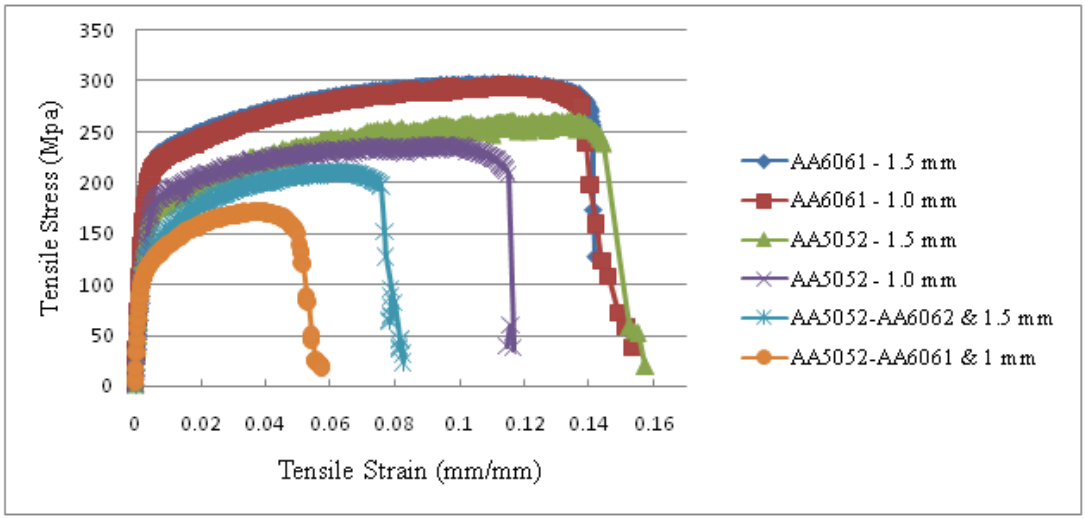

Fig. 4.6 Tensile stress vs. tensile strain plots of base materials and friction stirs welded samples.

Table 4.2 Mechanical properties of base material and friction stir welded samples.

Material	Thickness (mm)	Ultimate Tensile Strength (MPa)	Yield Strength (MPa)	Modulus of Elasticity (GPa)	Extension at Break (mm)
6061-*T6* (*Base*)	1	293.9	212.5	70.26	2.5
6061-*T6* (*Base*)	1.5	297.3	206.2	80.62	3.84
5052-*H32* (*Base*)	1	237.3	175.7	51.87	2.87
5052-*H32* (*Base*)	1.5	260.3	168	60.59	3.93
5052-6061 (*FSW*)	1	172.4	114.6	75.99	1.44
5052-6061 (*FSW*)	1.5	210.5	126.2	74.18	2.06

4.1.1.3 Hardness Properties

Micro hardness test for the welded blank samples were analysed along the perpendicular to the weld line. Micro-hardness distributions along the transverse cross-section of the welded zone for each sample are shown in *Fig. 4.7*. In the heat affected zone (*HAZ*) i.e. near the parent metal and tool shoulder edge junction the hardness values were found to be lowest. As *AA* 6061(*T6* tempered) being precipitation-hardened aluminium alloy, *FSW* creates a softer region at nugget zone than the corresponding base metal. Such phenomenon is due to the occurrence of heat treatment condition like over-ageing.

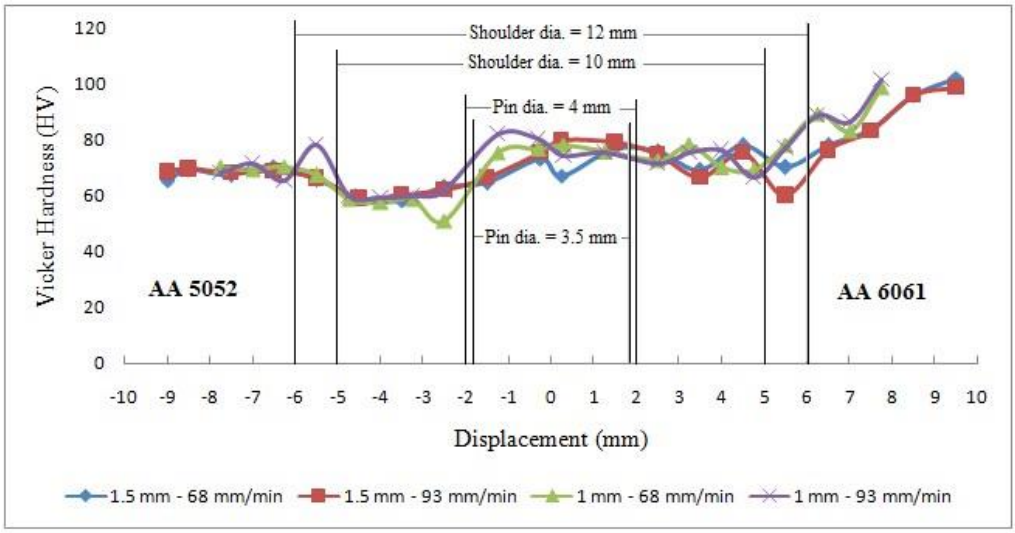

Fig. 4.7 Vickers micro hardness graph for friction stir welded samples.

McNelley *et al.* [205] suggested that the reason behind softening on *AA* 6061(*T6* tempered) side is due to the severe coarsening and dissolution of precipitates by the thermal effect of *FSW*. However, for *AA* 5052 *H32* the hardness in the nugget zone was slightly higher than that of the corresponding base material but lowest in *HAZ*. Park *et al.* [183] described the reason behind low hardness value at *HAZ* of *AA* 5052 side as annealing phenomena. However, the average hardness value at *HAZ* on *AA* 6061 side is more than that of *AA* 5052 side which had caused the failure of all tensile test samples on the *AA*5052 side.

4.1.1.4 Microstructural Analysis

Microstructure of the weld cross section was observed using an optical microscope and scanning electron microscope. No internal defects were found in the welded blanks. Microstructure image for 1.5 *mm* welded blank is shown in *Fig. 4.8* which shows no major defects such as porosity and worm holes. The grain structures found in the various welding zones of *FSWed* blank are shown in *Fig. 4.9*. The micrograph presented here consists of Base Metal (*BM*) (*a and f*), Thermo-Mechanically Affected Zone (*TMAZ*) (*b and e*) and Stir Zone (*SZ*) (*c and d*).

Fig. 4.8 Optical macrographs of the cross-section perpendicular to the tool traverse direction of FSW sample welded at 68 mm /min speed.

The *TMAZ* zone consists of both unmixed region and mechanically mixed region. In this region the flow of the grains on both the sides are found to be elongated towards *SZ* from the base metal, due to the stirring action of the tool pin. The thermo-mechanical effect of the tool pin affects the grains to get elongated near *SZ* which were plastically deformed. Thus, we obtain deformed grains in the *TMAZ*. The *TMAZ* of advancing side of *AA* 6061 alloy shows more intense distribution of materials around the tool compared to that of retreating side of *AA* 5052. Dynamic recrystallization of grains in *SZ* region takes place under heavy pressure and mechanical mixing. Fine-equiaxed recrystallized grains are visible in both *SZ* regions of *AA* 5052 and *AA* 6061 alloys due to effective stirring action of cylindrical profile tool pin at lower tool traverse feed rate.

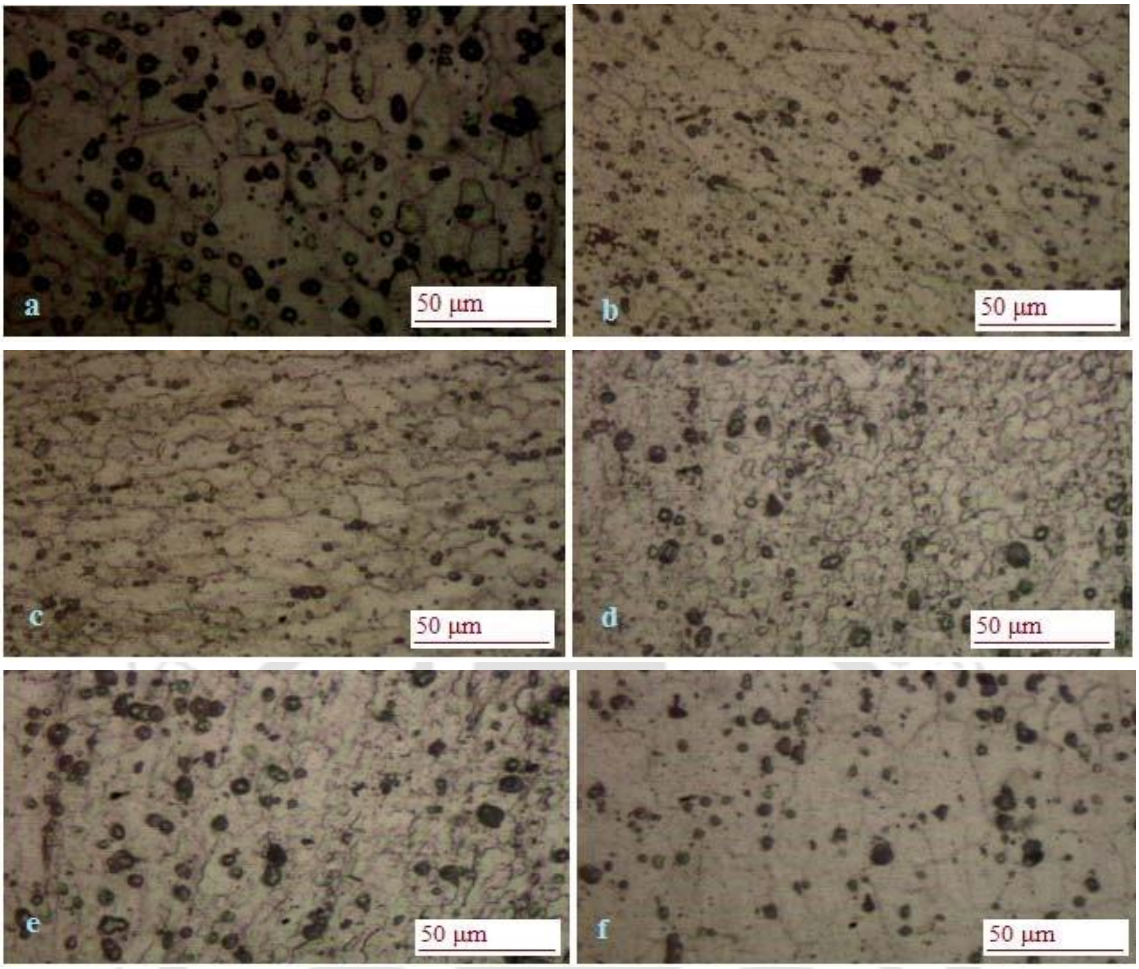

Fig. 4.9 Optical Micrograph image of (a) base AA 6061 alloy, (b) TMAZ at AA 6061 side, (c) SZ at AA 6061 side, (d) SZ at AA 5052 side, (e) TMAZ at AA 5052 side and (f) base AA 5052 alloy.

With the help of an Energy Dispersive Spectrometry (*EDS*) under Scanning Electron Microscope (*SEM*) images are taken at the centre of the stir zone (*Fig. 4.10*). At the centre three different spot shows spectrum distributions of constituent elements. It shows that there is a mix scattering of Magnesium (*Mg*) element, example in *spectrum 6* and *spectrum 8* the weight percentage of *Mg* exhibits constituent of *AA* 6061 while *spectrum 7* exhibit that of *AA* 5052. So we can conclude that at the centre of the stir zone uniform mixing of *AA* 5052-*H32* and *AA* 6061-*T6* alloys have taken place.

FESEM images (*Fig. 4.11*) of the stir zone show random distribution of a considerable amount of despersoids in α (Aluminium) matrix. The formations of these inter-metallic compounds which include incoherent *β-Mg2Si* and *β-Mg2Al3* phases are the result of frictional heat and pressure generation during tool rotation. The mechanical process of stirring and heating cause the diffusion of already present magnesium in the alloy into second phase compounds. These second phase particles favourably provide nucleation sites

for initiations of micro-voids during tensile and fatigue fracture, thus the presence of these compounds weaken the tensile properties of the weld and the formation of these particles are undesirable. During tensile testing these intermetallic compound particles favourably provide nucleation sites for initiations of micro-voids.

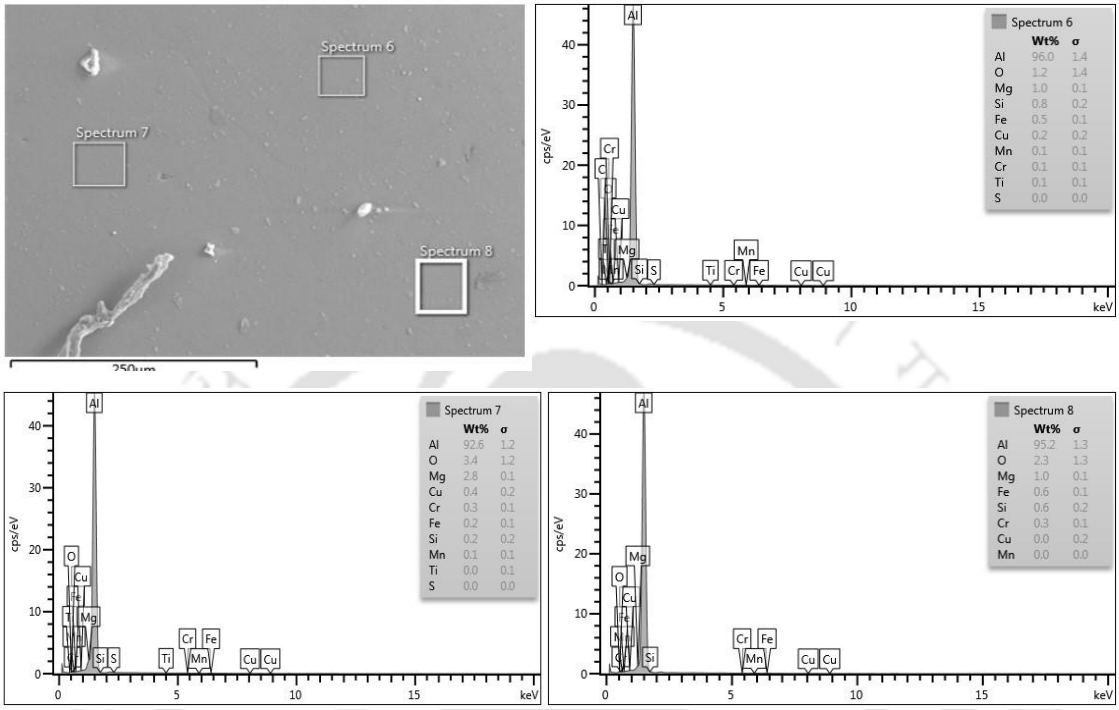

Fig. 4.10 SEM image and EDS spectrums showing the chemical compositions at the center of the weld.

The formation of intermetallic compounds could be avoided if the weld temperature is maintained just below eutectic temperature. In contrast there is a need for enough frictional heat for successful welding. Which in our case due to the thin size of the sheet the temperature rise is quite instant and it is difficult to maintain equilibrium.

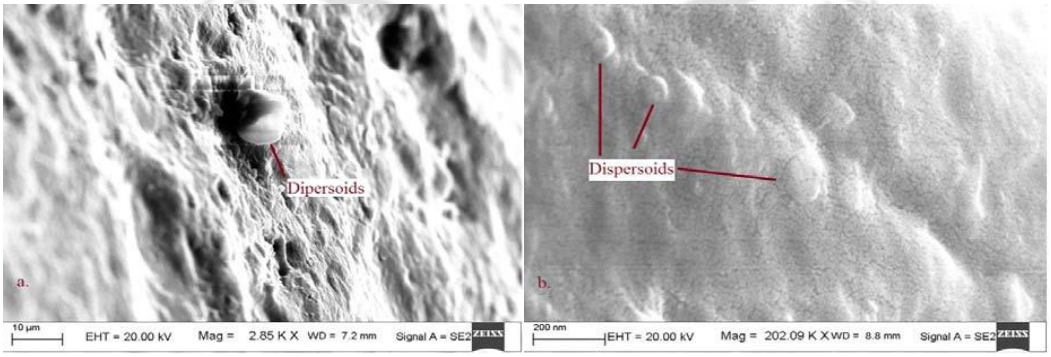

Fig. 4.11 FESEM images of the weld stir zone at tool rotational speed of 68 mm/min (a) at lower magnification and (b) at higher magnification.

Necking is mostly associated with ductile materials. In brittle materials, there is no necking region. Formation of necks is mainly due to the formation of micro-voids, which is formed during the plastic flow of metals under tension. The distribution of microvoids in the necked region controls the ultimate failure mode during plastic deformation. Ductile fracture consists mainly of three stages, (i) void nucleation, (ii) void growth and (iii) void coalescence.

The *FESEM* observations of the tensile-tested specimens revealed that the mode of failure is characterized by coalescence of micro voids (*Fig. 4.12*). Large sheared voids on the fractured specimen indicate that the mode of failure was ductile fracture. Higher magnification observation revealed multiple sheared micro void regions within a large void clearly indicating that the growth of these voids are results of amalgamation of micro voids.

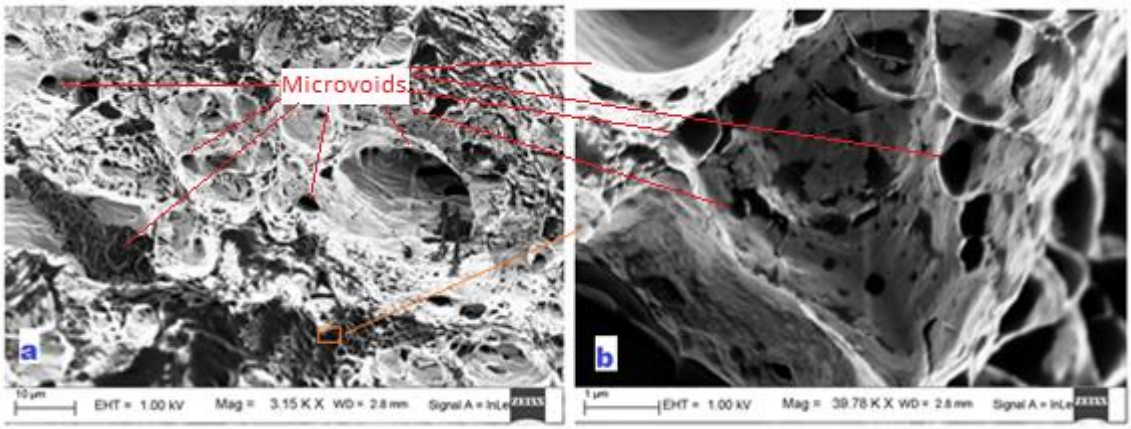

Fig. 4.12 FSEM images of the fracture surface of weld region of tensile specimen.

4.1.2 Summary

In the present study, mechanical and microstructure analysis of friction stir welded thin sheet aluminium alloy 5052-*H32* to 6061-*T6* were done. Effect of varying traverse speed with constant spindle speed on two different thicknesses of 1 *mm* and 1.5 *mm* sheets were evaluated. Grain distribution and mixing pattern in weld zone were examined. The observations we got from this study can be summarized as follows:

1. The welded joint produced at lower traverse speed (63 *mm/min*) produce better ductility than that at higher traverse speed (98 *mm/min*) for both the thicknesses of sheet and at constant spindle speed of 1500 *rpm*.

2. The ultimate tensile strength (*UTS*) of 1.5 *mm* thickness weld joint (210.4 *MPa*) was found to be 22 % more than that of 1 *mm* thickness joint (172.4 *MPa*) under same process parameters as the average hardness value at weld zone of 1.5 *mm* thickness was more than that of 1 *mm* thickness joint.
3. The average elongation before failure of 1.5 *mm* thickness welds was about 47 % more than that of 1 *mm* thickness weld samples this attribute is due to higher ductility due to the higher hardness at weld zone/*UTS* of 1.5 *mm* thickness weld.
4. Average micro hardness values at *SZ* was more than that of base *AA* 5052 alloy and less than that of *AA* 6061 alloy base, whereas lowest hardness value was found to be at heat affected zone of *AA* 5052.As *AA* 6061(*T6* tempered) being precipitation-hardened aluminium alloy, *FSW* creates a softer region at nugget zone than the corresponding base metal while non-heat treatable alloy i.e. *AA* 5052 has a lower hardness value at *HAZ* due to annealing phenomena.
5. Dynamic recrystallization and finer grains size was observed at the *SZ* with intense mixing of the materials were observed in the *AA* 6061side compared to *AA* 5052 due to precipitation-hardened nature of *AA* 6062 alloy. At the center of the weld there was uniform blending of *AA* 6061 and *AA* 5052 alloy constituents.
6. Intermetallic compounds were formed in weld zone which contribute negatively in the fracture strength of the joint. This results in lower weld joint strength then that of base materials.

4.2 Friction Stir welding of Thin Dissimilar Thickness Aluminium Alloys of AA 5052 and AA 6061

In this section, joining of different thickness aluminium alloys of 1 *mm* to 1.5 *mm* by friction stir welding technique was investigated. Different thickness blanks of aluminium alloy 5052 -*H32* and 6061-*T6* were joined respectively. The objective of the current work is to characterize the mechanical response and microstructure characteristics of different thicknesses *TWB* of *AA* 5052 and *AA* 6061 respectively. Further comparison between different thicknesses *TWB*s of *AA* 5052 with *TWBS* of *AA* 6061 were done.

4.2.1 Results and Discussions

The process parameters utilized for successful weld blanks were tool spindle speed of 1500 *rpm*, tool traverse speed of 36 *mm/min*, 63 *mm/min* and 98 *mm/min*, which were chosen on the basis of preliminary test runs. During *FSW* process backing plate was tilted at an angle of 3^0 with 1.5 *mm* aluminium blank at the advancing side in order to compensate different blank heights. Nomenclature of welded samples associated with the blank thickness and tool traverse rate combinations are given in *Table 4.3*.

Table 4.3 Process parameters for each sample nos.

Sample nos.	Thickness combination (mm)	Material	Tool rotational speed (rpm)	Tool traverse speed (mm/min)
1	1 – 1.5	*AA* 5052	1500	63
2	1 – 1.5	*AA* 5052	1500	98
3	1 – 1.5	*AA* 6061	1500	36
4	1 – 1.5	*AA* 6061	1500	63

4.2.1.1 Surface Morphology

All the successful welded blanks have visibly smooth surface without any macro defects (*Fig. 4.13*). Though on the outer surface of the welded blanks, have wavy distortion due to the surface strain. Varying traverse speed had no effect on the surface appearance of the welded blanks. The average heights of flash formations along the edge of weld path were bigger in *AA* 5052 than that of *AA* 6061 material for the same process parameters.

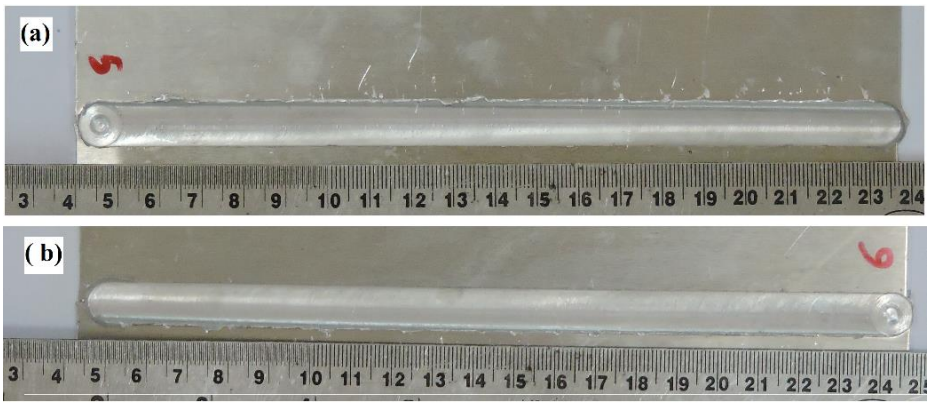

Fig. 4.13 Surface appearance of FSWed different thickness blanks (a) AA 5052 and (b) AA 6061.

4.2.1.2 Tensile Properties

Tensile test specimen was cut keeping the weld line in transverse direction. It was observed that all the tensile test samples fractured at weld zone (*Fig. 4.14*).

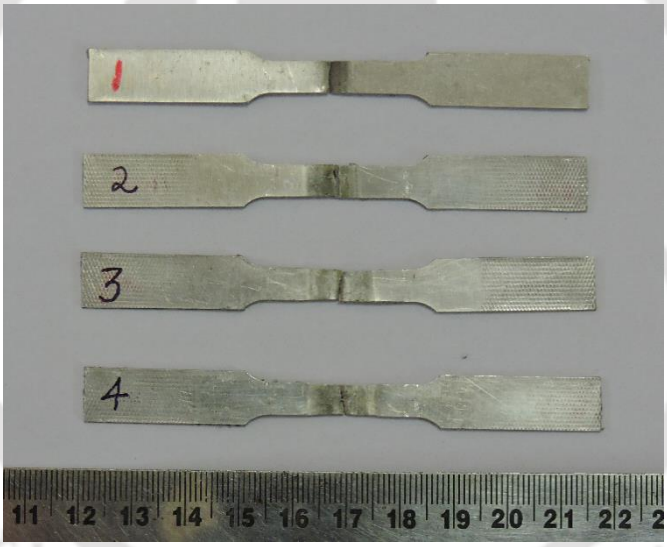

Fig. 4.14 Tensile test specimens showing fracture at weld.

The tensile test results of *sample 1* and *sample 2* in terms of average stress vs. strain are plotted in *Fig. 4.15*. It was found that samples welded at higher welding speed has higher strain reading although both *sample 1* and *sample 2* achieved approximately similar Ultimate Tensile Strength (*UTS*) of 185.5 *MPa* and 187.2 *MPa* respectively. The elongation at break for *sample 2* is 2.12 *mm* which was 14.6 % more than that of *sample 1* (1.85 *mm*). While in case of *sample 3* and *sample 4*, the sample welded at lower speed shows higher strength but still has lower ductility. From *Fig. 4.16* it can be interpreted that *sample 3* has *UTS* of 154 *MPa* and that of *sample 4* is 152.2 *MPa* though *sample 3* has elongation at break of 0.9 *mm* and *sample 4* has 1.23 *mm* (36.7 % more). So the optimum weld speed for

different thickness welded blank of *AA* 5052 alloy is 98 *mm/min* and for *AA* 6062 is 63 *mm/min* by *FSW* for the given setting.

Fig. 4.17 shows load vs. elongation of all welded blanks where *AA* 5052 material has more elongation reading than that of *AA* 6061. So,welded blanks of *AA* 5052 material show more ductility than of *AA* 6061 material. However, overall specimens welded at higher traverse speeds exhibited higher *UTS* and elongation than those welded at lower speeds.

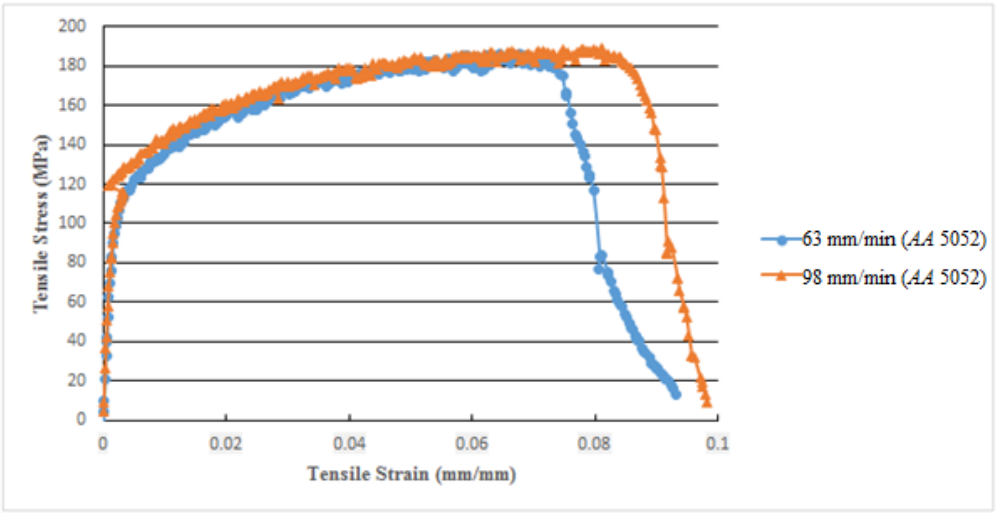

Fig. 4.15 Tensile test result of 1 mm thickness FSWed samples.

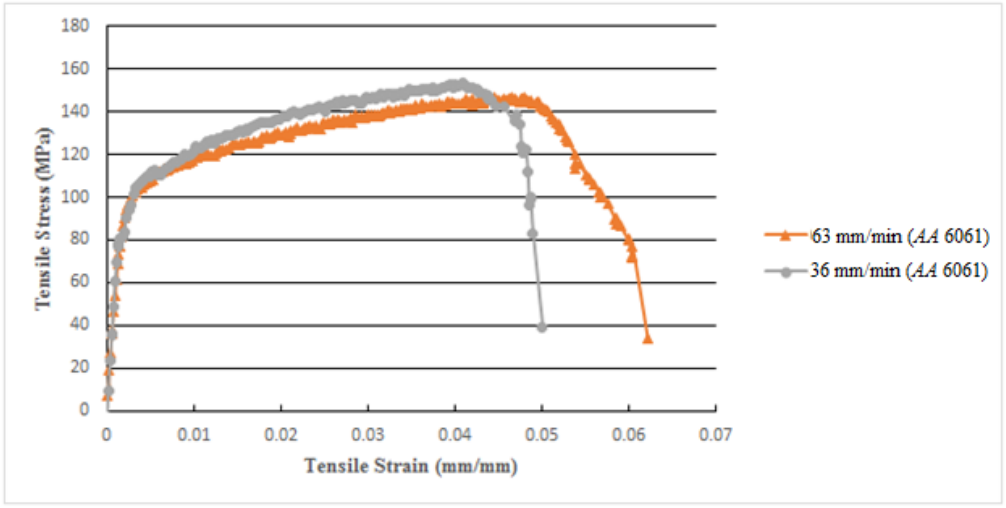

Fig. 4.16 Tensile test result of 1 mm thickness FSWed samples.

As expected the average strength of base material was found to be higher than that of the friction stir welded samples (*Fig. 4.18*), reason behind the fracture at welded joint during tensile testing of the samples (*Fig. 4.14*). The tensile properties of the base alloys and the *TWBs* are summarized in *Table 4.4*. The *FSWed* specimens exhibited lower yield strengths and elongations for all thickness categories.

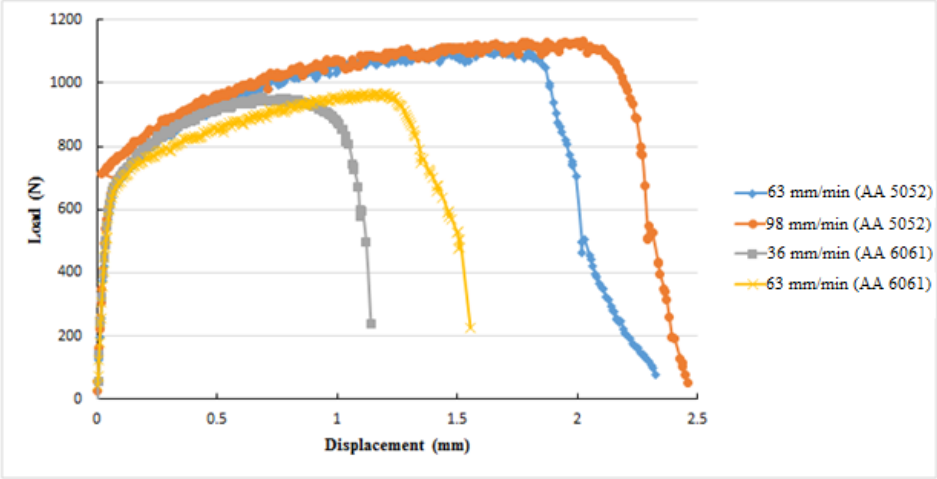

Fig. 4.17 Elongation corresponding to load applied for samples 1, 2, 3 and 4.

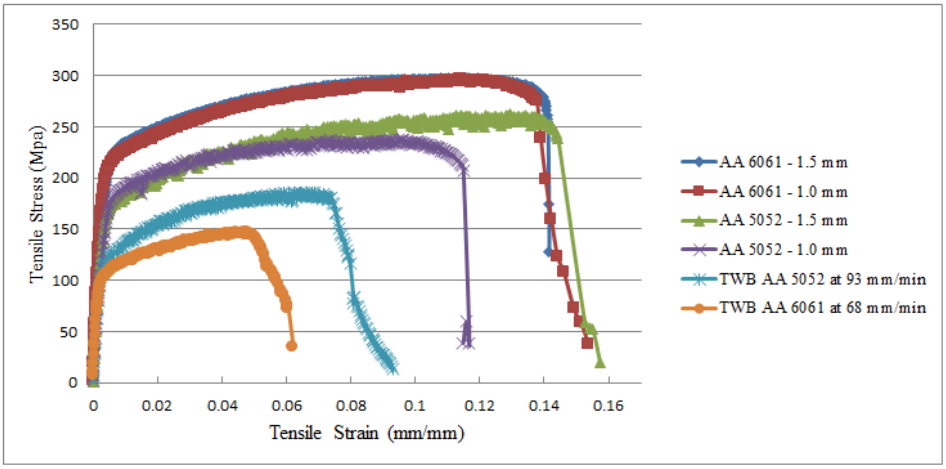

Fig. 4.18 Graph of tensile test results of base materials and different thickness FSW samples.

Table 4.4 Test results of mechanical properties of base material and friction stir welded samples.

Material	Thickness (mm)	Ultimate Tensile Strength (MPa)	Yield Strength (MPa)	Modulus of Elasticity (GPa)	Extension at Break (mm)
6061- *T6* (*Base*)	1	293.9	212.5	70.26	2.5
6061- *T6* (*Base*)	1.5	297.3	206.2	80.62	3.84
5052- *H32* (*Base*)	1	237.3	175.7	51.87	2.87
5052 - *H32* (*Base*)	1.5	260.3	168	60.59	3.93
TWB - *6061* (68 *mm/min*)	1-1.5	152.2	104.5	60.47	1.23
TWB -*5052* (93 *mm/min*)	1-1.5	187.2	128.2	80.49	2.12

4.2.1.3 Hardness Properties

Distributions of micro-hardness on the transverses cross-section of welded joints are shown in *Fig. 4.19.* Hardness at weld nugget of*AA* 5052 material is found to be more than that of base material for both different weld speeds. Being solid-solution-hardened aluminium alloy and because of annealing condition created by thermal environment of the process, *AA* 5052-*H32* alloy demonstrate such hardness characteristics.

While minimum hardness appeared in the weld zone of*AA* 6061 alloy for both the cases of weld speeds. The softening of hardness at nugget region of the joints can be attributed mainly due to the increase in the amount of dissolved precipitates and severe coarsening, which leads to increase in amount of alloying elements available for the precipitation hardening, causing over aging.

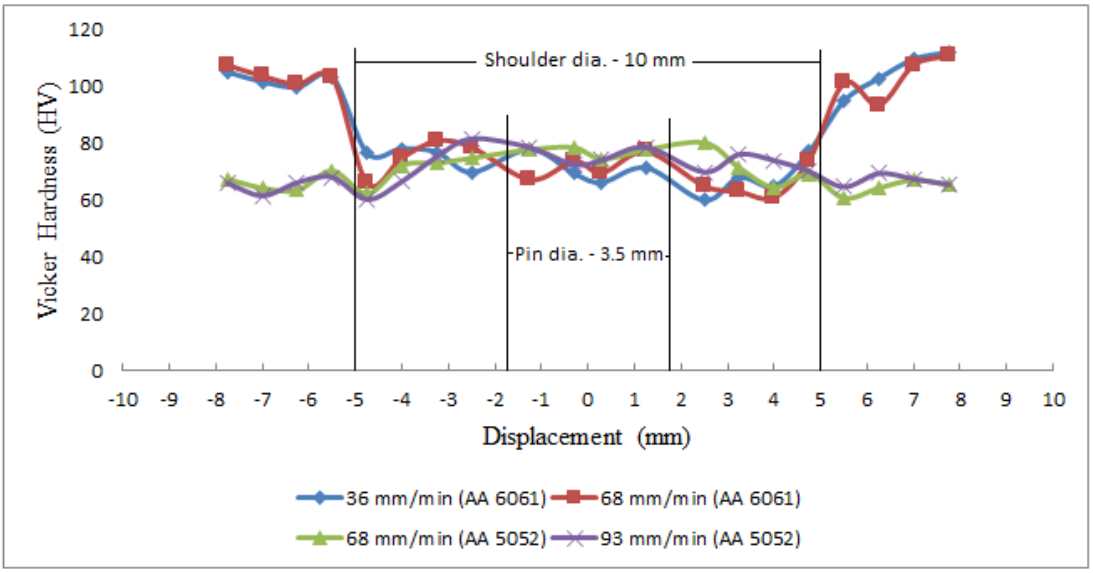

Fig. 4.19 Vickers hardness graph for friction stir welded samples.

4.2.1.4 Microstructural Analysis

Microstructures of various regions of weld cross section of the joint were observed by optical microscope. For microstructure analysis all the samples were polished to a mirror like surface finish with the help of emery papers up to 2000 grit and there after washed by alumina solution. Weld specimen of *AA* 5052 material were etched with Kroller's reagent solution and *AA* 6061 specimens with Keller's etchant solution [206]. All the weld joints observed were free from cracks and defects like tunnel, voids. We can identify the various weld zones in the *FSW* joint which are shown in *Fig. 4.20*, i.e. Base metal *[a]*, Heat affected zone *[b]*, Thermo mechanically affected zone *[c]* and Stir zones *[d1, d2, d3, d4, d5]*. Due

to the heat and pressure of rotating tool the material near the tool undergoes intense plastic deformation and flow, which leads to dynamic recrystallization of grains at the center of joints, commonly called as Stir zone (*SZ*). The mixing of material from adjacent sides of weld joint takes place in this region.

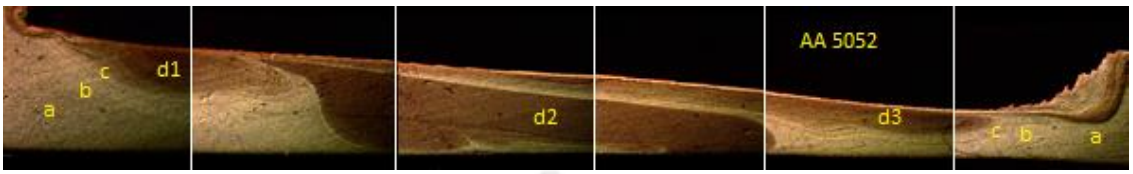

Fig. 4.20Macrostructure of weld joint of AA 6061 at welded at a speed of 68 mm/min.

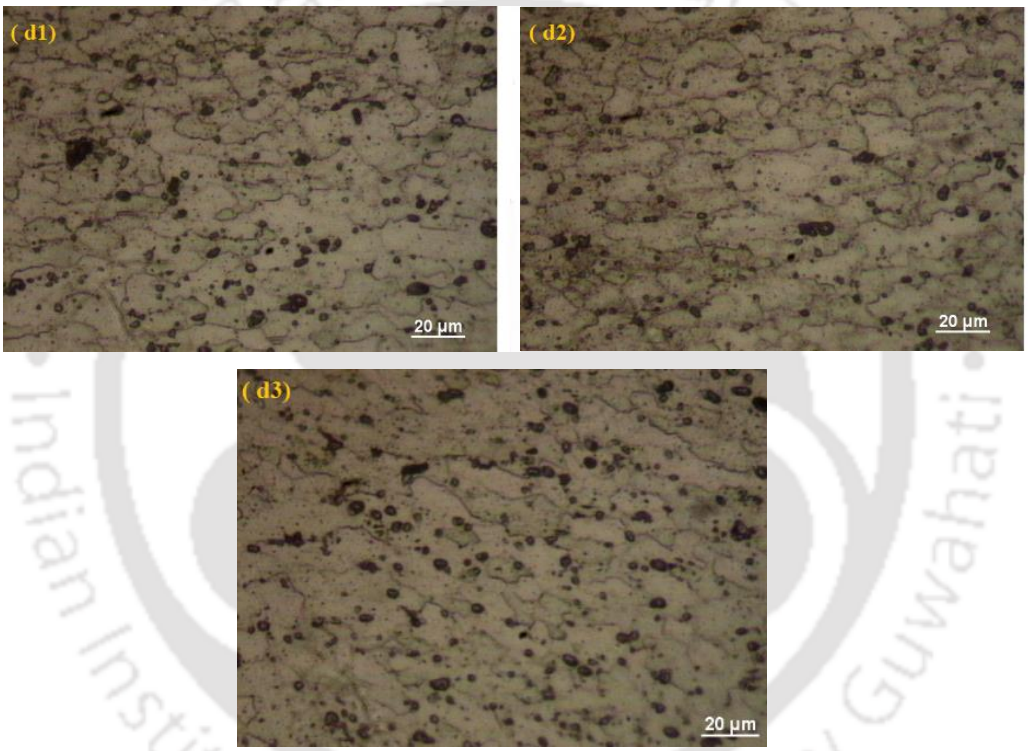

Fig. 4.21 Grain structures at SZs of AA5052 weld joint.

In *FSW* usually there is one single *SZ* in a joint however in one of our macrostructure of *AA* 5052 we found three *SZs* in the weld region (*Fig. 4.20*). This peculiar phenomenon occurred due to over feeding of the tool shoulder in to the blanks as we can see the thickness of the joint on retreating side is greatly reduced. As a result, even the tool shoulder has enough pressure and helps in stirring the grains of the blank below it. The grain structure found in the various *SZs* of the joint region of *AA* 5052 are shown *Fig. 4.21*. Dynamic recrystallization of grains occurred in these regions as we can see refined and elongated equiaxed grains structure within. This is due to combined effect of high temperature and severe deformation in this region.

*Fig. 4.22*shows the *SZ* of the *AA* 6061 weld joint where we can see a visibly clear onion ring pattern at the centre. At the left side of the weld which is being the thicker (advancing side) of the joint, we can see the individual piles of the onion rings structure gradually change its texture diminishing from the advancing side toward the retreating side. As shown in *Fig. 4.23* onion rings in the *SZ* of joint welded consisted of bands with fine and coarse grains.

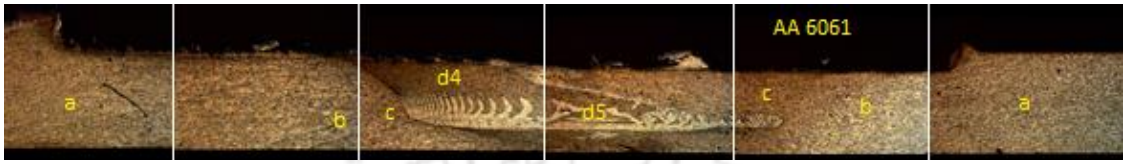

Fig. 4.22 Microstructure of weld joint of AA 6061 welded at a speed of 68 mm/min.

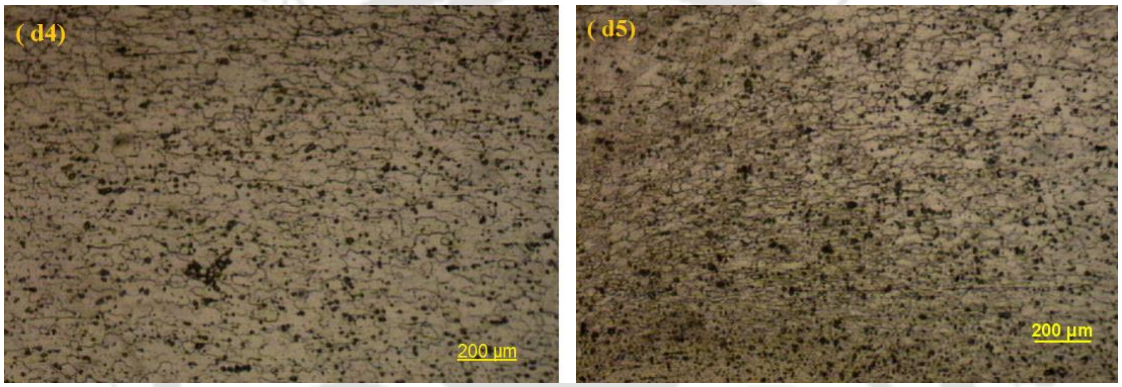

Fig. 4.23 Optical microstructure showing grain structure at SZ and onion ring region of AA 6061 weld joint.

The Field Emission Scanning Electron Microscope (*FSEM*) images of the surface of each fractured tensile-tested specimens are shown in *Fig. 4.24*. *FSEM* images revealed that the mode of failure for all samples are ductile in nature as large population of sheared voids can be seen at the fracture surface. The sheared voids indicate the finished phase of initial crack formation. The crack initiation during tensile test is due to the coalescence of micro voids which ultimately lead to fracture. So, it was observed that the variation of tool traverse speeds did not affect the ductile failure mode during tensile testing of the friction stir welds.

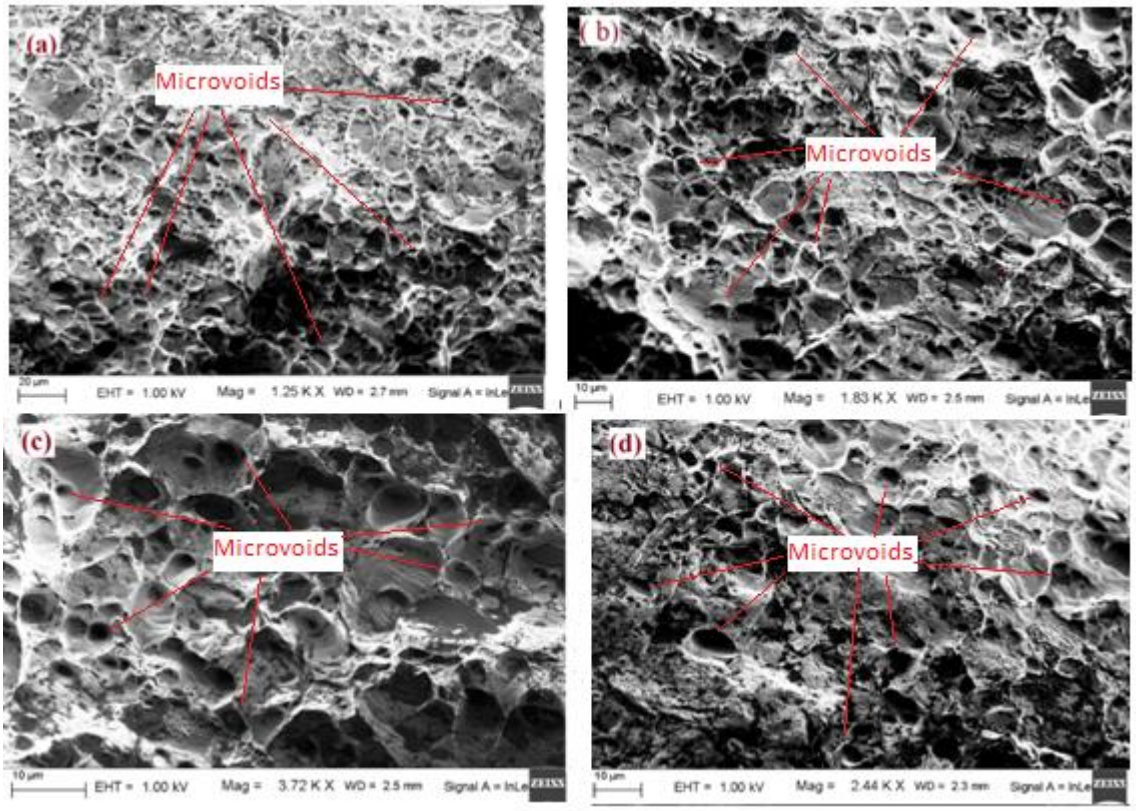

Fig. 4.24 FSEM images of the fracture surface of weld region of (b) AA 5052 welded at 68 mm/min (b) AA 5052 welded at 93 mm/min (c) AA 6061 welded at 36 mm/min and (d) AA 6061 welded at 68 mm/min.

4.2.2 Summary

Dissimilar thickness blanks of 1 *mm* to 1.5 *mm* for each *AA* 5052-*H32* and *AA* 6061-*T6* aluminium alloys are joined by *FSW* process. Welding by welding at a constant tool rotation speed of 1500 *rpm* the effects of variant weld speed on, tensile properties, micro-hardness distributions and microstructures of the joints were analysed. Based on the study presented, the following conclusions are drawn accordingly.

1. Successful joint of different blank thickness of 1 *mm* to 1.5 *mm* of each *AA* 5052 and *AA* 6061 respectively were obtained by *FSW* process. The required tool tilt angle was 3^0.

2. All the joints failed at positions in heat affected zone of the thinner 1 *mm* thickness side of the welded blank. The ultimate tensile strength (*UTS*) of different thickness *AA* 5052 weld joint (187.2 *MPa*) was found to be 23 % more than that of *AA* 6061 joint (152.2 *MPa*) with similar effect in elongation

prior fracture also, which showed an increase of 72.4 % than that of *AA* 6061 specimen. The process also produced a softened region in the weld nugget which may be due to the dissolution and growth of possible precipitates.

3. Both *AA* 5052 and *AA* 6061 have exhibited similar average micro hardness values at the weld region, however there was an uneven distributions of micro hardness profile. Average micro hardness values of the solid-solution-hardened *AA* 5052 at weld region was more than that of the base due to annealing phenomena while for *T6* tempered *AA* 6061 micro hardness decreases at weld compartment compared to base due to age hardening.

4. Both *AA* 5052 and *AA* 6061 alloys have gone through dynamic recrystallization showing fine equiaxed grain structures. The microstructure images of fractured surfaces of tensile tested specimen shows a large amount of equiaxed sharp cut dimples with different size characterizing ductile mode of failure which shows weld was successful.

Chapter 5

Electromagnetic Forming of Friction Stir Welded Blank

5 Electromagnetic Forming of Friction Stir Welded Blanks

5.1 Electromagnetic Forming of Friction Stir Weld Blank of Dissimilar Grade AA 5052-AA 6061

The objective of the presented work, in the current chapter, is to analyse the effect of weld line on the formability of Friction Stir Welded (*FSWed*) *TWB* by *FSW* process and to compare the forming behaviour of *TWB by FSW* with conventional hydraulic press forming. Formability was characterized with Limit Dome Height (*LDH*) tests and Forming Limit Curve (*FLC*) diagrams.

5.1.1 Results and Discussions

Blanks welded at tool traverse speed of 63 *mm/min* with a different grade combination of *AA* 5052-*H32* to *AA* 6061-*T6* were considered for formability analysis. The final *TWB* dimension was 200 *mm* × 200 *mm* with a thickness of 1 *mm*.

5.1.1.1 Limit Dome Height (LDH) Test

To study the influence of weld line on the formability of *TWB* at high speed, *LDH* tests were carried out by *EMF* process. Two orientations were considered; in one situation welded blank was offset by 25 *mm* towards *AA* 6061 side and another towards *AA* 5052 side by 25 *mm*. The sample numbering with weld orientations are illustrated in *Fig. 5.1*. In *Figure 5.2* all the dome heights of the *TWBs* with failure are plotted against different applied voltages. *Sample 2* has higher dome height over *sample 3* prior failure which is 19.1 *mm* as against 12.2 *mm* for the later. When weld line is offset towards *AA* 6061 more portion of *AA* 5052 cover up the copper coil for deformation which is in favour for occurrence of more deformation. As *AA* 5052-H32 has better formability characteristics over *AA* 6061-T6 which can be seen from tensile tests results (Please refer to section *4.1.1.2*). The maximum dome height reached is 17.4 *mm* for weld line centred *sample 1* but it is lower than that of *sample 2* (*Fig. 5.2*).

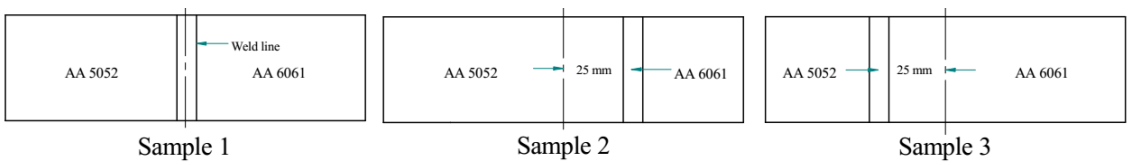

Fig. 5.1Orientation of weld line of FSWed blanks.

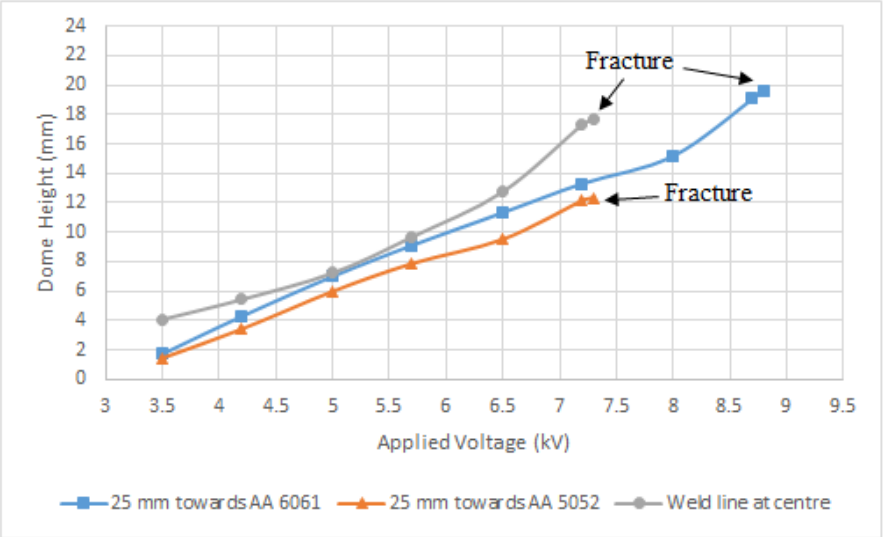

Fig. 5.2 Dome heights of weld line orientated samples obtained by EMF process.

Fig. 5.3 shows the graph of transient current flowing through the coil at highest discharge voltage. Current curves were acquired using Cathode Ray Oscilloscope (*CRO*). The current frequency was found to be 14.88 *kHz* for the given coil tool. The cycle time was equal to 67.2 *μs*, so the maximum deformations in *TWBs* were expected to occur at 16.8 *μs*.

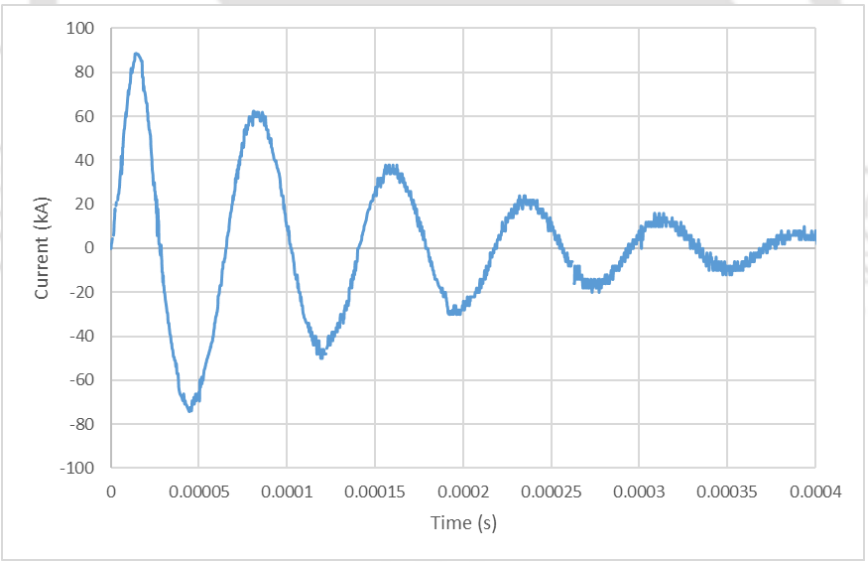

Fig. 5.3 Current variation over time at 8.7 kV discharge voltage.

The plotting of currents versus voltages for the *EMF* process is illustrated in *Fig. 5.4*. The change in peak current takes place due to change in mutual inductance of the circuit. Increase in peak current has been observed for increase in voltage. The highest current before failure for *sample 2* was found to be 88.85 *kA* which was highest among all welded blanks. For *sample 1* and *sample 3* the measured current is approximately equal to 82 *kA*.

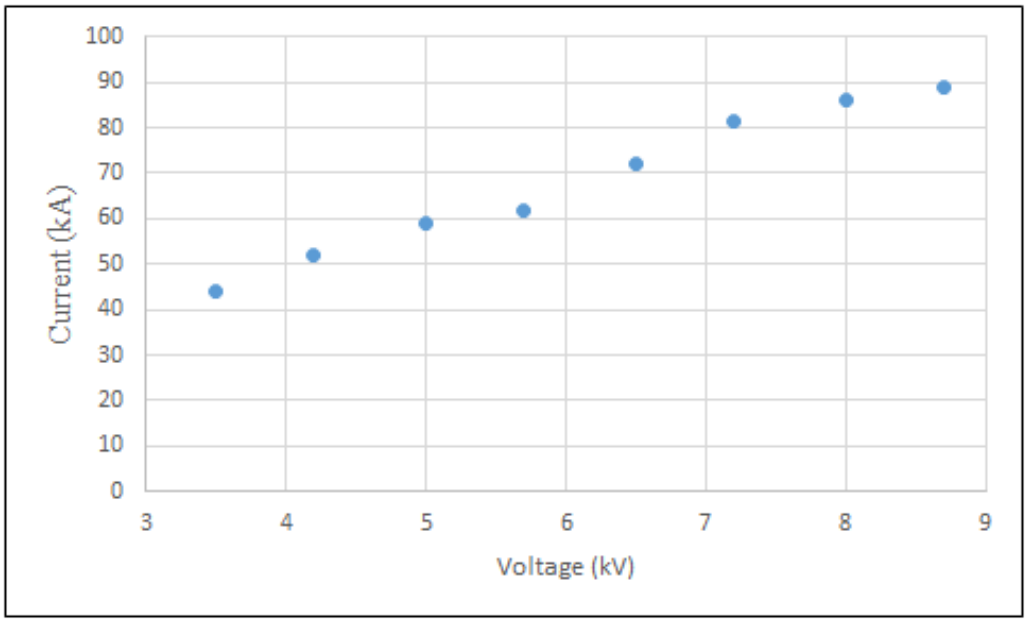

Fig. 5.4 Current variation over voltages.

LDH test is biaxial test causing stretching of the *FSWed* blanks both along and across the weld. So during the process the softest of all regions will experience larger deformation and finally failure will occur. *Fig. 5.5* shows the final deformed welded blanks before failure.

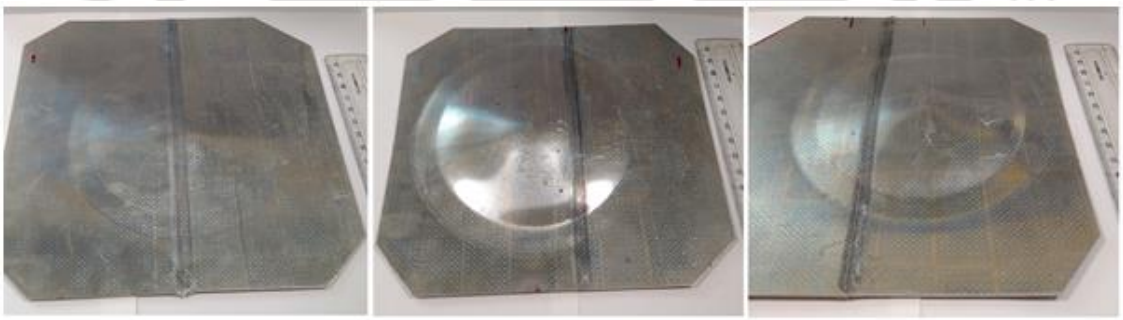

Fig. 5.5 Dome heights of weld line oriented samples formed by EMF.

Final fractured welded and base material blanks which were deformed by both quasi-static and *EMF* process are shown in *Fig. 5.6*. The shape of the electromagnetically deformed samples shows a hump (*Fig. 5.6*) at the centre which is due to the inertia effect. The intense magnetic field which is characterized by the shape of the coil causes a heterogeneous distribution of strains at the worksheet and at high speed this brings the inertia effect to deforming sheet.

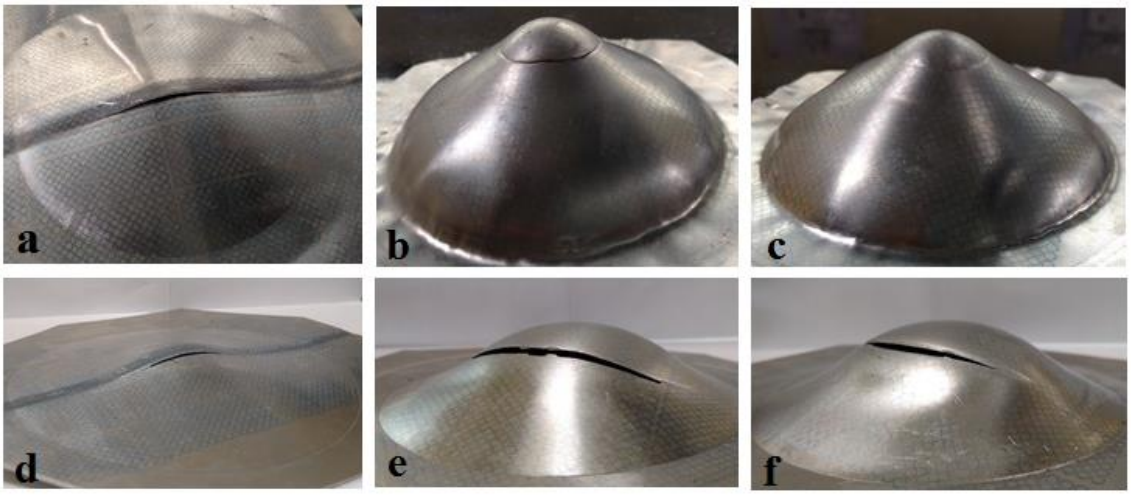

Fig. 5.6 Final fractured dome heights obtained by EMF process (a) TWB, (b) AA 5052, (c) AA 6061, by conventional HPF (d) TWB, (e) AA 5052 and (f) AA 6061.

The *LDH* test shows significant difference for maximum dome heights between conventional and *EMF* process as shown in *Fig. 5.7*. Dome height obtained with *EMF* process for *AA* 5052 is 40.95 *mm* and for *AA* 6062 it is 37.68 *mm*. There is a percentage increase of about 115% for base *AA* 5052 from conventional process to *EMF* while for *AA* 6062 it is about 83.4 %. The increase in dome height for *FSW* blank is 42 % by *EMF* as compared to conventional forming process. Here the strain rate sensitivity of the material plays an important part in increasing the formability of aluminium alloys by *EMF* process, the phenomenon although increases the flow stress of the material with speed but at the same time delay the onset of necking [215].

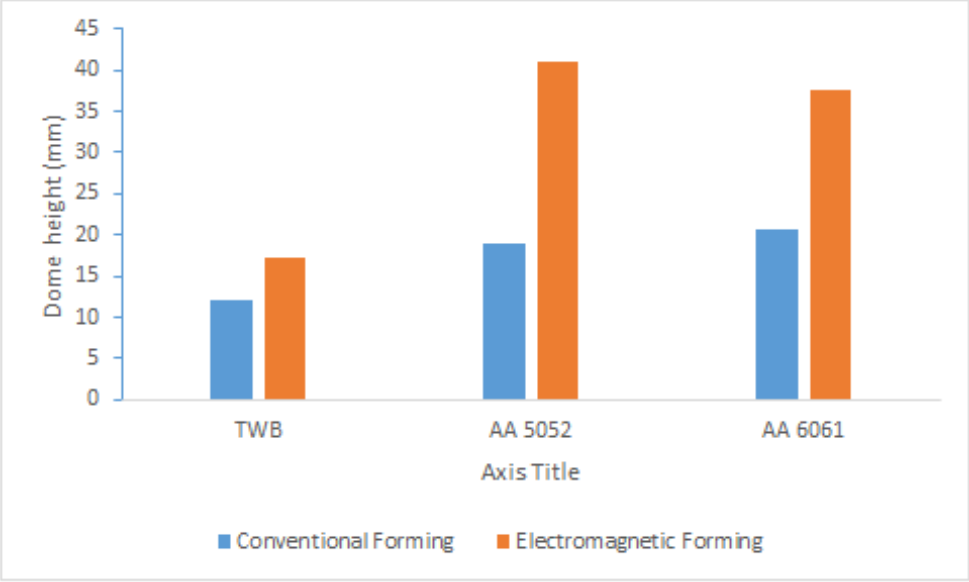

Fig. 5.7 Dome height of base and TWB samples formed by conventional and EMF process.

5.1.1.2 Forming Limit Diagram (FLD)

The experimental *FLCs* are plotted at border line of safe and failed grid circles and below the curve line lays all the safe grids. In case of *FLC* of welded blanks, *sample 2* is highest among *sample 1* and *sample 3* (*Fig. 5.8*). As expected *sample 2* with more ductility and dome height will show higher *FLC*. However, there is no significant increase in major strains as the rise in *FLC* is mainly due to the difference in minor strains. While for conventional and *EMF* process the difference in *FLCs* of welded blanks is more pronounce in terms of both major and minor strains. In *Fig. 5.9*, *FLC* of electromagnetically formed samples shows same shape with a higher *FLC* of about 18% more than that of *FLC* of conventionally formed samples. The uniform rise in *FLC* of alloys with *EMF* shows the proportional effect of strain rate sensitivity. At high velocity, forming is characterised by high strain rate, aluminium alloys are showing positive rate sensitivity. The *FLCs* of welded blanks with base materials formed by both processes are shown in *Fig. 5.10*. The *FLCs* of base materials showed an increase of about 89 % and 62.5 % for *AA* 5052 and *AA* 6061 respectively by *EMF* process. *AA* 6062 being harder material than *AA* 5052 exhibits lower *FLC* (please refer to section *4.1.3*). The curve of *AA* 5052 is highest when formed by *EMF* but it is lower than *AA* 6062 when formed by conventional forming process. This is consistence with forming results obtained with *LDH* test where *AA* 5052 attained maximum height with *EMF* process. The experiment shows significant improvement in formability of *FSWed* blank of *AA* 5052 to *AA*6062 by *EMF* process with respect to quasi-static process.

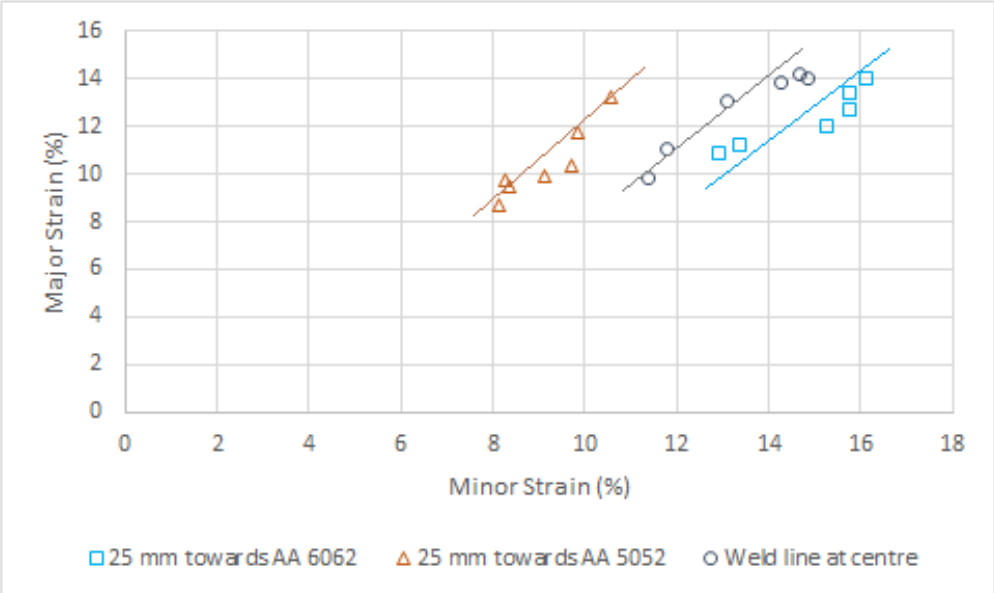

Fig. 5.8 FLD of different weld line orientated samples formed by EMF.

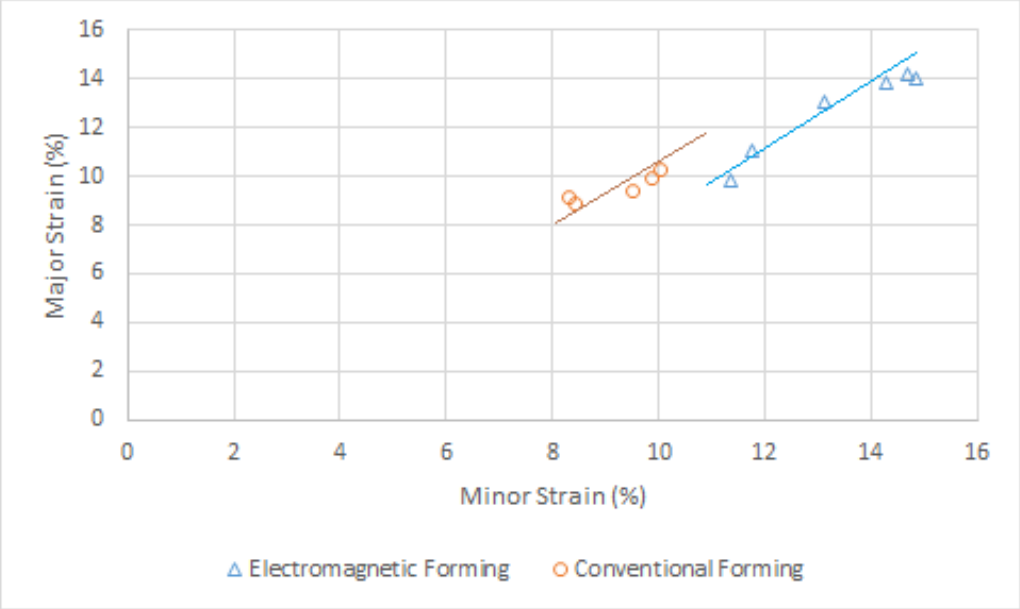

Fig. 5.9 FLD of FSWed samples formed by conventional and EMF process.

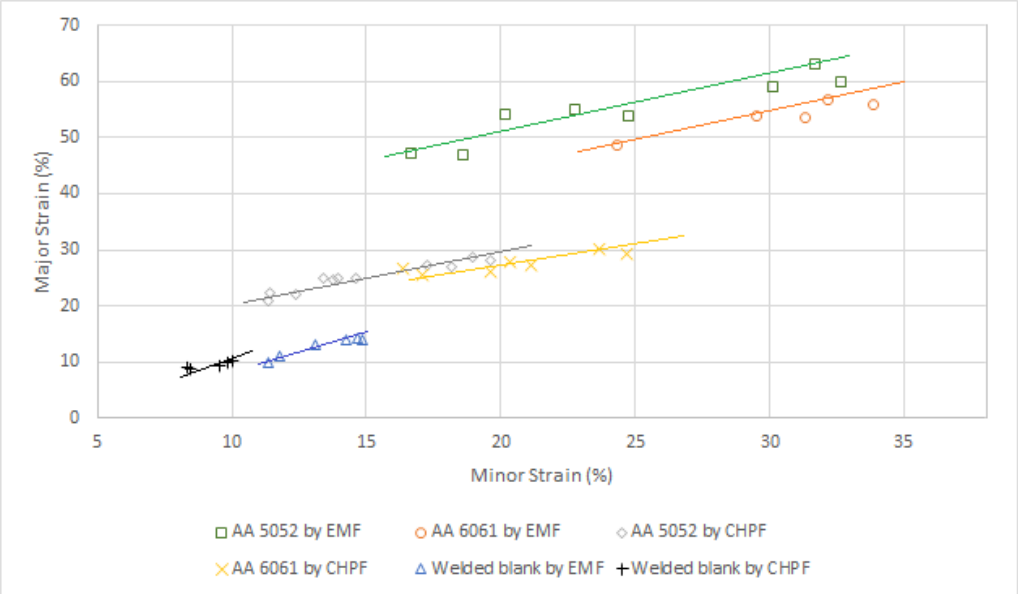

Fig. 5.10 FLD of base materials and FSWed samples formed by conventional and EMF process.

5.1.2 Summary

In this section formability analysis was performed for aluminium welded blanks by both conventional and high speed forming process. Welded blanks with combination of different grades of aluminium alloys specifically *AA* 5052-*H32* (work-hardened non-heat-treatable) and *AA* 6061-*T6* (heat-treatable) of 1 *mm* thickness which were welded together by *FSW* are taken for formability evaluation. The formability test was done in terms of *LDH* test and *FLD* diagram. The main conclusions can be summarized as follows:

1. Effect of weld line location when formed by *EMF* shows significant change in formability. Bulge test show more dome height can be achieved when weld line is offset by 25 *mm* towards *AA* 6062. Lowest *LDH* is obtained when weld was kept offset towards *AA* 5052 and intermediate height was obtained when formed at exactly with zero offset (at centre). This is also true with corresponding *FLCs*.

2. With *EMF* process *FSWed* blank achieved a greater height compared to conventional process. The percentage increase is 42% with *EMF* process. Dome heights attained by *FSWed* blanks in both conventional and *EMF* process are lesser than that of the base materials. The percentage increase in dome heights for both base *AA* 5052 and *AA* 6062 by *EMF* is 115% and 83% respectively against conventional process.

3. The *FLC* of blanks formed by *EMF* process shows significant increase in both major and minor strain from conventional process. This is also same for base *AA* 5052 and *AA* 6061 where the *FLCs* increase with *EMF* process against the conventional process.

5.2 Electromagnetic Forming of Different Thickness Tailor Welded AA 5052 Blank

In this section, *FSWed* different thickness *TWBs* of *AA* 5052-*H32* was formed by *EMF* process. The objective is to characterize the forming behaviour of different thickness *TWB* formed at high velocity. Further the formability of *TWBs* was compared with quasi-static forming process. The formability of the *TWB* in both the cases were analysed in terms of Limit Dome Height (*LDH*) and Forming Limit Curve (*FLC*).

5.2.1 Results and Discussions

FSWed blanks of different thickness combination of 1 *mm* to 1.5 *mm* of *AA* 5052 which were welded at tool transverse speed of 93 *mm/min* were considered for formability test. The final *TWB* dimension was 200 *mm* × 200 *mm*.

5.2.1.1 Limit Dome Height (LDH) Test

Experiments for free forming were done by electromagnetic forming process. Welded blanks (*TWB*) were deformed at various voltages until fracture. Both *TWB* and base materials were used to obtain dome heights. The maximum height attained before fracture by *TWB* was 18.31 *mm* at 8 *kV*, which lower than that of base materials (*Fig. 5.11*). The maximum dome height before fracture for *AA* 5052 1 *mm* thickness material was 40.24 *mm* at 12.4 *kV*until fracture and the largest dome height obtained with available system capacity was 33.68 *mm* at 13.1 *kV*. The dome heights obtained by 1.5 *mm* thickness was lower than 1 *mm* thickness aluminium alloy at every corresponding voltage, since 1.5 *mm* thickness alloy has higher tensile strength than that of 1 *mm* thickness aluminium alloy.

Current curves were acquired during experiment by using Cathode Ray Oscilloscope (*CRO*). *Fig.5.12* shows the graph of transient current flowing through the coil at a discharge voltage of 12.6 *kV*. The current frequency was found to be 14.88 *kHz* for the given coil tool with a cycle time of 67.2 *μs*, so the maximum deformation in welded blanks by the coil were expected to occur at 16.8 *μs*. The *LDH* test shows significant difference between heights obtained by conventional and *EMF* process which is shown in *Fig. 5.13*. Dome height attained by *TWB* with *EMF* process is about 43 % more than that of height obtained by the conventional process. Similarly, the percentage increase is 115 for base *AA* 5052 of 1 *mm* thickness from conventional hydraulic press forming to *EMF* process.

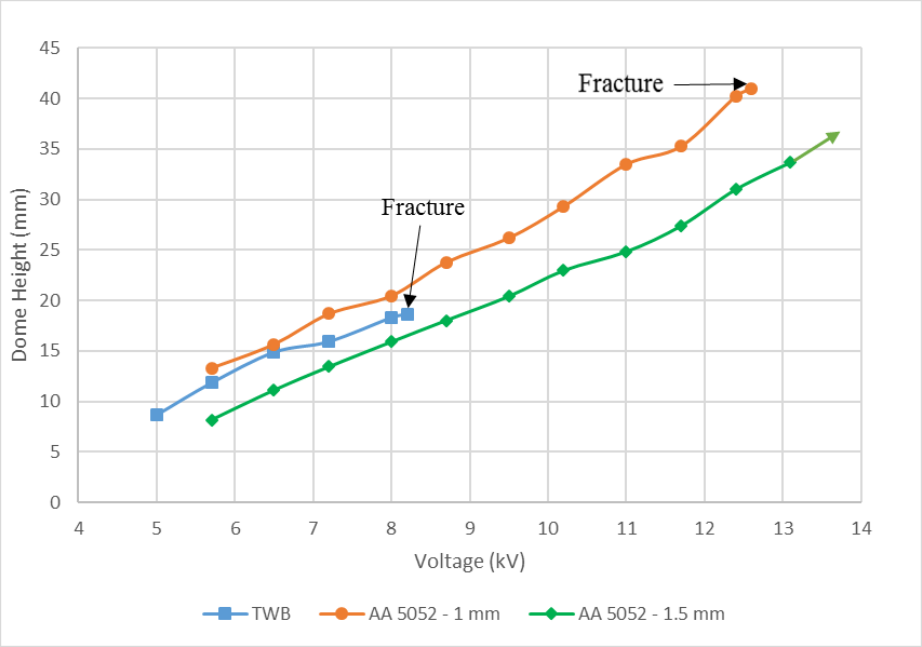

Fig. 5.11 Graph of dome heights attained by TWB and base alloy at various voltages.

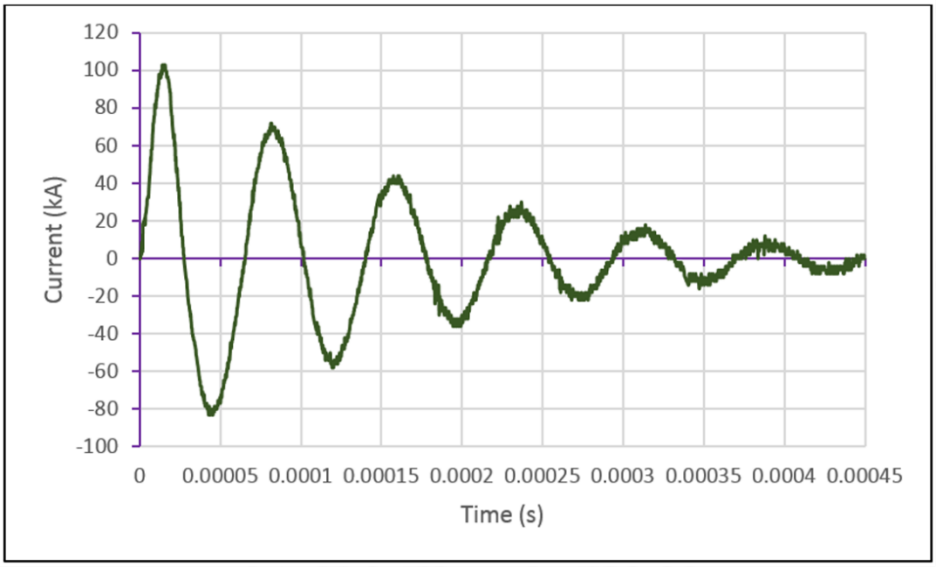

Fig. 5.12 Sinusoidal damped current curve for 12.6 kV discharge voltage.

With present *EMF* system, the percentage increase in height is 27.25 for 1.5 *mm* thickness *AA* 5052 alloy, which will be more if further experiment till fracture is considered. At high velocity the delay in initiation of necking of material and at the same time increase in flow stress of the material contributes to the increase formability of the aluminium alloy by *EMF* process.

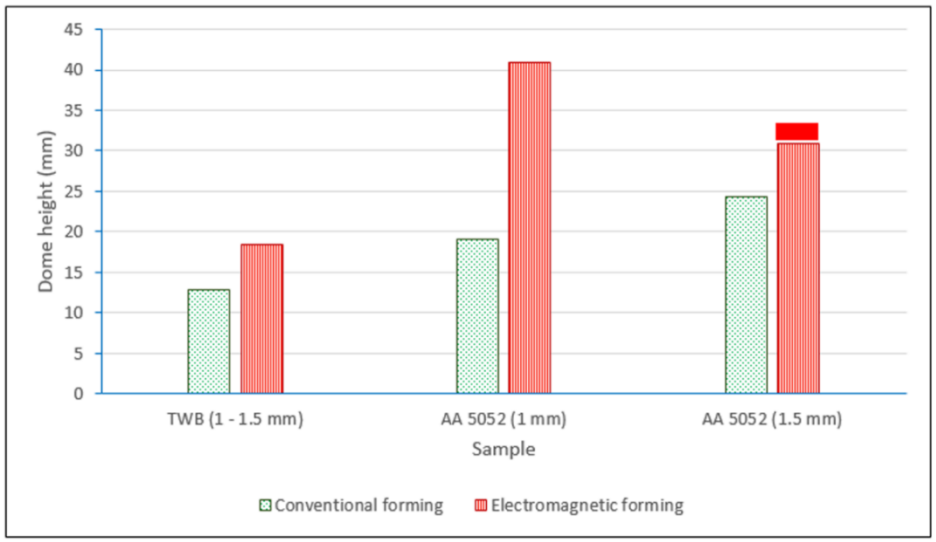

Fig. 5.13 Dome heights of TWB and base materials formed by conventional and EMF process.

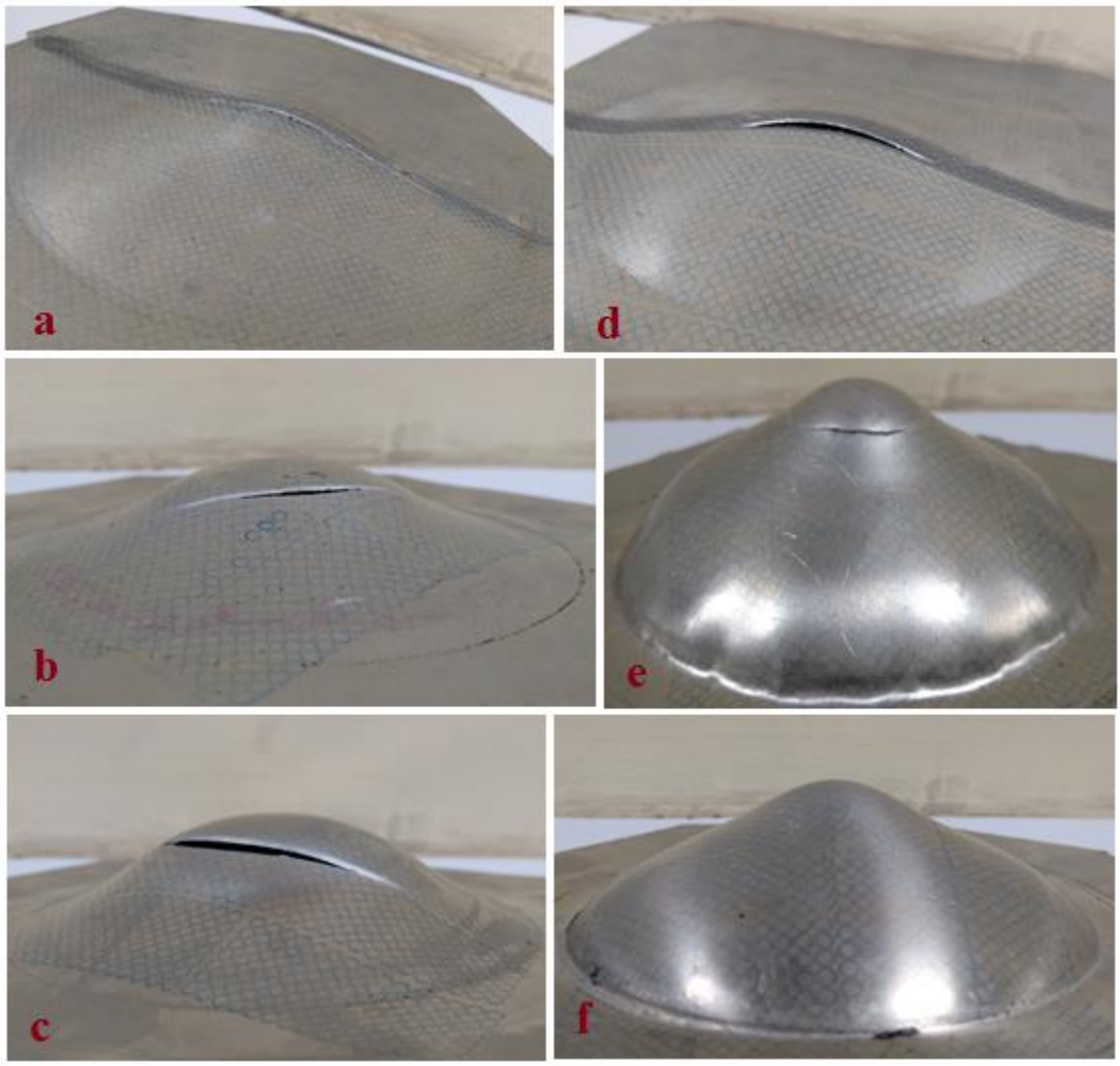

Fig. 5.14 Final fractured dome heights obtained by conventional forming process (a) TWB, (b) AA 5052 1 mm (c) AA 5052 1.5 mm and by EMF process (d) TWB, (e) AA 5052 1mm, (f) AA 5052 1.5 mm (No fracture).

In *Fig. 5.14* the final shape of all the domes which were obtained by both conventional and *EMF* process were shown. Due to inertia effect of the deforming *TWB* at high velocity there is a hump at centre of the dome when formed by *EMF* process. The intense Lorentz force generated by the instantaneous electric and magnetic field between coil and *TWB* work piece contributes to the heterogeneous distribution of strains at the worksheet at high speed causing an inertial effect to the deforming sheet.

5.2.1.2 Forming Limit Diagram (FLD)

From the final deformed *TWBs* Forming Limit Curves (*FLCs*) were plotted which is shown in *Fig. 5.15*. *FLC* was plotted each for conventional forming and electromagnetic forming process the measured grid circles printed at the *TWB* surfaces. The *FLCs* draws a border line between safe and failed grid circles. The *FLC* of *EMF* is more than that of the conventional forming as expected because of higher dome height. The increase of *FLC* by *EMF* in terms of major strain is about 28.6 % more than that of the *FLC* constructed from conventional process. The increase in *FLC* of *TWB* with *EMF* indicates positive strain rate sensitivity of the weld region. So, at high velocity forming formability of friction stir welded blanks increases.

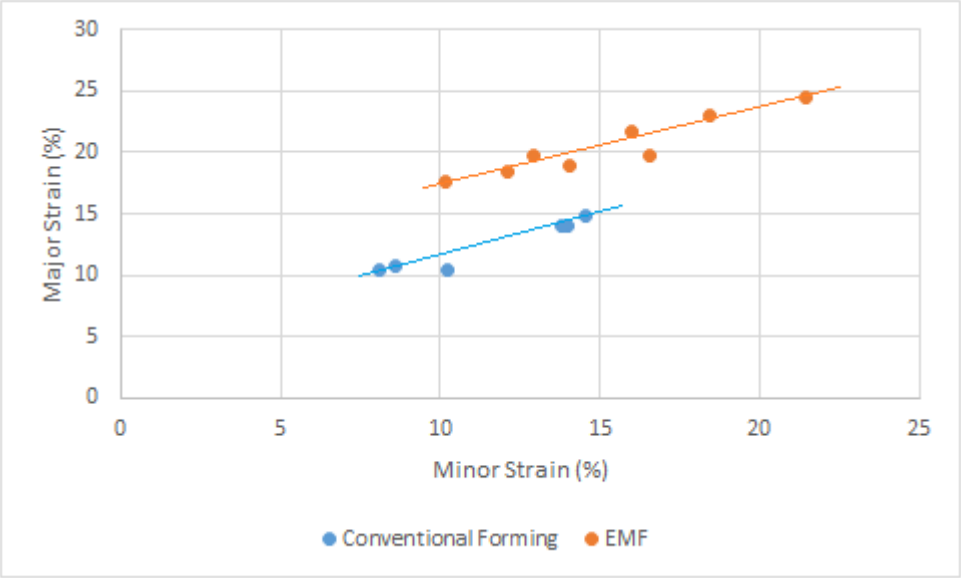

Fig. 5.15 FLD of FSWed TWB formed by conventional and EMF process.

In *Fig. 5.16*, *FLCs* were plotted for all the welded blanks and base materials. Forming curves of base material *AA* 5052 obtained from *EMF* process showed higher magnitude than that by quasi-static process, it is about 81.5 % more in major strain direction for 1 *mm* thickness.

The forming curve of welded blanks (from *EMF* process) is lower than that ofbase material *FLC* (from quasi-static process). This is due to weld region being weaker than that of base metals.

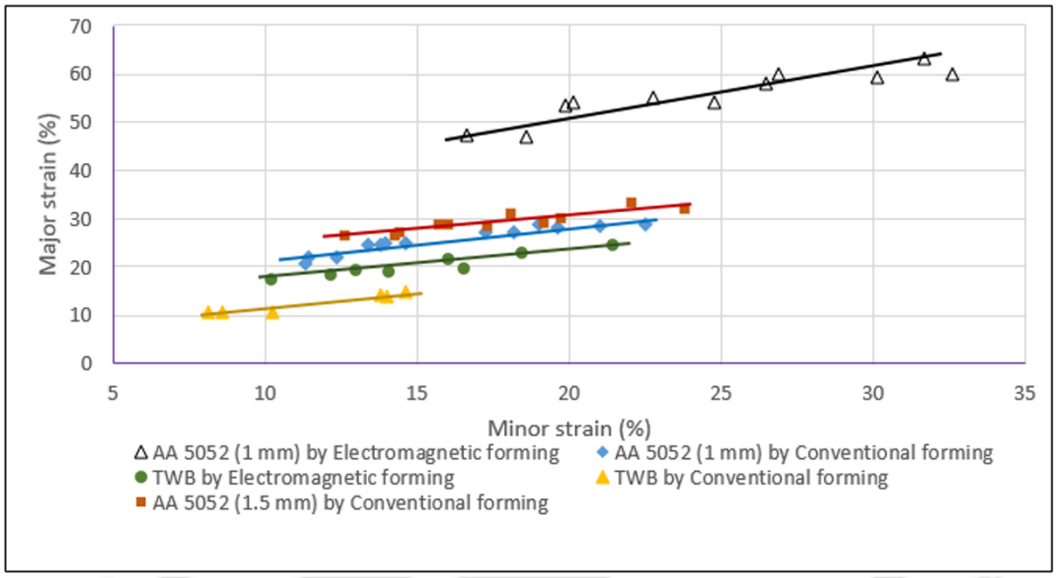

Fig. 5.16 FLCs of base materials and welded blanks obtained from conventional quasi-static and EMF process.

5.2.2 Summary

In this section, formability analysis of different thickness welded blank of *AA* 5052 material was done. The thickness difference was 1*mm* to 1.5 *mm* which was welded together by *FSW* process. The weld parameters were tool rotational speed of 1500 *rpm* and weld speed of 93 *mm/min.* forming characteristics were quantified by Limit dome height test and by constructing Forming limit curve. Both quasi-static and high velocity forming (*EMF*) were considered forming characterisation. Based on the study, the following conclusions can be drawn accordingly.

1. *EMF* process gives more deformation than the conventional quasi-static process for both welded blank and base materials. The increase in dome height before fracture for welded blank by *EMF* process is 43 %. The increase in height for 1 mm thickness base material *AA* 5052 it is 115 %. Similarly, the increase in height is 27.25 % for 1.5 *mm* thickness *AA* 5052 alloy, which will be more if further experiment till fracture is considered.

2. The forming limit curve obtained from welded blanks formed by *EMF* process shows significant increase in magnitude as compared to quasi-static process. The increase of forming curve by *EMF* in terms of major strain was found to be little over 28 %. Hence, high velocity forming process increases the formability of both base and welded blanks (different thickness).

Chapter 6

Numerical Simulation for Prediction of Failure in Electromagnetic Sheet Metal Forming

6 Numerical Simulation for Prediction of Failure in Electromagnetic Sheet Metal Forming

In this chapter, prediction of failure zone through simulation on the *EM* sheet forming process with respect to die entry radius was done. Simulation of a free formed dome height test of *AA* 6061 of 1 *mm* thickness with dimension 200 *mm* × 200 *mm* are performed in commercially available Finite Element Method (*FEM*) software. The *FEM* software utilized for the purpose is the beta version of *LS Dyna EM* module which is specially design for *EMF* application and utilizes strong coupling method. Strong coupling is the most difficult type of coupling strategy. It yields the best results compared to the other types (loose Coupling and sequential coupling), as the number of assumptions and simplifications are minimal in the said simulation. In a fully coupled method, the effects of the coupled Electromagnetic, mechanical and thermal fields are calculated in each element of the forming system. One major advantage of adopting this strategy is the instantaneous strong linking of the solvers of multi-physic equations. Which are absent in loose and sequential coupling (due to increased complexity).

6.1 FEM Simulation

LS-DYNA® Electromagnetism (*EM*) module is a special*FEM* software package being developed exclusively for electromagnetic manufacturing. It coupled a magnetic solver with mechanical solver and, with external current input into solid conductors and computes the corresponding magnetic field, electric field and induced current by solving the Maxwell equations in the eddy-current approximation [208]. All the solid or shell elements conductors corresponding Maxwell equations are solved by using a *FEM* and for the surrounding air Boundary Element Method (*BEM*) is used. Lorentz force *F*, is evaluated at each node of the element and added to the mechanical solver as input, once after computing electromagnetic fields by electromagnetic solver.

The Maxwell's equations solved by FEM magnetic solver is given by:

$$\vec{\nabla} \times \vec{E} = \frac{-\partial \overrightarrow{B_m}}{\partial t} \tag{6.1}$$

$$\vec{\nabla} \times \left(\frac{\overrightarrow{B_m}}{\mu}\right) = \vec{J} \tag{6.2}$$

$$\nabla . \overrightarrow{B_m} = 0 \tag{6.3}$$

$$\nabla . \varepsilon \vec{E} = 0 \tag{6.4}$$

$$\nabla . \vec{J} = 0 \tag{6.5}$$

$$\vec{J} = \sigma \vec{E} + \overrightarrow{J_s} \tag{6.6}$$

$$\vec{\nabla} \times \vec{H} = \vec{J} + \varepsilon \frac{\partial \vec{E}}{\partial t} \tag{6.7}$$

$$\vec{B}_m = \mu \vec{H} \tag{6.8}$$

Where,

σ = electrical conductivity, μ = magnetic permeability,

$\mathcal{E}$ = electrical permittivity, E = electric field,

B_m = magnetic flux density, H = magnetic field intensity,

ρ = total charge density, J = total current density,

J_s= source current density.

In the equation (6.3) the magnetic flux density is represent as:

$$\vec{B}_m = \vec{\nabla} \times \vec{A} \tag{6.9}$$

Where, A is the vector potential. Similarly equation (6.1) electric field is given by

$$\vec{E} = -\vec{\nabla}\emptyset - \frac{\partial \vec{A}}{\partial t} \tag{6.10}$$

Where, $\emptyset$ is the electric scalar potential.

Separating the vector potential from the scalar potential (gauge condition).

$$\nabla \cdot \sigma \vec{A} = 0 \tag{6.11}$$

From equations 6.5, 6.6, 6.10, and 6.11,

$$\nabla \cdot \sigma \vec{\nabla} \emptyset = 0 \tag{6.12}$$

By using eqns. 6.2, 6.6, 6.9, and 6.10, the induced total current density $\vec{J}$ over the workpiece can be expressed as get Maxwell equation in terms of potential as,

$$\vec{J} = \vec{\nabla} \times \frac{1}{\mu}\left(\vec{\nabla} \times \vec{A}\right) + \sigma \frac{\partial A}{\partial t} + \sigma \vec{\nabla} \emptyset \tag{6.13}$$

After computing the *EM* field, Lorentz force $\vec{f}$ is evaluated at the nodes and added to the mechanical solver. According to Maxwell's equation, the Lorentz force $\vec{f}$ is expressed by

$$\vec{f} = \vec{J} \times \overrightarrow{B_m} = \left(\vec{\nabla} \times \frac{\overrightarrow{B_m}}{\mu}\right) \times \overrightarrow{B_m} \tag{6.14}$$

The explicit mechanical solver computes the deformation of the work-piece with that the new geometry is used to compute the *EM* field in a Lagrangian way.

The boundary condition is given by,

$$\vec{n} \cdot \vec{\nabla} \emptyset = 0 \; on \Gamma \tag{6.15}$$

$$\emptyset = \emptyset_c on \Gamma_c \tag{6.16}$$

$$\vec{n} \times \vec{\nabla} \times \vec{A} = \overrightarrow{A_c} on \Gamma \tag{6.17}$$

$$\vec{n} \times \vec{A} = A_c on \Gamma_c \tag{6.18}$$

where,Γ represents the surface of the coil and tube, Γ_c represents the region where the coil is connected to the external current supply. Equation (*6.15*) states that the gradient of the electric potential is orthogonal to the surface normal$\vec{n}$, while equation (*6.16*) shows that the potential at the coil current input surface is equal to the source potential i.e. connection of the conductor to a voltage source and equation (*6.18*) to the current source

In order to evaluate the constitutive response of the aluminium alloy work piece material, the flow stress is determined as a function of the plastic strain; the strain rate and the temperature using the constitutive equation of Johnson cook [209]

$$\sigma = (A + B(\bar{\varepsilon})^n)(1 + C\ ln\left(\frac{\dot{\bar{\varepsilon}}}{\dot{\varepsilon}_0}\right))\left(1 - \left(\frac{T - T_{room}}{T_{melt} - T_{room}}\right)^m\right) \quad (6.19)$$

Where, $\bar{\varepsilon}$ = equivalent plastic strain,

$\dot{\bar{\varepsilon}}$ = equivalent plastic strain rate,

$\dot{\varepsilon}_0$= reference plastic strain-rate.

In *Eq. (6.19)* the parameter *A* is the initial yield strength of the material at room temperature. The equivalent plastic strain rate $\dot{\bar{\varepsilon}}$ is normalized with a reference strain rate $\dot{\varepsilon}_0$. The expressions in the second and third set of brackets represent the effects of strain rate and temperature, respectively. The equivalent flow stress σ is the product of three factors representing strain hardening, strain rate and temperature. *B*, *C*, *n* and *m* are the five material constants which are determined from the experimental data. Thus to describe the material behaviour the values of the constants *A*, *B*, *C*, *n* and *m* were required.

In the present work, Aluminium alloy *AA* 6061 has been used as worksheet for simulations. The dimensions of the blank were 200 *mm* × 200 *mm*× 1 *mm*. The constitutive parameters required by the *Johnson-Cook* constitutive model are given in *Tables 6.1* and *Table 6.2*. The material properties of the copper coil tool are given in *Table 6.3*.

Table 6.1 Johnson-Cook Parameters for Aluminium alloy.

Density (ρ)	*2700 Kg / m³*	**Johnson-Cook parameters**	
Modulus of rigidity (G)	26 *GPa*	*A*	324 *MPa*
Modulus of Elasticity (E)	68.9 *GPa*	*B*	114 *MPa*
Poisson's Ratio (γ)	0.31	*n*	0.42
Heat Capacity (C)	896 *J / Kg-K*	*C*	0.002
Thermal Conductivity (k)	167 *W / m-K*	T_m	925
Electrical Conductivity (σ)	25 *MS / m*	*m*	1.34

Table 6.2 EOS constants for Aluminium alloy.

C_0	C_1	C_2	C_3	C_4	C_5	C_6	E_0	V_0
0	74.2 *GPa*	60.5 *GPa*	36.5 *GPa*	1.96	0	0	0	1

Table 6.3 Material properties of the copper coil.

Material	Mass Density (kg/m^3)	Electrical conductivity (Ω^{-1}/m^{-1})	Poisson's ratio	Young's Modulus (GPa)
Cu coil	8940	5.96×10^7	0 .31	97

6.2 Simulation Work

The dimension of die fixture assembly actually used in experimental *EMF* process was modelled for the simulation. 5 *mm* entry radius is proposed at bottom of the hollow die for simulation and to save computing time the die was taken as shell elements. As shown in *Fig. 6.1*, the six-turn spiral copper coil tool with 110 *mm* diameter was modelled as solid element and aluminium blank was also modelled as solid element. Resistance, capacitance and induction (*RLC*) values were given according to our *EM* machine specification, i.e. resistance = 50 Ω, capacitance = 90 μF and inductance = 400 nH. Simulation was programed to terminate at 40 *ms* with varying input current voltages. The blank was constrained in a circular pattern to mimic the constraint given by the draw bead of the blank holder to blank in actual experiment.

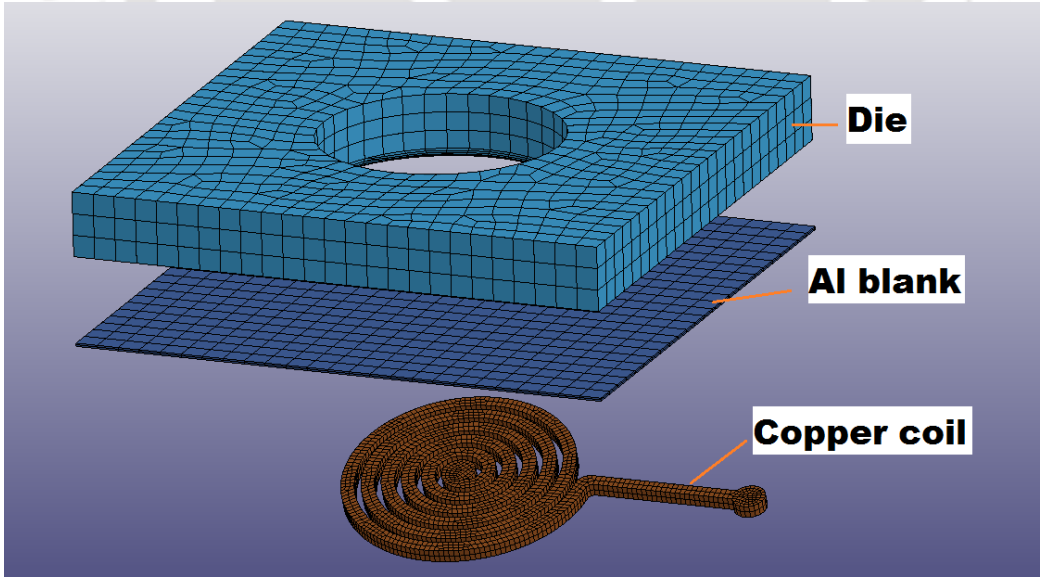

Fig. 6.1 Exploded view of EM free forming assembly used for simulation.

Simulation results of input voltage 8 *kV*is demonstrated in *Fig. 6.2*, *Fig. 6.3*, and *Fig. 6.4*, which shows the fringe pattern of pressure generated in the aluminium blank during various

time step of the simulation run. Initially at around 55 microseconds (*Fig. 6.2)*, the *EM* pressure is at maximum at the centre of the blank. Due to this the centre of the blank experience upward force and result in an upward movement of the central part of the blank creating a dome shape. Around 265 microseconds when the blank attained a full dome height the pressure is shifted to the circumference of the dome i.e. around the die entry corner (*Fig. 6.3*). The magnitude of the peak pressure is around 254 *MPa* while initially at the centre it was 143.5 *MPa*. At the end of the simulation the peak pressure value was found to be around 340.5 *MPa* at some zones around the circumference of the dome. *Fig. 6.4* shows the bottom view of pressure fringe pattern of the blank. From the simulation results we can interpret that the probable region for crack initiation for the aluminium blank would be around the die corner.

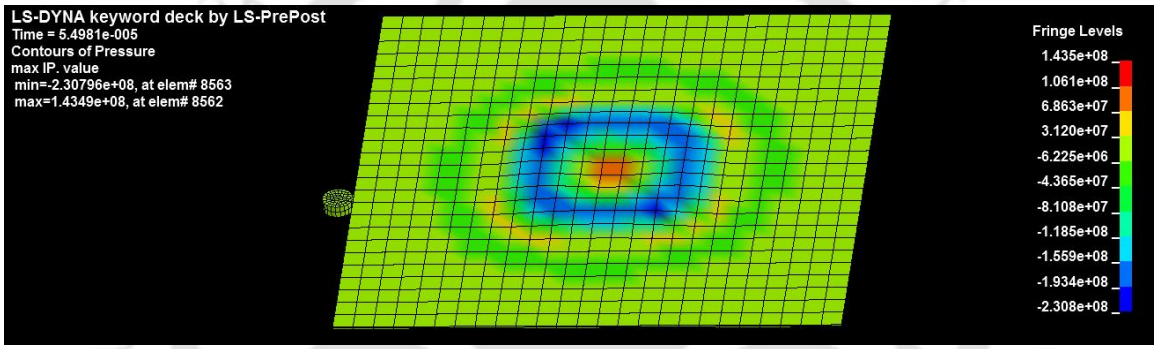

Fig. 6.2 Fringe pattern of electromagnetic pressure on the blank at 54.98 μs.

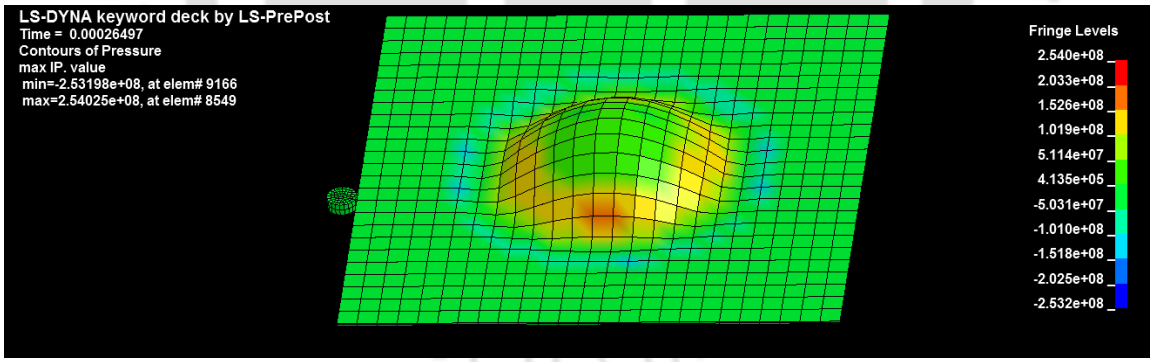

Fig. 6.3 Fringe pattern of electromagnetic pressure on the blank at 264.97 μs.

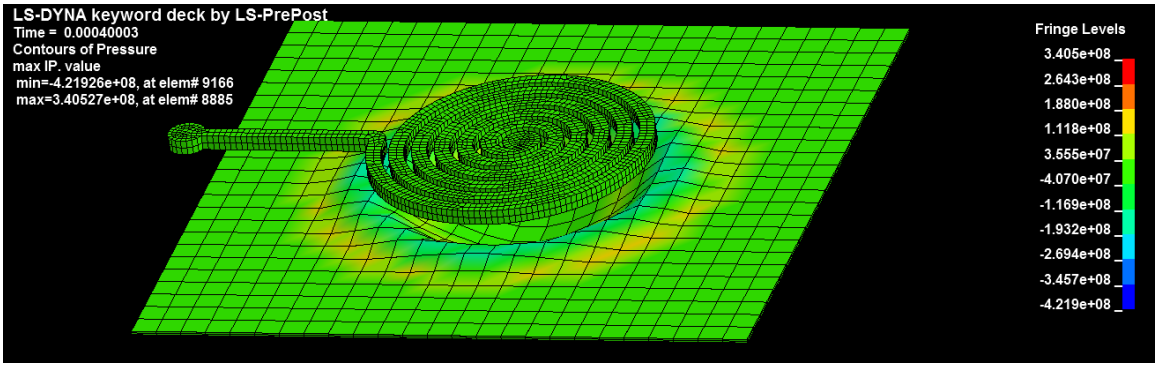

Fig. 6.4 Fringe pattern of electromagnetic pressure on the blank at 400 μs.

The interpretation is further rationalized with the result of *von Mises* stress representation in the blank. The *von Mises* criterion is used for analysing whether the stress combination at a given point will cause failure. In *Fig. 6.5*, the peak *von Mises* stress spread around the blank and die interface. This phenomenon indicates that initial failure will occur first at these regions. The vector representation of Lorenz force acting in the blank are shown in *Fig. 6.6*, in which we can clearly see a highest force value is around some pocket of the dome base.

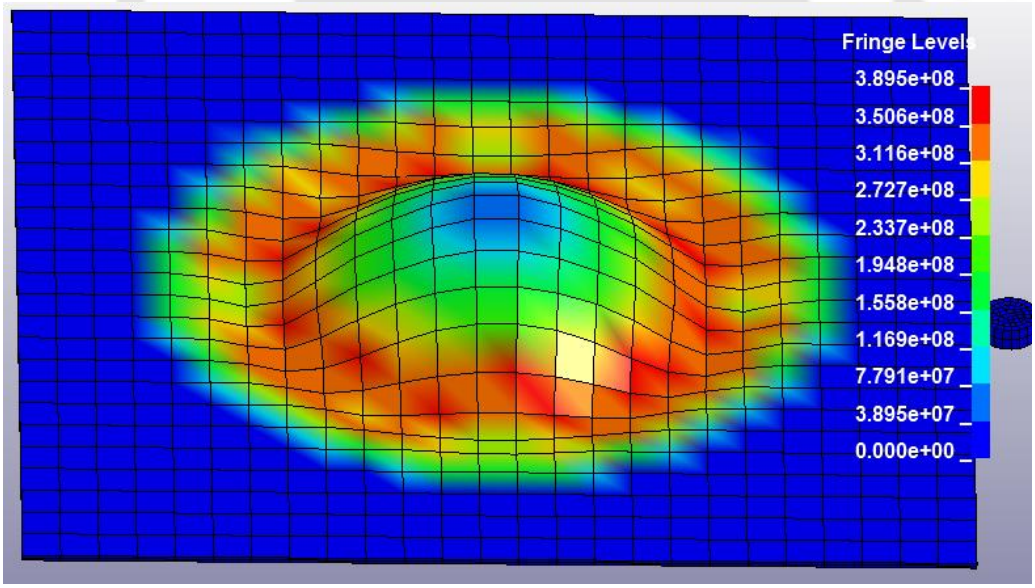

Fig. 6.5 Representation of von Mises stress fringe pattern at the blank.

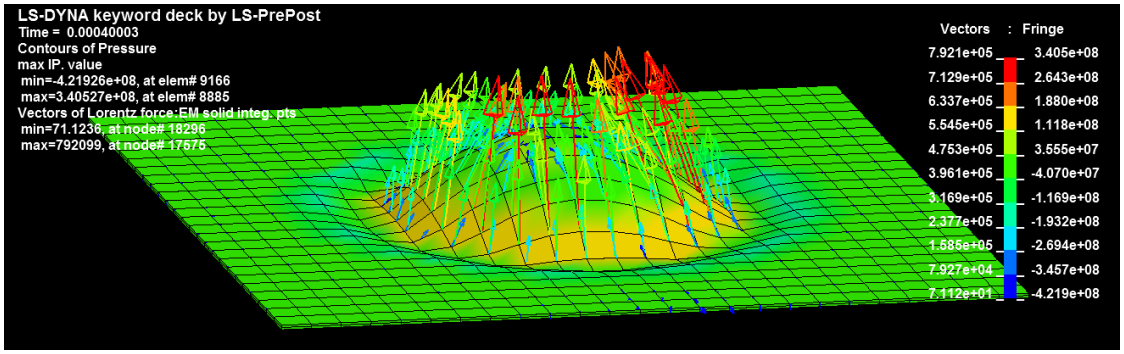

Fig. 6.6 Vector fringe pattern of Lorenz force acting on the blank.

6.3 Experimental Work

The free form die which was used for *EMF* experiment is shown in *Fig. 6.7*. The was bolted down to hold the blank in place with a cast iron base plate and the die is provided with the same entry radius of 5 *mm* which was used in simulation, as shown in *Fig.6.7*. The cavity of the free-form die was open to the atmosphere eliminating the requirement to evacuate the die chamber. To constraint the movement of the aluminium blank draw bead with a height of 3.5 *mm* was provided in a circular dimension on the lower part of die itself.

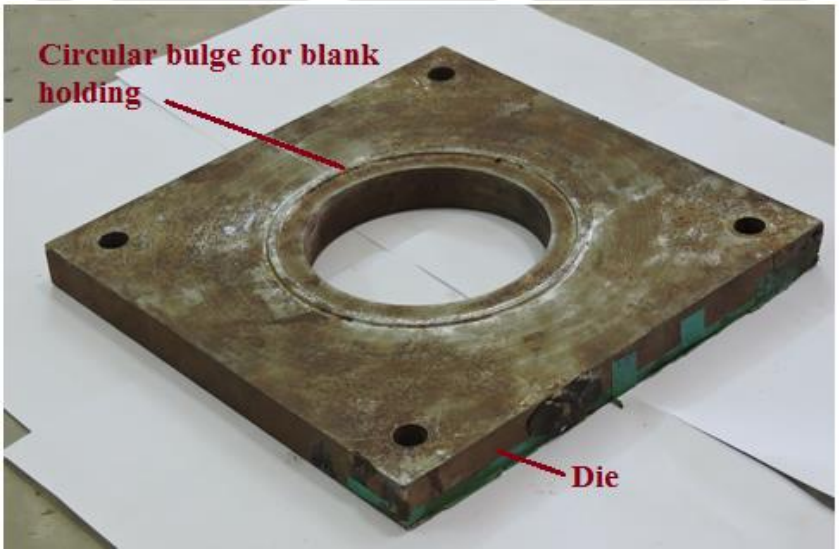

Fig. 6.7 Die cum blank holder.

The material tested was *AA* 6061 sheet cut into dimension of 200 × 200 × 1 *mm*. The stock material provided was graded *T6*, which is solution *heat-treated* then artificially aged.

The blanks were deformed at increasing voltages to obtain safe, necked and fractured parts. The energy levels are selected in terms of percentage output corresponding to total energy output of the machine, as it is easy to categorized energy level rather than specific voltage selection in the existing *EMF* machine (*Table 6.4*). So, the range of output charge voltages was from 7.7 *kV* to 12.75 *kV* which were utilized to obtain deformation height.

Table 6.4 Experimental process parameters.

Sl. No.	Material	Energy (kJ)	Charge voltage (kV)	Bulge height (mm)	Failure /safe
1	*AA* 6061	2.6 (50 %)	7.7	14	safe
2	*AA* 6061	3.7 (60 %)	9.4	18.5	safe
3	*AA* 6061	5.2 (70 %)	10.1	23.4	safe
4	*AA* 6061	6.4 (80 %)	11.7	28	Crack initiation at base.
5	*AA* 6061	6.9 (85 %)	12.75	36.5	Partial shear failure at the base.
6	*AA* 6061	7.1 (86 %)	12.88	_	Complete shearing at base.

The dome height of the blank increases with the corresponding increase in applied voltage. *Fig. 6.8* shows deformed samples at different voltage level. There was no wrinkling around the dome base as enough blank holding pressure was generated by the die. At voltage 11.7 *kV* crack initiation takes place around the base corner of the dome.

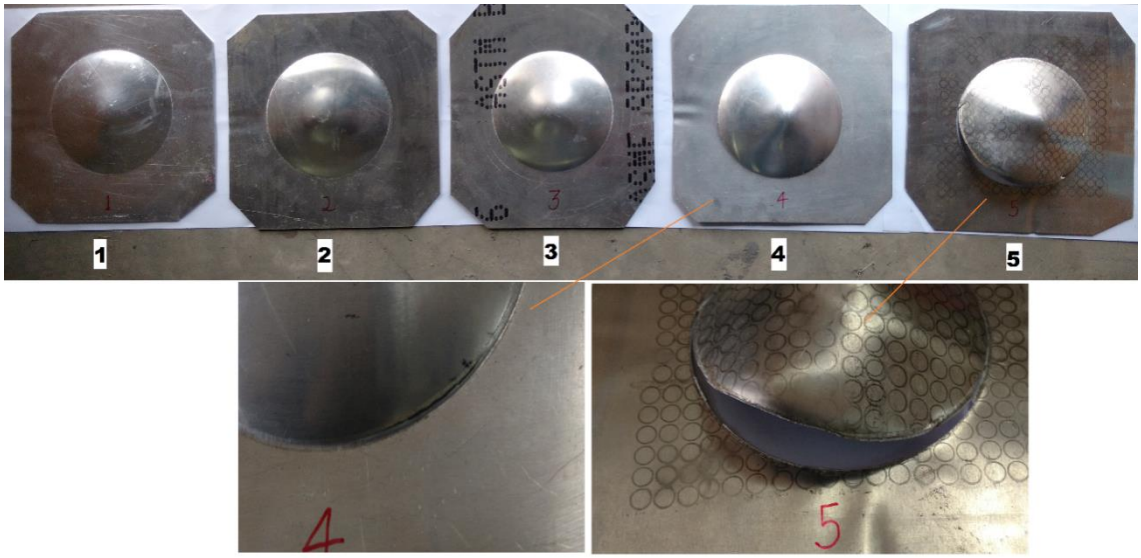

Fig. 6.8 Deformed blanks at various voltages.

As predicted in the simulation result maximum surface pressure occurs in this region. Extreme pressure and relatively sharp edge of die entry radius contribute excessive shear stress in the region. Further increase in voltage resulted in shearing of the blank at the bottom of the dome, which can be seen at 12.75 *kV*. Finally, at 12.88 *kV* the aluminium blank experienced a complete failure or shearing from the dome base area (*Fig. 6.9*).

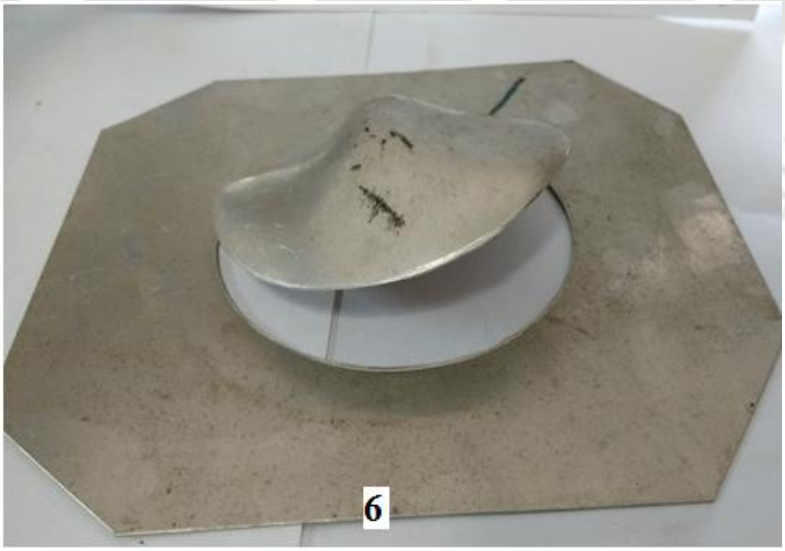

Fig. 6.9 Shearing of the blank at 12.88 kV.

6.4 Summary

Successful simulation result was obtained in *LS Dyna FEM* software to predict the failure region of *EM* sheet forming. With the help of simulation result correct prediction of failure region were obtained with respect to die entry radius. From the simulation result which indicated maximum pressure and stress occurs will occur at the base of the dome for 5 *mm* die entry radius, which was validated with experimental results. For experimental validation *AA* 6061 was free formed by electromagnetic forming machine. In experimental result shear failure of the blank occur at the base of the dome similar to the simulation result. The failure of the blank at base of the dome is due to the extreme shear stress generated between blank and die cavity opening.

Chapter 7

Conclusions and Future Scopes

7 Conclusions and Future Scopes

7.1 Conclusions

The research reported in this thesis shed light on the weldability and formability characteristics of two different types of aluminium alloys i.e. a non-heat-treatable aluminium alloy (*AA* 5052-*H32*) and another a heat treatable alloy (*AA* 6061-*T6*). These alloys have major application in the field of automobile production. With the arrival of innovating manufacturing concept like tailor welded blanks attempts were made to produce tailor welded blanks with *AA* 5052-H32 and *AA* 6061-T6 material by joining together with friction stir welding. Subsequently effect of high speed forming on the formability of the tailor welded blanks by electromagnetic forming was investigated. The detailed conclusion in the form of summary is given at the end of individual chapters. Therefore, in this final chapter, the main overall conclusions and contribution of the thesis are presented. The main overall conclusions are as follows:

1. Defect free friction stir welding of different grade *AA* 5052-*H32* to *AA* 6061-*T6* can be achieved in thicknesses of 1 *mm* and 1.5 *mm* respectively. The optimum process parameters are tool rotational speed of 1500 *rpm* and welding speed of 63 *mm/min* and 98 *mm/min*. All the tensile test samples fractured at weld zone near *AA* 5052 alloy. During welding intermetallic compounds were formed in weld zone which contribute negatively in the fracture strength of the joint.

2. Successful friction stir welding of different thickness blanks with thickness combination of 1 *mm* to 1.5 *mm* were obtained for *AA* 5052 -*H32* and *AA* 6061-*T6* respectively. Tool rotational speed of 1500 *rpm* and tool traverse speed of 36, 63 and 98 *mm/min* were the parameters for successful weld joint. All the weld samples fractured at weld zone near thinner 1 *mm* side during tensile testing.

3. Orientation of weld line during *EM* forming of different grade *TWB* shows significant change in formability. For *AA* 5052 to *AA* 6062 combination *TWB*, bulge test show more dome height obtained when weld line is offset by 25 *mm*

towards *AA* 6062. Further, with *EMF* process the height achieved by *TWB* is greater compared to conventional process. Dome heights attained by *TWB* are lesser than that of the base materials in both conventional and *EMF* process respectively. There is a significant increase in *FLC* of *TWB* which was formed by *EMF* process from that of conventional process.

4. *EMF* process gives more deformation than the conventional quasi-static process for different thickness *TWB* of *AA* 5052. The thickness combination was of 1 *mm* to 1.5 *mm*. Base materials also showed the same trend of increase formability with *EMF* process. Also, the *FLC* obtained from welded blanks formed by *EMF* process shows significant increase in magnitude as compared to quasi-static process. Hence, high velocity forming process increases the formability of both base and *TWBs*.

5. Optimum die design can be conceptualized using commercially available *FEM* software *LS Dyna*. The software was used to predict the failure region of *EM* sheet forming with respect to die entry radius. The simulation result was successfully validated with experiment.

7.2 Future Scopes

For the continuation of current work in to future we can look into both welding and high speed forming area. In welding area the tailor welded blanks made by different welding technique like laser, tungsten inert welding and friction stir welding can be further analysed and compared. The choice of material thickness and grade combination should be appropriate. Combination of different welding techniques to join a particular tailor welded blank would be an interesting field to study. For high speed forming processes, the welded blanks in the present work can be deformed and compared with Electro-hydraulic forming and explosive forming techniques. The dynamic behaviour of *FSWed* blanks at high speed can be studied by using finite element method. Further a practical car body part can be fabricated by combining friction stir welding and electromagnetic forming process.

References

1. Wilson, D. V., 1988. Aluminium versus steel in the family car-The formability factor. Journal of Mechanical Working Technology, v.16, pp. 257-277.

2. Mori, T., Hino, M., Iwaya, J. and Miyahara, M., 1992. Press formability of aluminum alloy sheets for automobile parts. KOBELCO Technology Review, n.14, pp. 49-53.

3. Miller, W. S., 2000. Recent development in aluminium alloys for the automotive industry. Materials Science and Engineering A, A280, pp. 37- 49.

4. Ezra A. A., 1973. Principles and Practices of Explosive Metallurgy, Metal Working. Industrial Newspapers Ltd., London.

5. Fengman He, Zheng Tong, Ning Wang and Zhiyong Hu, 2000. Explosive forming of thin-walled semi-spherical parts, Materials Letters, Vol. 45, pp. 133-137.

6. Golovashchenko, S. F., Gillard, A.J., Cedar, D.A., Illnich, A.M., 2009. Electrohydraulic forming tool. United States Patent 7,516,634 B1, 1–11.

7. Balanethiram, V. S., Daehn, G.S., 1992. Enhanced formability of interstitial free ironat high-strain rates. Scripta Metall. Mater. 27, 1783–1788.

8. Balanethiram, V. S., Daehn, G.S., 1994. Hyperplasticity – Increased forming limits at high workpiece velocity. Scripta Metall. Mater. 30, 515–520.

9. Rohatgi, A., Stephens, E. V., Soulami, A., Davies, R. W., Smith, M. T., 2010. High-strainrate forming of aluminum and steel sheets for automotive applications. In: Kolleck, R. (Ed.), International Deep Drawing Group (IDDRG). Graz, Austria, pp. 441–450.

10. Rohatgi, A., Stephens, E. V., Davies, R. W., Smith, M. T., Soulami, A., and Ahzi, S., 2012. Electro-hydraulic forming of sheet metals: Free-forming vs. conical-die forming. Journal of Materials Processing Technology, 212, pp. 1070–1079.

11. Maxwell, J. C., 1873. A Treatise of Electricity and Magnetism. Macmillan and Co. Publishers to the University of Oxford.

12. Conway, J. T., 2001. Exact solutions for the magnetic fields of axisymmetric solenoids and current distributions, IEEE transactions, Vol. 37, no.4, pp. 2977-2988.

13. Wilson, F. W., 1964. High-velocity forming of metals. Prentice-Hall Inc.

14. Jablonski, J. and Winkler R., 1978. Analysis of the electromagnetic forming process, Int. J. Mech. Sci., Vol. (20), pp. 315-325.

15. Heaviside, O., 1951. Electromagnetic theory. The Complete & Unabridged Edition.

16. Belyy, L. V., Fertik, S. M., Khimenko, L. T., 1977. Electromagnetic Metal Forming Handbook. (English translation by Altynova, M. M.) http://www.mse.eng.ohiostate.edu/~Daehn/metalforminghb/index.html.

17. Loschmann, F., Putz, M., Koch, T., 2006. Perspective accuracy requirements in the Automotive. In: Proceedings of the 2nd International Conference on Accuracy in Forming Technology—ICAFT06, Chemnitz, pp. 9–24.

18. Welleman, A., Fleischmann, W., 2006. High power semiconductor devices and solid state switches for pulsed discharge applications. In: Proceedings of the 2nd International Conference on High Speed Forming—ICHSF 2006, Dortmund, pp. 239–248, online available at https://eldorado.tudortmund.de/handle/2003/27056.

19. Psyk, V., Beerwald, C., Henselek, A., Homberg, W., Brosius, A., Kleiner, M., 2007. Integration of electromagnetic calibration into a deep drawing process of an industrial demonstrator part. Key Engineering Materials 344, 435–442.

20. Daehn, G. S., Vohnout, V. J., Herman, E. A., 2000. Hybrid matched tool-electromagnetic forming apparatus incorporating electromagnetic actuator. US-Patent, 6, 128, 935.Daehn, G. S., 2003. High velocity metal Forming, Draft for publication in ASM Handbook (2003/2004).

21. Plum, M., 1988. Electromagnetic forming. ASM Handbook Forming and Forging 14, 644–653.

22. Saha, P. K., 2005. Electromagnetic forming of various aircraft components. SAE Technical Papers 114, 999–1009, part 1 S.

23. Bruno, E. J., 1968. Editor, High-velocity forming of metals, American Society of Tool and Manufacturing Engineers, Dearborn, MI.

24. Weimar, G., 1963. High speed machining III- transformation from cough up and tubes by magnetic personnel. Workshop and business 96 (12),893–900.

25. Kleiner, M., Geiger, M., Klaus, A., 2003. Manufacturing of lightweight components by metal forming. CIRP Annals-Manufacturing Technology 52, 521–542.

26. Thyssen Krupp AG, 2013. www.tailored-blanks.com/en/products/tailored products .html (17.06.13).

27. Zadpoor, A. A., Sinke, J., Benedictus, R., 2007. Mechanics of tailor welded blanks: an overview. Key Engineering Materials 344, pp. 373–382.

28. Bruhn, E. F., 1971. Analysis and Design of Flight Vehicle Structures.

29. Staud, D., Merklein, M., Fratini, L., Buffa, G., 2007. Investigations on the mechanical properties and formability of friction stir welded and laser welded aluminium tailored blanks. Key Engineering Materials, 344, pp.143–150.

30. Dawes, C., Thomas, W., 1995. TWI Bulletin 6, November/December, p. 124.

31. Rhodes, C. G.,Mahoney, M. W., Bingel, W. H., Spurling, R. A.,Bampton, C. C., Scripta Mater. 36 (1997) 69.

32. Mishra, R. S., Ma, Z. Y., 2005. Friction stir welding and processing, Materials Science and Engineering, R 50, pp.1–78.

33. Sato, Y. D., Kokawa, H., 2003. Friction stir welding (FSW) process, Welding International, 17 (11), pp. 852-853.

34. Liu, G., Murr, L. E.,Niou, C. S., McClure, J. C., Vega, F. R., Scripta Mater. 37 (1997) 355.

35. Thomas, W. M., Nicholas, E. D., Smith, S. D., 2001. Aluminum automotive and joining sessions, TMS, 2001, pp. 213.

36. Guerra, M., McClure, J. C., Murr, L. E., Nunes, A. C., 2001. Friction stir welding and processing, TMS, Warrendale, PA, USA, pp. 25.

37. Colligan, K., 1999. Material flow behaviors during friction stir welding of aluminum. Weld. J., 78, pp. 229S–237S.

38. Ma, Z. Y., Mishra, R. S., Mahoney, M. W., 2003. Friction stir welding and processing II, TMS, pp. 221–230.

39. Sato, Y.S., Kokawa, H., Enomoto, M., Jogan, S., 1999. Microstructural evolution of 6063 aluminum during friction-stir welding. Metall. Mater. Trans. A 30, pp. 2429–2437.

40. Murr, L. E., Li, Y., Flores, R. D., Trillo, E. A., 1998. Mater. Res. Innovat. 2, 150.

41. Charit, I., Mishra, R.S., 2004. Evaluation of microstructure and superplasticity in friction stir processed 5083 Al alloy. J. Mater. Res. 19, 3329–3342.

42. Sato, Y. S., Park, S. H. C., and Kokawa, H., 2001. Microstructural factors governing hardness in friction-stir welds of solid-solution-hardened Al alloys. Metallurgical and Materials Transactions A, vol. 32, pp. 3033-3042.

43. Mahoney, M. W., Rhodes, C. G., Flintoff, J. G., Spurling, R. A.,Bingel, W. H., Metall. Mater. Trans., A 29, pp. 1955.

44. Scialpi, A., De Giorgi, M., De Filippis, L. A. C., Nobile, R., and Panella, F. W., 2008, Mechanical analysis of ultra-thin friction dtir welding joined sheets with dissimilar and similar materials, Mater. Des., 29(5), pp. 928–936.

45. Rodrigues, D. M., Loureiro, A., Leitao, C., Leal, R. M., Chaparro, B. M., and Vilaca, P., 2009. Influence of friction stir welding parameters on the microstructural and mechanical properties of AA 6016-T4 thin welds. Mater. Des., 30(6), pp. 1913–1921.

46. Leal, R. M., Leit~ao, C., Loureiro, A., Rodrigues, D. M., and Vilac, P., 2008. Material flows in heterogeneous friction stir welding of thin aluminium sheets: effect of shoulder geometry. Mater. Sci. Eng., 498(1–2), pp. 384–391.

47. Patel, V. V., Sejani, D. J., Patel, N. J., Vora, J. J., Gadhvi, B. J., Padodara, N. R., and Vamja, C. D., 2016. Effect of tool rotation speed on friction stir spot welded AA5052-H32 and AA6082-T6 dissimilar aluminum alloys. Metallogr. Microstruct. Anal., 5(2), pp. 142–148.

48. Wagner, H. J., and Boulger, F. W., 1960. High velocity metalworking processes based on the sudden release of electrical of electrical energy. Memorandum prepared by the Battle Memorial Institute for the Defence Metals Information Center.

49. Harvey, G.W., Brower, D.F., 1958. Metal Forming Device and Method. US-Patent Nr. 2976907.

50. Wood, W.W., et al, 1963. Chance-Vought Corp., Dallas, TX, Report no. ASD-TDR-63-7-871, AD 416412.

51. Tobe, T., Kato, M. and, Obara, H., 1979. Mechanical properties at high rates of strain, J. Harding (ed.), Institute of Physics, London, Conf. ser. 47, 383.

52. Kobayashi, A., Nakao, A., Hashimoto, S. and, Zhou, Q., 1988. Journal de physique, Colloque C3, Supplement 9, c3-29.

53. Winter, R. E., 1979. In mechanical properties of high rates of strain, J. Harding (ed.), Institute of physics, London, Conf. ser, 47, 81.

54. Takatsu, N., Kato, M., Soto, K. and, Tobe, T., 1988. High-speed forming of metal sheets by electromagnetic force. JSME International Journal, Series III, Vol. 31, No. 1, pp. 142-148.

55. Daehn, G. S.,Vohnout, V. J. and, DuBois, L., 1999. Improved formability with electromagnetic forming: fundamentals and a practical example, sheet metal forming technology. The Minerals, Metals & Materials Society, pp.105-116.

56. Jablonski, J., and Winkler, R., 1978. Analysis of the Electromagnetic forming process, Int. J. Mech. Sci., Vol. 20(5), pp. 315-325.

57. Seth, M. and, Daehn, G., 2005. Effect of aspect ratio on high velocity formability of aluminum alloy. Trends in Materials and Manufacturing Technologies for Transportation Industries, TMS.

58. Hu, X., and Daehn, G. S., 1996. Effect of velocity on localization in uniaxial tension.ActaMaterialia, Vol. 44, pp.1021-1033.

59. Hassani, S. T. S., Duncan, J. L., and Johnson, W., 1969. Techniques for designing electromagnetic forming coils. Proc. Second International Conference on High Rate Forming, Colorado, USA, pp. 5.1.2 -5.1.16.

60. Yudaev, V. D., 1989. Manufacture of large sheet-metal parts by incremental electromagnetic forming, Kuznechno-ShtampovochnoeProizvodstvo ~Forging and Stamping Industry Journal, **7**, pp. 1–2.

61. Vohnout, V. S., 1998. A hybrid quasi-static/dynamic process for forming large sheet metal parts from aluminum alloys. Ph.D. thesis, The Ohio State University.

62. Oliveira, D. A., and Worswick, M. J., 2003. Electromagnetic forming of aluminum alloy sheet. J. Phys. IV, 110, EDP Sciences, Les Ulis, DOI: 10.1051/jp4:20030709, pp. 293–298.

63. Imbert, J., Winkler, S., Worswick, M., Oliveira, D., and Golovashchenko, S., 2005. The effect of tool-sheet interaction on damage evolution in electromagnetic forming of aluminum alloy sheet, Journal of Engineering Materials and Technology, vol. 127, no. 1, pp. 145-153.

64. Padmanabhan, M., 1997. Wrinkling and springback in electromagnetic sheet metal forming and electromagnetic ring compression, Ph.D. dissertation, The Ohio State University.

65. Ning Li, Haiping Yu, Zhu Xu, Zhisong Fan, Lin Liu, 2016. Electromagnetic forming facilitates the transition of deformation mechanism in 5052 aluminum alloy, Materials Science & Engineering, A 673, pp. 222–232.

66. Kamal, M., Shang, J., Cheng, V., Hatkevich, S. and, Daehn, G., 2001. Agile manufacturing of a micro-embossed case by a two-step electromagnetic forming process. Journal of Materials Processing Technology, vol. 190 -1, pp. 41-50.

67. Golowin, S., Kamal, M., Shang, J., Portier, J., Din, A., Daehn, G. S., Bradley, J. R., Newman, K. E. and Hatkevich, S., 2007. Application of a uniform pressure actuator for electromagnetic processing of sheet metal. Journal of Materials Engineering and Performance, vol. 16, no. 4, pp. 455-460.

68. Noh, H. G, Song, W. J, Kang, B. S, Kim, J., 2015. Two-step electromagnetic forming process using spiral forming coils to deform sheet metal in a middle-block die. Int J AdvManuf Technol,76, pp. 1691-97.

69. Li, F., Mo, J., Li, J., Zhao, J., 2016. Formability evaluation for low conductive sheet metal by novel specimen design in electromagnetic forming. Int J AdvManufTechnol doi:10.1007/s00170-016-8893-9.

70. Xiaohui Cui, Jianjun Li, Jianhua Mo, Jinxiu Fang, Bo Zhou, Xiaoting Xiao, 2016. Effect of the sheet thickness and current damping exponent on the optimum current frequency in electromagnetic forming. Int J AdvManufTechnol, 85, pp. 843-851.

71. Mamalis,A., Manolakos, D., Kladas, A. and, Koumoutsos, A., 2004. Electromagnetic forming and powder processing: Trends and developments, Applied Mechanics Reviews, vol. 57, no. 4, pp. 299-324.

72. Psyk, V., Risch, D., Kinsey, B., Tekkaya, A. and Kleiner, M., 2011. Electromagnetic forming|a review. Journal of Materials Processing Technology, vol. 211, no. 5, pp. 787-829.

73. Rooks, B., 2001. Tailor-welded blanks bring multiple benefits to car design. Assembly Automation, vol. 21, pp. 323-328.

74. Kusuda, H., Takasago, T., and Natsumi, F., 1997. Formability of tailored blanks. Journal of Materials Processing Technology, vol. 71, pp. 134-140.

75. Merklein, M., Johannes, M., Lechner, M. and, Kuppert, A., 2014. A review on tailored blanks—Production, applications and evaluation. Journal of Materials Processing Technology 214, pp. 151– 164.

76. Montgomery, A., Wild, P., and Clapham, L., 2004. Defect characterization using magnetic flux leakage inspection of tailor-welded blanks. Insight, vol. 46, pp. 260-264.

77. T. W. B. P. Team, 2001, Tailor welded blank applications and manufacturing - a state of the art survey, Auto-Steel Partnership.

78. Stasik, M.C., Wagoner, R.H., 1998. Forming of tailor-welded aluminum blanks. Int. J. Form. Process., 1, 9–34.

79. Zhao, H., White, D. R., and DebRoy, T., 1999. Current issues and problems in laser welding of automotive aluminium alloys. International Materials Reviews, vol. 44, pp. 238- 266.

80. Cao, X., Wallace, W., Poon, C., and Immarigeon, J. P., 2003. Research and progress in laser welding of wrought aluminum alloys. I. Laser welding processes. Materials and Manufacturing Processes, vol. 18, pp. 1-22.

81. Cao, X., Wallace, W., Immarigeon, J. P., andPoon, C., 2003. Research and progress in laser welding of wrought aluminum alloys. II. Metallurgical microstructures, defects, and mechanical properties. Materials and Manufacturing Processes, vol. 18, pp. 23-49.

82. Daeyong K., Wonoh, L., Junehyung, K., Kyung-Hwan, C., Chongmin, K., Kazutaka, O., Wagoner, R. H., Kwansoo, C., 2010. Macroperformance evaluation of friction stir welded automotive tailor welded blank sheets: part II—formability. Int J Solids Struct 47(7–8):1063–1081, ISSN 0020–7683.

83. Staud, D., Merklein, M., Fratini, L., Buffa, G., 2007. Investigations on the mechanical properties and formability of friction stir welded and laser welded aluminium tailored blanks. Key Engineering Materials, 344, pp. 143–150.

84. Taban, E. and Kaluc, E., 2007. Comparison between microstructure characteristics andjoint performance of 5086-H32 aluminium alloy welded by MIG, TIG and friction stir welding processes. Kovove Mater., 90 (262), pp. 11–14.

85. Malarvizhi, S. andBalasubramaniam, V., 2011. Effect of welding processes on AA2219 aluminium alloy joint properties.Trans. Nonferrous Met.Soc. China, vol. 21, pp. 962-973.

86. Thomas, W. M., Nicholas, E. D, Needham, J. C, Murch, M. G, Templesmith, P., Dawes, C.J., G.B. Patent Application No. 9125978.8 (December 1991).

87. Tang, W.,Guo, X., McClure, J. C., and Murr, L. E., 1999. Heat input and temperature distribution in friction stir welding. Journal of Materials Processing and Manufacturing Science, vol. 37, pp. 163-172.

88. Mahoney, M. W., Rhodes, C. G., Flintoff, J. G., Spurling, R. A., and Bingel, W. H., 1998. Properties of friction-stir-welded 7075-T651 aluminum. Metallurgical and Materials Transactions A, vol. 29, pp. 1955-1964.

89. Reynolds, A. P., Lockwood, W. D., and Seide, T. U., 2000. Processing property correlation in friction stir welds. Material Science Forum, 331-337, pp. 1719-1724.

90. Rhodes, C. G., Mahoney, M. W., Bingel, W. H., Spurling, R. A., Bampton, C. C., 1997. Effect of friction stir welding on microstructure of 7075 aluminum. Scripta Mater.,36(1), pp. 69–75.

91. Liu, G., Murr, L. E., Niou, C. S., McClure, J. C., Vega, F. R., 1997. Microstructural aspects of the friction-stir welding of 6061-T6 aluminum. Scripta Mater, 37(3), pp. 355–61.

92. Thomas, W. M., Johnson, K. I., Wiesner, C. S., 2003. Friction stir welding-recent developments in tool and process technologies. AdvEng Mater.,5, pp. 485–90.

93. Thomas, W. M., 2003. Friction stir welding – recent developments. Mater Sci Forum, 426–432, pp. 229–36.

94. Thomas, W. M., Nicholas, E. D., Smith, Das, S. K., Kaufman, J. G., Lienert, T. J.,2001. Aluminum 2001—Proceedings of the TMS 2001 Aluminum Automotive and Joining Sessions, TMS, pp. 213.

95. Nandan, R., DebRoy, T., Bhadeshia, H.K.D.H., 2008. Recent advances in friction-stir welding – Process, weldment structure and properties. Progress in Materials Science, 53, pp. 980–1023.

96. McClure, J., Tang, W., Murr, L. E., Guo, X., Feng, Z., Gould, J. E., 1998. A thermal model for friction stir welding. Trends in welding research. Ohio, USA: ASM International; pp. 590–5.

97. Jata, K. V., Semiatin, S. L., 2000. Continuous dynamic recrystallization during friction stir welding. Scripta Mater, 43, pp. 743–8.

98. Masaki, K., Sato, Y. S., Maeda, M., Kokawa, H., 2008. Experimental simulation of recrystallized microstructure in friction stir welded Al alloy using a plane-strain compression test. Scripta Mater, 58, pp. 355–60.

100. Zhang, H. W., Zhang, Z., Chen, J. T., 2005. Effect of angular velocity of pin on material flow during friction stirs welding. ActaMetall Sin, 41, pp. 853–9.

101. Khandkar, M. Z. H., Khan, J. A., Reynolds, A. P., 2003, Prediction of temperature distribution and thermal history during friction stir welding: input torque based model. SciTechnol Weld Join,8, pp.165–74.

102. Svensson, L. E., Karlsson, L., Larsson, H., Karlsson, B., Fazzini, M., Karlsson, J., Microstructure and mechanical properties of friction stir welded aluminium alloys with special reference to AA 5083 and AA 6082. SciTechnol Weld Join, 5(5), pp. 285–96.

103. Lockwood, W. D., Tomaz, B., Reynolds, A. P., 2002. Mechanical response of friction stir welded AA 2024: experiment and modeling. Mater. Sci. Eng. A 323, pp. 348–353.

104. Sutton, M., Reynolds, A., Wang, D. Q., Hubbard, C., 2002. A study of residual stresses and microstructure in 2024-T3 aluminum friction stir butt welds. J Eng Mater Technol Trans ASME, 124(2), pp. 215–21.

105. Genevois, C., Deschamps, A., Denquin, A., DoisneauCottignies, B., 2004. Quantitative investigation of precipitation and mechanical behaviour for AA2024 friction stir welds. Acta Mater. 53 (8), pp. 2447–2458.

106. Jones, M. J., Heurtier, P., Desrayaud, C., Montheillet, F., Allehaux, D., Driver, J.H., 2005. Correlation between microstructure and microhardness in a friction stirwelded 2024 aluminium alloy. Scr. Mater., 52, pp. 693–697.

107. Yan, J., M. A., Reynolds, A. P., 2006. Notch tensile response of mini-regions in AA 2024 and AA 2524 friction stir welds. Materials Science and Engineering A, vol. 427, pp. 289-300.

108. Fu, R. D., Zhang, J. F., Li, Y. J., Kang, J., Liu, H. J., Zhang, F. C., 2013. Effect of welding heat input and post-welding natural aging on hardness of stir zone for friction stir-welded 2024-T3 aluminum alloy thin sheet. Mater. Sci. Eng., A 559, pp. 319–324.

109. Zhang, Z., Xiao, B. L., Ma, Z. Y., 2014. Influence of water-cooling on microstructure and mechanical properties of friction stir welded 2014 Al-T6 joints. Mater. Sci. Eng., A 614, pp. 6–15.

110. Fonda, R. W., Bingert, J. F., 2006. Precipitation and grain refinement in AA 2195 Alfriction stir weld. Metall. Mater. Trans., A 37, pp. 3593–3604.

111. Elangovan, K., Balasubramanian, V., 2008. Influences of tool pin profile and welding speed on the formation of friction stir processing zone in AA 2219 aluminium alloy. J Mater Process Technol, 20, pp. 163–75.

112. Jie, L. H., Jie, Z. H., Xian, H. Y., Lei, Y., 2010. Mechanical properties of underwater friction stir welded 2219 aluminium alloy. Trans Nonferrous Met. Soc. China, 20, pp. 1387–1391.

113. Zhang, Z., Xiao, B. L., Ma, Z. Y., 2012. Effect of welding parameters on microstructure and mechanical properties of friction stir welded 2219 Al-T6 joints. J. Mater.Sci., 47, pp. 4075–4086.

114. SreeSabari, S., Balasubramanian, V., Malarvizhi, S., Madusudhan Reddy, G., 2015. Influence of post weld heat treatment on tensile properties of friction stir welded AA 2519-T87 aluminium alloy joints. J. Mech. Behav. Mater., 24, pp. 195–205.

115. Rodrigues, D. M., Loureiro, A., Leitao, C., Leal, R. M., Chaparro, B. M., Vilaça, P., 2009. Influence of friction stir welding parameters on the microstructural and mechanical properties of AA 6016-T4 thin welds. Mater Des, 30(6), pp. 1913–1921.

116. Cavaliere, P., Squillace, A., Campanile, G., Panella, F., 2006. Effect of welding parameters on mechanical and microstructural properties of AA 6056 joints produced by friction stir welding. J. Mater. Process. Technol., 180, pp. 263–270.

117. Cabibbo, M., McQueen, H.J., Evangelista, E., Spigarelli, S., Di Paola, M., Falchero, A., 2007. Microstructure and mechanical property studies of AA 6056 friction stir welded plate. Mater. Sci. Eng., A 460–461, pp. 86–94.

118. Shigematsu, I., Suzuki, K., Imai, T., Kwon, Y. J., Saito, N., 2005. Friction stir welding of recycled AA 6061 aluminum plates fabricated by hot-extrusion of machined chips. J Mater Sci, 40(11), pp. 2971−2974.

119. Soundararajan, V., Zekovic, S., Kovacevic, R., 2005. Thermo-mechanical model with adaptive boundary conditions for friction stir welding of Al 6061. Int. J. Mach. Tools Manuf., 45, pp. 1577–1587.

120. Dinaharan, I., Murugan, N., Parameswaran, S., 2012. Developing an empirical relationship to predict the influence of process parameters on tensile strength of friction stir welded AA 6061/0–10 wt% ZrB2 in situ composite. Trans Indian Inst Met, 65(2), pp. 159–70.

121. Heidarzadeh, A., Khodaverdizadeh, H., Mahmoudi, A., Nazari, E., 2012. Tensile behavior of friction stir welded AA 6061-T4 aluminum alloy joints. Mater Des, 37, pp. 166–73.

122. Trueba Jr., L., Heredia, G., Rybicki, D., Johannes, L. B., 2015. Effect of tool shoulder features on defects and tensile properties of friction stir welded aluminum 6061-T6. Journal of Materials Processing Technology, 219, pp. 271–277.

123. Sato, Y.S., Kokawa, H., 2001. Distribution of tensile property and microstructure in friction stir weld of 6063 aluminum. Metall. Mater. Trans.,A 32, pp. 3023–3031.

124. Imam, M., Racherla, V., Biswas, K., 2014. Effect of post-weld naturalaging on mechanical and microstructural properties of friction stir welded 6063-T4 aluminium alloy. Mater. Des., 64, pp. 675–686.

125. Cavaliere, P., Squillace, A., Panella, F., 2008. Effect of welding parameters on mechanical and microstructural properties of AA 6082 joints produced by friction stir welding. Journal of Materials Processing Technology, vol. 200, pp. 364-372.

126. Scialpi, A., De Filippis, L.A.C., Cavaliere, P., 2007. Influence of shoulder geometry on microstructure and mechanical properties of friction stir welded 6082 aluminium alloy. Mater. Des., 28, pp. 1124–1129.

127. Kim, D., Lee, W., Kim, J., Kim, C., Chung, K., 2010. Formability evaluation of friction stir welded 6111-T4 sheet with respect to joining material direction. Int J MechSci, 52(4), pp. 612–625.

128. Gaafer, A. M., Mahmoud, T. S., Mansour, E. H., 2010. Microstructural and mechanical characteristics of AA 7020-O Al plates joined by friction stir welding. Mater SciEng, 527, pp. 7424–9.

132. Jata, K. V., Sankaran, K. K., Ruschau, J., 2000. Friction-stir welding effects on microstructure and fatigue of aluminum alloy 7050-T7451. Metall. Mater. Trans. 31A, pp. 2181–2192.

129. London, B., Mahoney, M., 2003. Material flow and temperature distribution during friction stir welding of 7050 aluminum alloy. TMS Symposium Proceedings. A Publication of TMS, pp. 3–10.

130. Rebecca, B., Wei, T., Reynolds, A. P., 2009. Multi-pass friction stir welding in alloy 7050-T7451: effects on weld response variables and on weld properties. Mater SciEng, A 513–514, pp. 115–121.

131. Fu, R. D., Sun, Z. Q., Sun, R. C., Li, Y., Liu, H. J., Liu, L., 2011. Improvement of weld temperature distribution and mechanical properties of 7050 aluminum alloy butt joints by submerged friction stir welding. Mater. Des. 32, pp. 4825–4831.

132. Rhodes, C. G., Mahoney, M. W., Bingel, W. H., 1997. Effects of friction stir welding on microstructure of 7075 aluminium. Scripta Mater., 36, pp. 69–75.

133. Fratini, L., Buffa, G., Shivpuri, R., 2010. Mechanical and metallurgical effects of in process cooling during friction stir welding of AA7075-T6 butt joints. Acta Mater, 58, pp. 2056–2067.

134. Rajakumar, S., Muralidharan, C., Balasubramanian, V., 2010. Optimization of the friction-stir-welding process and tool parameters to attain a maximum tensile strength of AA7075-T6 aluminium alloy. ProcInstMechEng Part B J EngManuf , 224, pp. 1175–91.

135. Liu, H. J., Fujii, H., Maeda, M., Nogi, K., 2003. Mechanical properties of friction stir welded joints of 1050-H24 aluminium alloy. SciTechnol Weld Joining,8, pp. 450–454.

136. Murr, L. E., Liu, G., McClure, J. C., 1997. Dynamic recrystallization in friction-stir welding of aluminium alloy 1100. J of Mats SciLettrs, vol. 16, pp. 1801-1803.

137. Kwon, Y. J., Shim, S. B., Park, D. H., 2009. Friction stir welding of 5052 aluminum alloy plates. Trans. Nonferrous Met. Soc. China, 19, pp. s 23-s 27.

138. Sato, Y. S., Yusuke, S., Yohei, S., Park, S. H. C, Hiroyuki, K., Keisuke, I., 2004. Post-weld formability of friction stir welded Al alloy 5052. Mater SciEng A, 369(1–2), pp. 138–143.

139. Moshwan, R., Yusof, F., Hassan, M. A., Rahmat, S. M., 2015. Effect of tool rotational speed on force generation, microstructure and mechanical properties of friction stir welded Al–Mg–Cr–Mn (AA 5052-O) alloy, Materials and Design, 66, pp. 118–128.

140. Peel, M., Steuwer, A., Preuss, M., Withers, P. J., 2003. Microstructure, mechanical properties and residual stresses as a function of welding speed in aluminium AA5083 friction stir welds. Acta Mater, 51(16), pp. 4791–801.

141. Hirata, T., Oguri, T., Hagino H., Tanaka, T., Chung, S. W., Takigawa, Y., 2007. Influence of friction stir welding parameters on grain size and formability in 5083 aluminum alloy. Mater SciEng, A456(1–2), pp. 344 –349.

142. James, M. N., Bradley, G. R., Lombard, H., Hattingh, D. G., 2005. The relationship between process mechanisms and crack paths in friction stir welded 5083-H321 and 5383-H321 aluminiumalloys. Fatigue Fract. Eng. Mater. Struct., 28, pp. 245–256.

143. Etter, A. L., Baudin, T., Fredj, N., Penelle, R., 2007. Recrystallization mechanisms in 5251 H14 and 5251 O aluminum friction stir welds. Mater. SciEng, A445–A446. pp 94–9.

144. Chen, H. B., Yan, K., Lin, T., Chen, S. B, Jiang, C. Y., Zhao, Y., 2006. The investigation of typical welding defects for 5456 aluminum alloy friction stir welds. Mater SciEng, A433(1–2), pp. 64–9.

145. Fonda, R. W., Pao, P. S., Jones, H. N., Feng, C. R., Connolly, B. J., Davenport, A. J., 2009. Microstructure, mechanical properties, and corrosion of friction stir welded Al 5456. Mater SciEng, A519(1–2), pp. 1–8.

146. Crawford, R., Cook, G. E, Strauss, A. M, Hartman, D. A, Stremler, M. A., 2006. Experimental defect analysis and force prediction simulation of high weld pitch friction stir welding. SciTechnol Weld Join, 11, pp. 657–65.

147. Liu, H. J, Fujii, H., Maeda, M., Nogi, K., 2004. Tensile fracture location characterization of friction stir welded joints of different aluminium alloys. J Mater SciTechnol, 20, pp.103–5.

148. Long, X., Khanna, S. K., 2005. Modeling of electrically enhanced friction stir welding process using finite element method. SciTechnol Weld Join, 10, pp. 482–7.

149. Leal, R., Loureiro, A., 2004. Defect formation in friction stir welding of aluminium alloys. Adv Mater Forum II, 455– 456, pp. 299–302.

150. Lee, W. B., Yeon, Y. M., and Jung, S. B., 2003. The joint properties of dissimilar formed Al alloys by friction stir welding according to the fixed location of materials. Scr. Mater., 49, pp. 423–428.

151. Ahmed, M. M. Z., Ataya, Sabbah, El-Sayed Seleman, M. M., Ammar, H. R., Essam Ahmed, 2017. Friction stir welding of similar and dissimilar AA7075 and AA5083. J of Mat ProcsTechn, 242, pp. 77–91.

152. Sivachidambaram, S., Rajamurugan, G., Amirtharaj, D., 2015. Optimizing theparameters for friction stir welding of dissimilar aluminium alloys AA 5383/AA7075. ARPN J. Eng. Appl. Sci., 10 (12), 5434–5437, SSN 1819-6608.

153. Dilip, J., Koilraj, M., Sundareswaran, V., Janaki Ram, G.D., Koteswara, S.R., 2010. Microstructural characterization of dissimilar friction stir welds between AA2219 and AA5083. Trans. Indian Inst. Metals, 63, pp. 757–764.

154. Guo, J., Gougeon, P., Chen, X.-G., 2012. Microstructure evolution and mechanical properties of dissimilar friction stir welded joints between AA1100-B4C MMC and AA6063 alloy. Mat Sci and Engg., A 553, pp. 149– 156.

155. Sundaram, N. S, Murugan, S., 2010. Tensile behavior of dissimilar friction stir welded joints of aluminum alloys. Materials and Design, 31, pp. 4184–4193.

156. Cavaliere, P., Nobile, R., Panella, F. W. and Squillace, A., 2006. Mechanical and microstructural behaviour of 2024–7075 aluminiumalloy sheets joined by friction stir welding. Int. J. Mach. Tools Manuf., 46, pp. 588–594.

157. Muruganandam, D., Ravikumar, S., and Das, S. L., 2010. Mechanical and micro structural behavior of 2024–7075 aluminum alloy plates joined by friction stir welding. 978-1-4244-9082-0/10/$26.00 c2010 IEEE , pp. 247- 251.

158. Cavaliere, P., De Santis, A., Panella, F., Squillace, A., 2009. Effect of welding parameters on mechanical and microstructural properties of dissimilar AA6082–AA2024 joints produced by friction stir welding. Materials and Design, 30, pp. 609–616.

159. Hatamleh, O., DeWald, A., 2009. An investigation of the peening effects on the residual stresses in friction stir welded 2195 and 7075 aluminum alloy joints. Journal of Materials Processing Technology, 209, pp. 4822–4829.

160. Rodriguez, R. I., Jordon, J. B., Allison, P. G., Rushing, T., Garcia, L., 2015. Microstructureand mechanical properties of dissimilar friction stir welding of 6061-to-7050 aluminum alloys. Mater. Des. 83, pp. 60–65.

161. Ghosh, M., Kumar, K., Kailas, S. V., Ray, A. K., 2010. Optimizations of friction stir welding parameters for dissimilar aluminum alloys. Materials and Design, 31, pp. 3033–3037.

162. Kasman, S., Yenier, Z., 2014. Analyzing dissimilar friction stir welding of AA5754/AA7075. Int. J. Adv. Manuf. Technol. 70, pp. 145–156.

163. Da Silva, A. A. M., Arruti, E., Janeiro, G., Aldanondo, E., Alvarez, P., Echeverria, A., 2011. Material flow and mechanical behaviorof dissimilar AA2024-T3 and AA7075-T6 aluminum alloys friction stir welds. Materials and Design, 32, pp. 2021–2027.

164. Amancio-Filho, S. T., Sheikhi, S., dos Santos, J. K., and Bolfarini, C., 2008. Preliminary study on the microstructure and mechanical properties of dissimilar friction stir welds in aircraft aluminium alloys 2024- T351 and 6056-T4. J. Mater. Process. Technol., 206, pp. 132–142.

165. Koilraj, M., Sundareswaran, V., Vijayan, S., Koteswara Rao, S. R., 2012. Friction stir welding of dissimilar aluminum alloys AA2219 to AA5083 – Optimization of process parameters using Taguchi technique. Materials and Design, 42, pp. 1–7.

166. Shojaeefard, M. H., Behnagh, R. A., Akbari, M., Givi, M. K. B., Farhani, F., 2013. Modelling and optimization of mechanical properties of friction stir welded AA7075/AA5083 butt joints using neural network and particle swarm algorithm. Mater. Des. 44, pp. 190–198.

167. Steuwer, A., Peel, M. J., and Withers, P. J., 2006. Dissimilar friction stir welds in AA5083–AA6082: the effect of process parameters on residual stress. Mater. Sci. Eng. A, A441, pp. 187–196.

168. Gan, W., Okamoto, K., Hirano, S., Chung, K., Kim, C., Wagoner, R.H., 2008. Properties of friction-stir welded aluminum alloys 6111 and 5083. J. Eng. Mater. Technol., 130, pp. 1–15.

169. Gungor, B., Kaluc, E., Taban, E., Sik, A., 2014. Mechanical, fatigue and microstructural properties of friction stir welded 5083-H111 and 6082-T651aluminum alloys. Mater. Des., 56, pp. 84–90.

170. Leitao, C., Louro, R., Rodrigues, D. M., 2012. Analysis of high temperature plastic behaviour and its relation with weldability in friction stir welding for aluminum alloys AA5083-H111 and AA6082-T6. Mate.Des., 37, pp. 402–409.

171. Moreira, P. M. G. P., Santos, T., Tavares, S. M. O., Richter-Trummer, V., Vilaca, P., de Castro, P. M. S. T., 2009. Mechanical and metallurgical characterization of

friction stir welding joints of AA 6061-T6 with AA 6082-T6. Materials and Design, 30, pp. 180–187.

172. JamshidiAval, H., Serajzadeh, S., Kokabi, A. H., 2011. Evolution of microstructures and mechanical properties in similar and dissimilar friction stir welding of AA5086 and AA6061. Mats Sci and Engg, A 528, pp. 8071– 80853.

173. Palanivel, R., Mathews, P.K., Murugan, N., Dinaharan, I., 2012. Effect of tool rotational speed and pin profile on microstructure and tensile strength of dissimilar friction stir welded AA5083-H111 and AA6351-T6 aluminum alloys. Mater. Des., 40, pp. 7–16.

174. Hong, S.-T., Kwon, Y.-J. and Son, H.-J. 2008. The mechanical properties of friction stir welding (FSW) joints of dissimilar aluminum alloys. Proc. 1st Int. Symp. on 'Hybrid materials and processing', Busan, South Korea, pp. 69.

175. Park, S.-K., Hong, S.-T., Park, J.-H., Park, K.-Y., Kwon, Y.-J., and Son, H.-J., 2010. Effect of material locations on properties of friction stir welding joints of dissimilar aluminium alloys. Sci and Tech Weld and Joining, 15, pp. 331-336.

176. Stasik, M. C., Wagoner, R. H., 1996. Forming of tailor-welded aluminum blanks. In: Aluminum of Magnesium for Automotive Applications. A Publication of TMS, Warrendale, pp. 69–83.

177. Sato, S. Y., Sugiura, Y., Shoji, Y., Park, S. H. C., Kokawa, H., Ikeda, K., 2005. Post-weld formability of friction stir welded Al alloy 5052. Mater SciEng, A 369, pp. 138–143.

178. Hirata, T., Oguri, T., Hagino, H., Tanaka, T., Wook ,C. S., Tsujikawa, M., 2007. Formability of friction stir welded and arc welded 5083 aluminum alloy sheets. Key Engineering Materials, 340–341, pp. 1473–1478.

179. Hirata, T., Oguri, T., Hagino, H., Tanaka, T., Chung, S. W., Takigawa, Y., 2007. Influence of friction stir welding parameters on grain size and formability in 5083 aluminum alloy. Mater Sci Eng. A 456, pp. 344–349.

180. Kang, S. H., Chung, S. H., Han, N. H., Oh,H. K., Lee, G. C., Kim, J. S., 2007. Relationship between formability and microstructure of Al alloy sheet locally modified by friction stir processing. Scr Mater., 57, pp. 17–20.

181. Leitao, C., Zhang, B. K., Padmanabhan, R., Rodrigues, D. M., 2011. Influence of weld geometry and mismatch on formability of aluminium tailor welded blanks.SciTechnol Weld Join, 16(8), pp. 662–668.

182. Miles, M. P., Decker, B. J., Nelson, T. W., 2005. Formability of friction-stir welded dissimilar-aluminum alloy sheets. Metall Mater Trans, 35, pp. 3335–3342.

183. Miles, M. P., Decker, B. J., Nelson, T. W., 2005. Formability and strength of friction-stir-welded aluminum sheets. Metall Mater Trans, 35, pp. 3461– 3468.

184. Kim, D., Lee, W., Kim, J., Kim, C., Chung, K., 2010. Formability evaluation of friction stir welded 6111-T4 sheet with respect to joining material direction. Int J Mech Sci., 52, pp. 612–625.

185. Leitao, C., Emilio, B., Chaparro, B. M., Rodrigues, D. M., 2009. Formability of similar and dissimilar friction stir welded AA 5182-H111 and AA 6016-T4 tailored blanks. Mater Des, 30, pp. 3235–3242.

186. Lee, W., Chung, H. K., Kim, D., Kim, C., Okamoto, K., Wagoner, R. H.,Chung, K., 2009. Experimental and numerical study on formability of friction stir welded TWB sheets based on hemispherical dome stretch tests. Int J Plast., 25, pp.1626–1654.

187. Rodrigue,s D. M., Loureiro, A., Leitao, C., Leal, R. M., Chaparro, B. M., Vilaça, P., 2009. Influence of friction stir welding parameters on the microstructural and mechanical properties of AA 6016-T4 thin welds. Mater Des, 30(6), pp. 1913–1921.

188. Saunders, F. I. and Wagoner, R. H., 1996. Forming of tailor-welded blanks. Metallurgical and Materials Trans. A,(v27A), pp. 2605-2616.

189. Buste, A., Lalbin, X., Worswick, M. J., Clarke, J. A.,Altshuller, B., Finn, M., Jain, M., 2000. Prediction of strain distribution in aluminum tailor welded blanks for different welding techniques. Canadian Metallurgical Quarterly,(v39 n4), pp. 493-502.

190. Shakeri, H. R., Buste, A., Worswick, M. J., Clarke, J. A., Feng, F., Jain, M., 2002. Study of damage initiation and fraction in aluminum tailor welded blanks made via different welding techniques. J Light Metals, 2, pp. 95–110.

191. Kim, D., Lee, W., Kim, J., Kim, C., Chung, K., 2010. Formability evaluation of friction stir welded 6111-T4 sheet with respect to joining material direction. Int J MechSci, 52(4), pp. 612–625.

192. Parente, M., Safdarian, R., Santos, A. D., Loureiro, A., and Vilaca, P., Natal Jorge, R. M., 2015. A study on the formability of aluminum tailor welded blanks produced by friction stir welding. Int J AdvManufTechnol, DOI 10.1007/s00170-015-7950-0.

193. Cayssials, F., 2000. An industrial application of specific forming limit curves for tailor-welded blanks. In: Proceedings of the 2000 International Deep Drawing Research Group, Ann Arbor, MI, pp. 17–22.

194. Chan, S. M., Chan, L. C, Lee, T. C., 2003. Tailor-welded blanks of different thickness ratios effects on forming limit diagram. J Mater Process Techn, 132, pp. 95–101.

195. Ramulu, P. J., R. G., Kailas, S. V., 2013. Forming limit investigation of friction stir welded sheets: influence of shoulder diameter and plunge depth, Int J AdvManufTechnol, 69, pp. 2757–2772.

196. Arora, A., De, A., Deb Roy, T., 2011. Toward optimum friction stir welding tool shoulder diameter. ScriptaMaterialia, 64(1), pp. 9–12.

197. Keeler, S. P., Backofen, W. A., 1963. Plastic instability and fracture in sheets stretched over rigid punches. ASM TRANS Q, 56(1), pp. 25–48.

198. Goodwin, G. M., 1968. Application of strain analysis to sheet metal forming problems in the press shop (No. 680093). SAE Technical Paper.

199. Hecker, S. S., 1974. Met Eng Q 14 , 30.

200. Nakazima, K., Kikuma, T., Hasuka, K., 1968. Study on the formability of steel sheets. Yawata Tech Rep, 264, pp. 8517–30.

201. ASTM International (2008) Standard test method for determining forming limit curves. ASTM E2218:1–15.

202. ASTM International (2016) Standard Test Methods for Tension Testing of Metallic Materials1 ASTM E8/E8M-16a.

203. Scialpi, A., De Giorgi, M., De Filippis, L. A. C., Nobile, R., Panella, F. W., 2008. Mechanical analysis of ultra-thin friction stir welding joined sheets with dissimilar and similar materials. Materials and Design, 29(5), pp. 928–36.

204. Patel, Vivek V., Sejani, Devang J., Patel, Nandish J., Vora, Jay J., Gadhvi, Bhargav J., Padodara, Neel R., Vamja, Chintan D., 2016. Effect of tool rotation speed on friction stir spot welded AA5052-H32 and AA6082-T6 dissimilar aluminum alloys. Metallogr. Microstruct. Anal., 5, pp. 142–148.

205. McNelley, T. R., Swaminathan, S., Su, J. Q., 2008. Recrystallization mechanisms during friction stir welding/processing of aluminum alloys. Scripta Mater, 58, pp. 349–54.

206. Vander Voort, G. F. and Manilova, E. P., 2015. Metallographic etching of aluminum and its alloys. http://cdn.intechopen.com/pdfs-wm/13406.pdf.

207. D., Li., 1984. Sheet steel formability. American Iron and Steel Institute, Washington, DC.

208. L'Eplattenier, P., Ashcraft, C., Ulacia, I., 2010. An MPP version of the electromagnetism module in LS-DYNA for 3D coupled mechanical-thermal-electromagnetic simulations, 4th International Conference on High speed forming. pp. 250-263.

209. Johnson, G., Cook, W., 1983. A constitutive model and data for metals subjected tolarge strains, high strain sates and high temperatures. In: Proc. 7th International Symposium on Ballistics, pp. 541–547.

Lists of Publications:

International Journals

1. Doley,Jyoti K., Kore,Sachin D., 2019. A Comparative study on formability of a different thickness FSWed AA 5052 blank by conventional and EM forming. Journal of Testing and Evaluation, American Society of Testing and Materials, Vol. 47, No.4, pp.-, https://doi.org/10.1520/JTE20170463. ISSN 0090-397

2. Doley,Jyoti K., Kore,Sachin D., 2017. Comparison of electromagnetic forming of friction stir-welded blanks of dissimilar material AA 5052-AA 6061 with conventional forming process. International Journal of Advance Manufacturing & Technology, Springer, vol. 93, pp. 3789-3797.

3. Doley,Jyoti K., Kore,Sachin D., 2016. A study on friction stir welding of dissimilar thin sheet aluminium alloys AA 5052 – AA 6061. Journal of Manufacturing science and Engineering, American Society of Mechanical Engineers, V-138, pp. 1145021-6.

4. Doley, Jyoti K., Kore, Sachin D., 2014. Electromagnetic Formability of an Aluminium ice tray. Key Engineering Materials, Vol. 611-612, pp.1124-1131. ISSN 1662-9795.

5. Doley,Jyoti K., Kore,Sachin D., 2012. Fully coupled numerical Simulation of Electromagnetic Forming, Key Engineering Materials, Vol. 504-506,pp. 1201-1206. ISSN 1662-9795.

International Conferences:

1. Doley, Jyoti K., Kore, Sachin D., Fully coupled numerical Simulation of Electromagnetic Forming, 15th Conference of the European Scientific Association on Material Forming (ESAFORM 2012), March 14 -16, 2012, Feiedrich-Alexander Universitat, Erlangen-Nurenberg, Germany, Editors: M. Merklein and H. Hagenah.

2. Doley, Jyoti K., Kore, Sachin D., Strong Coupling in Electromagnetic Forming, International Conference on Computational Methods in manufacturing, December 15-16, 2011, Indian Institute of Technology Guwahati, India.